NON-INVASIVE DETECTION OF A TUMOR IN A HUMAN BREAST

Koushik Das
Roll No: 126103027

DEPARTMENT OF MECHANICAL ENGINEERING
INDIAN INSTITUTE OF TECHNOLOGY GUWAHATI
April 2015

NON-INVASIVE DETECTION OF A TUMOR IN A HUMAN BREAST

A Thesis Submitted for the Award of the Degree of

Doctor of Philosophy

by

Koushik Das

to the

DEPARTMENT OF MECHANICAL ENGINEERING

INDIAN INSTITUTE OF TECHNOLOGY GUWAHATI

April 2015

C E R T I F I C A T E

It is certified that the work contained in the thesis entitled **Non-Invasive Detection of a Tumor in a Human Breast**, by Koushik Das, a student in the Department of Mechanical Engineering, Indian Institute of Technology Guwahati, India, for the award of the degree of the Doctor of Philosophy has been carried out under my supervision, and that this work has not been submitted elsewhere for a degree.

Dr Subhash C Mishra
Professor
Department of Mechanical Engineering
Indian Institute of Technology Guwahati
Guwahati, Assam-781039, India
April 2015

To

My family

Acknowledgements

This research work is made possible through the help and support from many prominent personalities of my life. Especially, please allow me to dedicate my acknowledgment of gratitude toward the following significant advisors and contributors. First and foremost, I would like to thank my guide and supervisor Dr. Subhash C. Mishra for his most support and encouragement. His mentorship was eminent in planning implementation of my long-term goals. He encouraged me to not only grow as a researcher but also as an instructor and an independent thinker.

I would like to thank all the members of the research group under Prof. Mishra, especially Rupesh for his invaluable advice towards this research work. I would also like to thank my friend and wall-mate Niraj for his support and encouragement during the time of discouragements. My sincere thanks also goes to the department of Mechanical Engineering at IIT Guwahati, especially those members of my doctoral committee for their input, valuable discussions and accessibility. The guidance of Dr. Manmohan Pandey and Dr. Chandramohan Somayaji from the Department of Mechanical Engineering and Dr. Dipankar Bandyopadhyay from the Department of Chemical Engineering, IIT Guwahati, was really preeminent.

The on time successful accomplishment of this thesis wouldn't have been possible without the backing of my friends, Dipjyoti, Dipankar, Rohan, Prashant, Alekh and Ashish. I really thank them for having faith on me. I would also like to thank my friend and fiancé Saroj for her love, consistent support and fortitudes. I thank my parents, and my sisters, for their faith in me and allowing me to be as ambitious as I wanted. It was under their watchful eye that I gained so much drive and an ability to tackle challenges. Towards the end, I thank the God for giving me everything.

List of Publications from this Thesis Work

International Journal

1. K. Das, S. C. Mishra; Estimation of tumor characteristics in a breast tissue with known skin surface temperature, Journal of Thermal Biology, 2013 (38) 311 – 317.
2. K. Das, S. C. Mishra; Non-invasive estimation of size and location of a tumor in a human breast using a curve fitting technique, International Communications in Heat and Mass Transfer, 2014 (56) 63–70.
3. K. Das, S. C. Mishra; Study of thermal behavior of a biological tissue: an equivalence of Pennes bioheat equation and Wulff continuum model, Journal of Thermal Biology, 2014(45) 103–109
4. K. Das, S. C. Mishra; Simultaneous estimation of size and location of a tumor in a breast using curve fitting technique, Computers in Biology and Medicine (Revised manuscript submitted)
5. K. Das, S. C. Mishra; Simultaneous estimation of size, radial and angular locations of a tumor in a 3-D human breast - A numerical study, Journal of Thermal Biology. (Communicated)

International Conference

1. S. C. Mishra, K. Das, M. Ganguly, P. Goswami; Thermal estimation of properties and location of tumor in a 2-D biological tissue using surface temperature profile, 9thInternational Conference on Flow Dynamics, Sendai, Japan, September 19– 21, 2012.
2. K. Das, S. C. Mishra; Non-invasive detection of breast tumor using curve fitting technique, 10thInternational Conference on Flow Dynamics, Sendai, Japan, November 25 – 27, 2013.
3. K. Das, S. C. Mishra; A comparative study of heat transfer in a biological tissue with Pennes bioheat equation and Wulff continuum model, 22nd National and 11th International ISHMT-ASME Heat and Mass Transfer Conference, IIT Kharagpur, India, December 28 –31, 2013.
4. K. Das, S. C. Mishra; Thermal investigation of human breast and utilization of curve fitting technique in inverse estimation of tumor characteristics, 11th International Conference on Flow Dynamics, Sendai, Japan, October 8 – 10, 2014.

SYNOPSIS

Name of the student: **Koushik Das** Roll No.: **126103027**

Degree for which submitted: **PhD** Department: **Mechanical Engineering**

Thesis Title: **Non-Invasive Detection of a Tumor in a Human Breast**

Name of the Supervisor: **Prof. Subhash C. Mishra**

Month & Year of Submission: **October 2014**

Cancer is a life threatening disease. All over the globe, millions of people are in its grip. No country is spared of this disease. It is growing like an epidemic. Controlling its growth and curing the affected ones, remain a great challenge. As per the latest report of GLOBOCAN, the number of new cases of cancer (incidence) in 2012 was 14.1 million; and 8.2 million people died of cancer in that year. Within 5 years of diagnosis (ending 2012), 32.6 million people were found living with cancer. Among all, breast cancer has been the second most common cancer in the world for several decades, with the highest mortality rate in women. Presently, every 1 out of 4 women carries the risk of having cancer of the breast. In the year 2012, with a mortality rate of 32%, 1.67 million new cases of breast cancer have been diagnosed globally. In the USA and India these numbers were 2,32,714 and 1,44,937, with mortality rate of 15% and 25.8%, respectively.

Breast cancer normally starts in the lobules and the milk ducts. Lobular Carcinoma in Situ (LCIS), in its non-invasive form, is a pre-cancerous condition that forms and stays in the lobules. Invasive LCIS is the type of cancer that invades through lobules with a potential to spread to other parts of the body. Ductal Carcinoma in Situ (DCIS), in its non-invasive form, develops in the milk ducts and it does not spread. If cancer spreads beyond the milk ducts, it is known as ductal carcinoma. Sometimes, cancer in a breast starts in the stromal tissues, fatty and fibrous connective tissues of the breast.Treating any cancer, more so the breast cancer, at an early stage is very important. If left untreated, it has a potential to invade healthy breast tissues and lymph nodes. After it enters the lymph system, there is a likelihood of cancer spreading very easily to other parts of the

body. Depending on the stages of the breast cancer, the size of the cancerous tumor may vary from few millimetres to 5 cm or bigger.

Prognosis and survival rate for any cancer including the breast cancer vary depending on its type, stage and geographical location of the patient. In the western countries, the survival rates are high. More than 8 out of 10 women in England diagnosed with breast cancer survive for at least 5 years. This number is low for the developing and underdeveloped countries. The above statistics indicates the volume of research needed for the diagnosis and the treatment of a breast cancer.

Diagnosis is the first and the foremost step in the treatment of any disease. Earlier diagnosis means better chances of cure and survival. This is more so for a cancer. Modern techniques and equipment like computed tomography scan, magnetic resonance imaging, X-ray mammography etc., quite efficiently detect malignancies in the body. But, many a times, a patient has to undergo cumbersome procedures related to these techniques, such as long duration of the diagnostic procedure, side-effects of radiation, high diagnosis cost, etc. Thus, research is needed to develop a simple diagnostic procedure without any side effect. The present work focuses on potential application of one such procedure. Consideration is given to the estimation of various attributes of a tumor in a human breast.

Any malignancy in a tissue leads to abnormal characteristics and behaviors. All the tissues in a human body at a particular condition have its own thermal signature. A slight variation in its condition, change these signatures. This is very much true for a cancerous tissue. Temperature profile in a cancerous tissue is different from that of a healthy one. Measurement of the changed thermal signals, such as the temperature profiles, temporal transmittance and reflectance signals can be a helpful tool in estimation of the presence of any abnormality in a tissue. The degree of abnormality, its location and size yield a specific signal. Thus, its measurement in an indirect way can reveal various attributes of the abnormality in the tissue. Present work focuses on estimation of various attributes of malignancy in a human breast, using the temperature profile of its skin surface.

From heat transfer point of view, human body is a thermal system. Mathematically, heat transfer in a biological system is governed by Pennes bioheat equation. In a simplified

form, Pennes bioheat equation is similar to an energy equation with a temperature dependent volumetric heat generation. Various numerical methods like the finite difference method, the lattice Boltzmann method, the finite volume method (FVM), the finite element method (FEM), etc. have been used by many researchers to solve this equation. Present work consists of discretization and solution of Pennes bioheat equation to obtain temperature field of a breast tissue, with the help of FVM and FEM. To estimate various characteristics of a tumor in a breast, inverse analysis of numerically obtained temperature distribution of the breast skin surface is performed. Present work utilizes stochastic method like the genetic algorithm (GA) in non-invasive detection of a tumor in the breast. The work also proposes an algorithm based on curve fitting method (CFM) for application in human breast in conjunction with FVM and FEM. Starting with a simple rectangular geometry of breast tissue, analysis is done for a semi-circular section of the breast; and finally a 3-D model is analyzed numerically to estimate the size, the radial location, the polar and the azimuthal angular position of a tumor. During the analysis of various aspects of a bioheat problem, a mathematical relation between average blood velocity and blood perfusion rate of a tissue is developed for a simplified case using equivalence of Pennes equation and Wulff's model of bioheat transfer.

In a healthy condition, the skin temperature of the breast is always uniform. A healthy tissue always has uniform blood perfusion and metabolic heat generation rate. In the presence of a malignancy such as a tumor, the value of the blood perfusion rate and the metabolic generation rate of the affected tissues increase by many fold. In spite of having higher value of blood perfusion rate, due to higher rate of metabolic activities, the overall temperature of the affected portion of the breast elevates. It manifests in the form of raised skin surface temperature of the breast. The size and the location of the malignancy in the breast also affect the skin surface temperature. The skin surface temperature of the breast rises for bigger sizes of the tumor. Closer the tumor located near the skin surface, higher is the temperature rise. In the present work, using the skin surface temperature of the breast, the parameters of malignancy inside the breast are estimated using inverse analysis. Consideration is given to a 2-D rectangular geometry of the breast tissue, and the inverse analysis is performed using the GA. Estimation of parameters using the GA requires solution of the governing bioheat equation. This is needed for every generation. The solution of the bioheat equation is an iterative one. This adds to the computational

time. Often the GA requires a large population size. The large population size combined with iterative procedure, the approach of the GA turns out to be computationally very expensive. Thus, there remains a need for a computationally efficient tool in the inverse analysis.

Breast skin surface temperature profile is tumor specific. The characteristics of the temperature profile vary according to the size and location of the tumor. In the present work, it has been found that irrespective of the size and location of the tumor, the skin surface temperature profile is Gaussian in nature. This forms the basis of the newly proposed CFM for inverse analysis. With this as a tool, simultaneous estimation of various parameters of a tumor in a 2-D rectangular tissue of breast is performed. Compared to the stochastic techniques like the GA, the CFM allows us to estimate more number of unknown parameters of the tumor with better accuracy. Further, the analysis is extended to a semi-circular section of breast and a 3-D hemispherical model. With the CFM, the time required in the estimation is also much smaller.

The PhD thesis consists of 7 chapters. Chapter 1, entitled “Introduction”, starts with a general discussion about cancer, and its effect in the human society. The global statistics of cancer and its root in connection with human activities are elaborated. Human body is a thermal system. Its analysis is complicated due to the presence of structural inhomogeneity, the counter-current flow of blood in vessels, the lymphatic systems and the metabolic activities. With a discussion of various models to describe bioheat transfer, its importance and scope in cancer diagnosis are discussed in this chapter. This chapter of the thesis is also devoted to the review of pertinent literature. The chapter describes briefly, the extent of various work done in the area of bioheat transfer and its application in cancer diagnosis. The review work forms the basis of the problem statement defined for the current research work. With a brief about the motivation of the current work, the following chapter (chapter 2) defines the problem statement and the roadmap.

The basic mathematical formulations, the governing equations and the numerical discretization of the solution domains are presented in chapter 3. The considered bioheat equations and the physical significance of its terms are described. The FVM and/or the FEM is used to solve the governing equation. A detailed approach is presented in this chapter. For the inverse analysis, the methodology of the GA is also presented.

The present work is aimed to analyze and non-invasively detect and estimate various attributes of a tumor present in a human breast using thermal means. The inverse methodology used in the defined problem uses the GA or the CFM. The results obtained from the direct analysis of a 2-D rectangular tissue is analyzed and are presented in chapters 4. This chapter also incorporates the inverse estimated data obtained for the geometry of tissue using both the GA and CFM. In chapter 5, similar analysis is done on a 2-D and 3-D realistic human breast. A comparative study between the efficacies of both the inverse methods are also presented.

Thermal modelling of a living tissue becomes very difficult when the vascular architecture of a tissue is taken into account. In the year 1948 and 1972, Pennes and Wulff, respectively, proposed the bioheat models with a few simplified assumptions. Contrary to the Pennes bioheat equation that considers blood perfusion rate, the Wulff continuum model considers the blood velocity in a tissue. Compared to the Pennes bioheat model, the Wulff continuum model is more realistic. However, measurement of the blood velocity in a tissue is cumbersome. To get rid of this measurement, a mathematical relationship is derived to calculate the average blood velocity from the blood perfusion rate for the 1-D tissue. The derived relation is established numerically for different cases. Details are presented in chapter 6.

The concluding remarks on various direct and inverse study, and the scope of the future work are presented in chapter 7.

CONTENTS

CHAPTER	TITLE		PAGE NO.
	SYNOPSIS		xi
	CONTENT		xvii
	LIST OF FIGURES		xxi
	LIST OF TABLES		xxvii
	NOMENCLATURE		xxix
	ABBREVIATIONS		xxxi
1.	**INTRODUCTION**		**1 – 6**
	1.1.	Cancer Statistics	2
	1.2.	Breast Cancer	2
	1.3.	Work Done in the Area of Bioheat Transfer	3
	1.4.	Summary	6
2.	**PROBLEM STATEMENTS AND GEOMETRY**		**7 - 12**
	2.1.	Motivation for the Proposed Work	8
	2.2.	Problem Statements and Roadmap	9
	2.3.	Geometry	9
	2.4.	Summary	12
3.	**METHODOLOGY AND FORMULATIONS**		**13 – 26**
	3.1.	Fourier's Law of Heat Conduction	14
	3.2.	Bioheat Transfer	15
		3.2.1. Pennes' bio-heat transfer equation	16
		3.2.2. Wulff continuum model	17
	3.3.	Normalized Form of Governing Bioheat Equations	17
	3.4.	Finite Volume Method	18

CHAPTER	TITLE		PAGE NO.
	3.5.	Finite Element Method	21
	3.6	Inverse Analysis	21
		3.6.1 Genetic algorithm	22
		3.6.2 Curve fitting technique	24
	3.5.	Summary	25
4.	**THERMAL MODELLING OF 2-D TISSUE**		**27 – 44**
	4.1.	Validation	27
		4.1.1. Validation of the numerical solver	27
		4.1.2. Equivalence of 2-D and 3-D numerical simulation of human breast	30
	4.2.	Thermal Analysis of a Tissue	32
		4.2.1. Based on properties given by Gonz´alez (2007)	32
		4.2.2. Based on properties given by Gautherie (1980)	35
	4.3.	Inverse Analysis	37
		4.3.1. Genetic algorithm	38
		4.3.2 Curve fitting technique	40
	4.4	Summary	44
5.	**THERMAL MODELING AND INVERSE ANALYSIS OF A REALISTIC BREAST GEOMETRY**		**45 – 70**
	5.1.	Geometry	45
	5.2	Validation	47
		5.2.1. Closeness of 2-D semicircular and 3-D hemispherical model of breast	47
		5.2.2 Validation with experimental data	49

CHAPTER	TITLE		PAGE NO.
	5.3.	Effects of Tumor Size and Location on the Skin Surface Temperature	50
		5.3.1. 2-D semicircular breast	50
		5.3.2. 3-D hemispherical breast	54
	5.4.	Inverse Analysis	56
		5.4.1. 2-D semicircular breast	56
		5.4.2. 3-D hemispherical breast	60
	5.5.	Effect of Measurement Error on Inverse Analysis	63
		5.5.1. 2-D semicircular breast	63
		5.5.2. 3-D hemispherical breast	65
	5.6.	Summary	69
6.	**EQUIVALENCE OF PENNES BIOHEAT EQUATION AND WULFF CONTINUUM MODEL**		**71 – 82**
	6.1.	The $v-\eta_b$ Relation	72
	6.2.	Comparison of Numerical Results with Experimental Data	75
	6.3.	Numerical Validation of the $v-\eta_b$ Relation	77
	6.4.	Calculation of Local Mean Blood Velocity	79
	6.5.	Effect of boundary conditions	80
	6.6.	Summary	82
7.	**CONCLUSIONS AND SCOPE FOR FUTURE WORK**		**83 –84**
	7.1.	Future Scope	84
	REFERENCES		**85 – 89**

LIST OF FIGURES

Figure	Title	Page No.
2.1	Schematics of (a) 1-D and (b) 2-D geometry of tissue.	10
2.2	Schematic of (a) human breast affected by a malignant tumor (b) 3-D model of hemispherical human breast and its simplified representation in the form of (c) 2-D semicircular planar tissue with tumor.	11
3.1	Schematics of (a) the 2-D and (b) the 1-D discretized solution space with nomenclatures of the control volume nodal points and description of the (c) 2-D and (d) 1-D FVM control volume.	19
3.2	Schematics of the (a) 2-D and (b) 3-D FEM discretized solution space.	21
3.3	Flow chart showing optimization steps in GA.	23
3.4	Schematic of a Gaussian distribution.	24
4.1	Comparison of (a) transient spatial distribution of temperature in 1-D tissue and steady-state temperature distribution in 2-D tissue along (b) the skin surface (x, L) and (c) the centerline (L, y) with Zhang (2008).	29
4.2	Schematic of (a) a 3-D hemispherical breast with an imbedded tumor and (b)a 2-D equivalent system of the 3-D model	31
4.3	A comparison of SS centerline (L, y) temperature distribution for the breast with and without tumor	32
4.4	Steady-state temperature distributions along the skin surface (x, L) of the breast tissue imbedded with a tumor $(\text{size:}1.25\,\text{cm}\times 1.25\,\text{cm})$ at position (a) top: $(0.625L \le y \le 0.875L)$ (b) center: $(0.375L \le y \le 0.625L)$ and (c) bottom $(0.125L \le y \le 0.375L)$.	34

Figure	Title	Page No.
4.5	Steady-state temperature distributions along the skin surface (x, L) of the breast tissue with a centrally imbedded tumor of thickness (a) $L/4$, (b) $L/2$ and (c) $3L/4$.	35
4.6	Steady-state skin surface (x,L) temperature distribution: Effect of locations $(L-\mathrm{Y})$ of tumor for tumor of size (a) 0.5 cm and (b) 2.5 cm, (c) effect of sizes of the tumor located at $(L-\mathrm{Y})$ = 2.75 cm.	37
4.7	(a) Schematic of a Gaussian profile, and variation of its (b) amplitude and (c) area for different sizes of tumors at its different locations *Y* in a 2-D tissue.	41
4.8	Effect of change of blood perfusion rate (η_b) on steady-state skin surface (x,L) temperature distribution for a tumor of size 3 cm located at *Y*= 3.0 cm.	42
5.1	Schematic of (a) 3-D model of hemispherical human breast and its simplified representation in the form of (b) 2-D semicircular planar tissue with tumor.	46
5.2	Schematics of the (a) 3-D and (b) 2-D FEM discretized solution space.	47
5.3	Comparison of SS (a) centerline $\left(r, \pi/2\right)$ and (b) skin surface (R,ϕ) temperature distribution of 3-D hemispherical model with 2-D section of human breast with tumor of size 2.5 cm located at a depth of 3 cm on *y*- axis.	49
5.4	Steady-state temperature distribution along (a) the centerline $\left(r,\theta=0,\phi=\pi/2\right)$ and (b) the skin surface $\left(r_b,\theta=0,\phi\right)$ of the 3-D breast validating the results with experimental data (Gautherie, 1980).	50

Figure	Title	Page No.
5.5	Steady-state temperature distribution of (a, b) surface (R,ϕ) and (c, d) centerline $\left(r,\pi/2\right)$ of the 2-D breast tissue with tumor of size 1.0 cm (a, c) and 2.5 cm (b, d) located on the centerline $\left(\phi=\pi/2\right)$ at different *r*.	51
5.6	Variation of SS temperature distributions along (a) the skin surface (R,ϕ) and (b) centerline $\left(r,\pi/2\right)$ of the 2-D breast tissue with tumors of different sizes located at $(r_o=4.5\,\text{cm})$.	52
5.7	Schematic of 2-D semicircular tissue with tumors at same depths from skin and with different offset from Y-axis.	53
5.8	Variation of SS temperature distributions along the skin surface of the breast having tumor of size 1 cm with different angular positions, located on radius (a) $r_o=7.0\,\text{cm}$ and (b) $r_o=6.5\,\text{cm}$.	54
5.9	Steady-state temperature distribution of surface $(R,\theta=0,\phi)$ of the breast with tumor (a) of various sizes, at $r_t=4.75\,\text{cm}$ and (b) at various depths $(R-r_o)$ with tumor radius (r_t) 1.5 cm, located on the centerline $\left(\theta=0,\phi=\pi/2\right)$.	55
5.10	Variation of SS temperature distributions along the skin surface of the breast with tumor of size 1.5 cm located at various (a) θ-position with $\phi=\pi/2$ and (b) ϕ-position with $\theta=0$ at $r_o=6.25\,\text{cm}$.	56
5.11	Schematic of a general Gaussian profile.	57
5.12	Variation of (a) amplitude (*A*) and (b) *Area* of SS Gaussian temperature profile for wide range of locations and sizes of tumor in	59

Figure	Title	Page No.
	2-D semicircular tissue.	
5.13	Variation of (a) amplitude, *A* and (b) Area of the Gaussian distribution of temperature for different sizes of the tumor at various radial locations.	61
5.14	Steady-state temperature contours of the skin surface of the breast with 1.5 cm tumor located at a depth of 3.75 showing (a) the point of maximum surface temperature, (b) the circumferential curve passing through the point of maximum temprature and (c) the virtual semicircular plan subtended on the curve passing through the center of the tumor.	62
5.15	Steady-state distributions of temperature along the skin surface of the breast with an accuracy of ±1% for the tissue-tumor configuration as shown in table 5.1.	64
5.16	Steady-state distributions of temperature along the skin surface of the breast with an accuracy of ±0.75% for the tissue-tumor configuration as shown in table 5.3.	67
5.17	Steady-state distributions of temperature along the skin surface of the breast with an accuracy of ±1% for the tissue-tumor configuration as shown in table 5.3.	68
6.1	Schematic of 1-D (a) tissue with a tumor and (b) FVM grid used in the analysis.	73
6.2	Comparison of 3-D numerical and experimental data for a human breast (a) without and (b) with tumor showing the closeness of the results with a 1-D planar geometry.	77
6.3	θ vs. X profile of 1-D geometry of tissue showing equivalence of PBHE and WCM.	78

Figure	Title	Page No.
6.4	Temperature profile for 1-D tissue geometry for different cases of having tumor and no tumor condition with and without metabolic heat generation.	80
6.5	Temperature (θ) distribution along the length (X) of the 1-Ddomain of tissue showing equivalence of PBHE and WCM with heat flux of strength (a, b) $q^* = 1$ and (c, d) $q^* = -1$ on the east boundary.	81

LIST OF TABLES

Table	Title	Page No.
4.1	Value of blood perfusion rate (η_b) and metabolic heat generation rate (Q_m) of human breast with reference to different literatures.	30
4.2	Estimated values of blood perfusion rate η_b of a healthy and malignant breast tissue.	38
4.3	Estimation of location of the top y_t^* and the bottom y_b^* surfaces of the tumor in a breast tissue.	39
4.4	Simultaneous estimation of blood perfusion rate η_b and location (y_t^*, y_b^*) of a tumor in breast tissue.	39
4.5	Inverse estimated value of location and size of a tumor in 2-D breast tissue.	43
5.1	Inverse estimated value of location and size of a tumor in semi-circular 2-D human breast.	59
5.2	Effect of blood perfusion rate on estimation of size and location of tumor in breast.	60
5.3	Inverse estimated values of size (r_t) and location (r_T, θ, ϕ) of a tumor in a breast	63
5.4	Inverse estimated value of location and size of a tumor using skin surface temperature of 2-D human breast with an accuracy of ±1%.	65
5.5	Effect of blood perfusion rate on estimation of size and location of tumor in a breast using skin surface temperature of ±1% accuracy.	65
5.6	Inverse estimated value of location (r_T, θ, ϕ) and size (r_t) of a tumor using skin surface temperature of 3-D human breast with an accuracy of ±0.75%.	67

5.7 Inverse estimated value of location (r_T, θ, ϕ) and size (r_t) of a tumor using skin surface temperature of 3-D human breast with an accuracy of ±1%. 68

6.1 Values of blood perfusion rate and metabolic heat generation rate for different cases breast tissue (Gautherie, 1980). 79

NOMENCLATURE

A	-	area, m^2
A_p, B_p	-	normalized function associated with Pennes bioheat equation
A_w, B_w	-	normalized function associated with Wulff's continuum model
c_p	-	specific heat at constant pressure, $\mathrm{J/kg \cdot K}$
c_pb	-	specific heat of the blood, $\mathrm{J/kg \cdot K}$
CV	-	total number of control volumes
k	-	thermal conductivity, $\mathrm{W/m \cdot K}$
L	-	length, m
q	-	heat flux, $\mathrm{W/m^2}$
$\dot{Q}_g$	-	volumetric heat generation rate, $\mathrm{W/m^3}$
Q_m	-	metabolic heat generation rate, $\mathrm{W/m^3}$
Q_s	-	distributed volumetric heat source due to spatial heating, $\mathrm{W/m^3}$
t	-	time, s
T	-	temperature, K or $^\mathrm{o}$C
T_a	-	temperature of the artery, K or $^\mathrm{o}$C
T_e	-	local heat source temperature, K or $^\mathrm{o}$C
v	-	mean blood velocity, $\mathrm{mm/s}$
V	-	volume of cell, m^3
x	-	space variable

X - non dimensional length

Greek symbols

α - thermal diffusivity, m^2/s

ρ - density, kg/m^3

ρ_b - density of blood, kg/m^3

η_b - blood perfusion rate, $\mathrm{ml/s \cdot ml}$

Superscript

$*$ - nondimensional variable

n - time level

Subscripts

E - east

N - north

P - cell center

S - south

W - west

ABBREVIATIONS

CFM	curve fitting method
DCIS	ductal carcinoma in situ
FEM	finite element method
FVM	finite volume method
GA	genetic algorithm
LCIS	lobular carcinoma in situ
PBHE	Pennes bioheat equation
SS	steady-state
WCM	Wulff continuum model
1-D/2-D/3-D	one-/two-/three-dimensional

CHAPTER 1

INTRODUCTION

Quest to understand the physics of the biological systems, like the human body has remained a challenge. This quest has led to the development of a new branch of science called bioengineering or popularly known as biotechnology. Since old ages, people are trying to understand and apply various aspects of biotechnology in their lives. The oldest known record of its use is in mummies of human and animals in ancient Egypt. Biotechnology is the application of basic laws of science in a biologically oriented technical problem. The proposed work focuses on biotechnical aspects of heat transfer in a living biological tissue.

Though, with advancement in science and technology, mortality rate from diseases like plague, polio, malaria, etc., has been drastically reduced, however, the overall mortality remains almost the same due to manifestation of diseases like cancer. Cancer is a condition of malignancy in a living body due to various causes like pollution, smoking, intake of alcohol and contaminated food, unhealthy lifestyle, etc. (National Cancer Institute). Some other reasons may include exposure to nuclear radiation and excessive sunlight, and of having family history of cancer, etc. The word ‘malignancy’ is of Latin origin; ‘male’ means ‘badly’ and ‘-gnus’ means ‘born’. Malignancy is a tendency of medical condition to become progressively worse leading to death. In cancer, a lump of malignant tissues called tumor, characterized by uncontrolled growth, get formed in the living body. The lump so formed, in due course of time has the ability to invade the

adjacent tissues and get transported in blood stream. In such a condition, the tumor is in the metastatic state. It attains the ability to form colonies in other parts of the body.

1.1. Cancer Statistics

Millions of people are in the grasp of cancer all over the globe. No country is spared. Controlling its growth and curing the affected ones, remain a great challenge. As per the latest report of GLOBOCAN, the number of new cases of cancer (incidence) in 2012 was 14.1 million; and 8.2 million people died of cancer in that year. Within 5 years of diagnosis (ending 2012), 32.6 million people were found living with cancer. Among all, the breast cancer has remained the second most common cancer in the world for several decades, with the highest mortality rate in women. Presently, every 1 out of 4 women carries the risk of having cancer of the breast. In the year 2012, with a mortality rate of 32%, 1.67 million new cases of breast cancer have been diagnosed globally. In the USA and India these numbers were 2,32,714 and 1,44,937, with mortality rate of 15% and 25.8%, respectively.

1.2. Breast Cancer

A breast is a part of the female human body situated at the upper region of the torso that carries the mammary glands to feed the infants. Breast cancer normally starts in the area where the milk is produced i.e., lobules and the milk ducts. Lobular Carcinoma in Situ (LCIS), in its non-invasive form, is a pre-cancerous condition that forms and stays in the lobules. Invasive LCIS is the type of cancer that invades through lobules with a potential to spread to other parts of the body. Ductal Carcinoma in Situ (DCIS), in its non-invasive form, develops in the milk ducts and it does not spread (National Breast Cancer Foundation). If cancer spreads beyond the milk ducts, it is known as ductal carcinoma. Sometimes, cancer in a breast starts in the stromal tissues, fatty and fibrous connective tissues of the breast. Treating any cancer, more so the breast cancer, at an early stage is very important. If left untreated, it has a potential to invade healthy breast tissues and lymph nodes. After it enters the lymph system, there is a likelihood of cancer spreading very easily to other parts of the body (National Breast Cancer Foundation). Depending on the stages of the breast cancer, the size of the cancerous tumor may vary from few centimeters to 5 cm or may be bigger (Fisher et al., 1969).

In the last decade, the application of hyperthermia and hypothermia opened new vistas in the area of treatment of benign and malignant tumors, which included the study of bioheat transfer. One such application might be the analysis of thermal behavior of a tissue in noninvasive diagnostic procedure of tumors in a living body. Limited to few cases, invasive mode of diagnosis is becoming obsolete; and after a few years, it is expected to no longer be in practice. Hence, in the current scenario, application of the thermal means in diagnosis of malignancy may prove to be a potential one.

1.3. Work Done in the Area of Bioheat Transfer

Human body is a complicated system, and that too when we talk of heat transfer in it, the analysis becomes complex. In the year 1876, Bernard, a French physiologist carried out the first experiment (Cho, 1992) in order to analyze effect of blood flow on heat transfer in living tissues. Since then, many physiologist, physicians and engineers have contributed to the area of bioheat transfer. The first model explaining mathematical relation between blood flow and heat transfer was proposed by Pennes in August, 1948. His experimental work, explaining the observation done on human forearm, lead to development of a bioheat equation known as Pennes bioheat equation (PBHE) (Pennes, 1948). The PBHE is based on the assumption that the heat transfer between tissue and blood takes place only in the capillaries. It neglects the effect of large blood vessels, and this, therefore is the simplified continuum approach (Shih, 2007). In his experiment, Pennes used thermocouples invasively to measure the temperature inside the forearm of a subject in a controlled environment.

In the year 1998, Wissler revisited the work of Pennes. The main purpose of his study was to re-establish the work of Pennes, as it had been facing criticisms, questioning the experimental and model data mismatch (Wissler, 1998). In his work, Wissler showed his analysis supporting the theory of Pennes, mentioning that, Pennes model was still a good approximation to predict temperature field in blood perfused biological tissue even after its simplified assumptions.

The first quantitative relation that described heat transfer in human tissue including the effect of blood flow on thermal condition of a tissue on continuum basis was the Pennes bioheat model. Essentially taking care of the blood perfusion, vascular architecture and

inhomogeneity in thermal properties of tissue, many researchers proposed various models on bioheat (Rai and Rai, 1999; Bhowmik et al., 2013). A discussion on mathematical models of bioheat transport can be found in work by Charny (1992), Arkin et al. (1994), Shih et al.(2007), and Ahmadikia et al.(2012). Charny (1992) has given a review of different models, their applicability and limitations mentioning that, in a tissue, blood perfusion rate is an important parameter, as it plays a vital role in heat transfer analysis. A review of developments of different models in a blood perfused tissue has been provided by Arkin et al. (2012). Shih et al. (2007) and Ahmadikia et al. (2012) did analytical study of the skin tissue subjected to different tissue surface conditions. Shih et al. (2007) has shown an analytical approach to solve the PBHE with sinusoidal heat flux condition on the skin surface. Since, analytical solutions are limited to simplified cases, several researchers have numerically studied various aspects of heat transfer in a biological tissue (Zhang, 2008; Fan and Wang, 2011). The PBHE is a modified form of the heat conduction equation, and it can be solved using different numerical methods, viz., the finite difference method (Yuan, 2009; Jiji, 2009; Zolfaghari and Maerefat, 2010), the lattice Boltzmann method (Zhang, 2008; Mishra et al., 2005), the finite volume method (FVM) (Versteeg and Malalasekera, 1995; Das et al., 2013), the finite element method (FEM) etc.

Nakayamma and Kuwahara (2008) have treated the anatomical structure of a tissue as a fluid saturated porous media through which the blood infiltrates, and have derived a volume averaged governing equations for the bioheat transfer and blood flow. The final governing equations derived are then compared with the existing models of bioheat transfer. An effort has also been made in their work to derive the existing models from the derived model. Zhao et al. (2005) have developed a new two-level finite difference scheme for the 1-D PBHE. The scheme developed is unconditionally stable and convergent. Numerical studies for a skin-heating model are also conducted in their work. A spectral element method is developed for the numerical solution of the Pennes bioheat transfer equation by Dehghan and Sabouri (2012). Explanation of the proposed method is given for implementation in one- and two-dimensional cases. Both the triangular and quadrilateral grids were investigated for two-dimensional cases using spectral element method. In the spectral element method, the high accuracy can be achieved with only few grid points for smooth solutions because approximating functions are higher order

polynomials. Fan and Wang (2011) have proposed a general bioheat model for macro-scale study. The model shows that both blood and tissue macro scale temperatures satisfy the dual phase lagging energy equations.

Trobec and Depolli (2011) have studied the effect of blood perfusion on central part of the human forearm using Pennes bioheat model. A 3-D model is built using 100 sliced models of forearm. Consideration is given to a non-homogeneous medium to study the effect of blood flow on temperature inside the system. The results were compared with the analytical and experimental data. Zolfaghari and Maerefat (2010) have proposed their own bioheat model for evaluating thermal response of the human body to transient environment. The model has been validated against the published experimental and analytical results, where a good agreement has been found. Despite the simplicity of the model, it is able to accurately predict the temperature and its changed rate in the cutaneous layer under a wide range of environmental conditions.

Agnelli et al. (2011a) have presented a methodology to determine unknown thermo-physical or geometrical parameters of a tumor region using the temperature profile on the skin surface that may be obtained by infrared thermography. To solve these inverse problems, a second order finite difference scheme was used to solve the PBHE with mixed boundary conditions in two and three dimensions. Then, the pattern search algorithm was used to estimate the different parameters by minimizing a fitness function. Agnelli et al. (2011a) have successfully estimated various parameters of a tumor. For a particular size and position of the tumor, estimation of metabolic heat generation is shown with acceptable accuracy. In the same article, similar study was done on a 2-D geometry in simultaneous estimation of radius and position of the center of the tumor. Effect of noise on the estimated parameters was also studied, and results obtained were within acceptable limit.

In another work by Agnelli et al. (2011b), abnormal skin surface temperature is utilized for optimization of shape of a tumor located inside a 2-D tissue. The methodology presented is concluded to be a useful tool to locate tumor regions. Similar study has also been carried out by Partridge and Wrobel (2007) for estimation of location and size of a tumor inside a 2-D tissue using surface temperature profile. In their work, the dual reciprocity method is coupled to genetic algorithm (GA) in an inverse procedure through

which the size and location of a skin tumor are obtained from temperature measurements at the skin surface.

Bezerra et al. (DOI: 10.1016/j.sigpro.2012.06.002) have developed an experimental setup using infrared imaging and inverse algorithm to estimate the thermal conductivity and blood perfusion rate of the breast tumor. Certain protocols were followed in the experiment done on a number of volunteers. Noise was also added to the measured thermogram, and the results obtained were considered good estimations for the thermal parameters. Thermal analysis of a three-dimensional model of breast tissue was done by Amri et al. (2011). Different sizes and locations of the tumor were considered for the study. Various issues related to effect of location, size and shape of the tumor were discussed in their work.

1.4. Summary

With an introduction to the broad area of the proposed work, various studies done till date have been reviewed. It is observed from the study that, though the PBHE is based on simplifying assumptions, it provides correct estimation for many cases. The PBHE has been used by many researchers in detection of cancer using various techniques. However, there still remains the scope for further work. Subsequent chapters deal with the problem statement and the geometry under consideration.

CHAPTER 2

PROBLEM STATEMENTS AND GEOMETRY

"Cancer" - a life threatening disease of current time, is spreading like a pandemic. These days, due to increasing adoption of unhealthy behaviors and lifestyles, cancer is showing its presence more frequently. Ancient Egyptians were the first one to note the disease, more than 3,500 years ago. Their descriptions include, "bulging tumors of the breast that has no cure" (Rayter and Mansi, 2003). Cancer is a condition in which growth of tissues becomes uncontrollable due to internal or external factors, forming a tumor. All parts of a human body are vulnerable to this disease. And once it affects, it has the tendency to spread, making condition worse for the patient. Thus, cancer in any form remains the cause of worry for everyone. Even today, we do not have a sure shot way to cure this disease.

Prognosis and survival rate of any cancer including breast cancer vary depending on its type, stage and geographical location of the patient. In western countries, the survival rates are high. More than 8 out of 10 women in England diagnosed with breast cancer survive for at least 5 years (World Cancer Report 2008). This number is lower for the developing countries. The above statistics indicates the volume of research work needed for the diagnosis and the treatment of a breast cancer.

2.1. Motivation for the Proposed Work

Towards the treatment of any disease, the diagnosis plays a vital role. Better the diagnosis better is the treatment. And, in case of a cancer, there is nothing better than an early diagnosis. For the disease like cancer, the available conventional diagnostic methods like X-ray, CT scan, MRI, mammography etc., are although effective, but they come with high operational cost, radiation hazard, complexity and cumbersome use (Byrns et al., 2000). As per the National Institutes of Health, in the year 2010 in the USA, the overall cost on cancer was $263.8 billion. Thus, research is needed to develop a simple and less expensive diagnostic procedure without any side effect. The proposed work focuses on potential application of one such procedure. Consideration is given to the estimation of the nature of the tumor in a biological tissue.

Any malignancy in a tissue leads to abnormal characteristics and behaviors. All the tissues in a human body at a particular condition have its own thermal signatures. A slight variation in its condition, changes these signatures. It is very much true for a cancerous tissue. Temperature profile in a cancerous tissue is different from a healthy tissue. Measurement of the changed thermal signals, such as the temperature profiles, temporal transmittance and reflectance signals can be a helpful tool in estimation of the presence of any abnormality in a tissue. The degree of abnormality, its location and size yield a specific thermal signal. Thus, its measurement in an indirect way may reveal various attributes of the abnormality in the tissue. The proposed work consists of the usage of the PBHE on a human breast, and simultaneous estimation of various parameters associated with a tumor using inverse analysis.

Numerical estimation of thermo-physical properties by solving the governing equation may lead to reach the key of the defined problems. It requires a well-defined geometry of the tissue and the considered conditions, to which the tissue is subjected. Keeping in mind, the complexity of the actual scenario, attempt has been made with 1-D and 2-D rectangular geometry of tissue first, and then the work is extended to a realistic 3-D geometry. The details of the considered geometry along with problems are described in the following sections.

2.2. Problem Statements and Roadmap

The main motive of the present work is to non-invasively detect inhomogeneity inside a tissue. The inhomogeneity may be in the form of a benign or a cancerous tumor. For the present study, cancerous tumors are taken into account, and the work has been divided into well-defined problems. For the problems considered, the defined roadmap is as follows:

I. To develop and validate solver for thermal analysis of a tissue using the PBHE for 1-D and 2-D rectangular geometry.
II. Simulation of a cancerous tumor inside the tissue, and to generate surface temperature profiles for 2-D rectangular tissue geometry of the human breast.
III. To analyze inversely, the surface temperature profiles of the 2-D tissue for simultaneous estimation of the thermal properties, the location and the size of the embedded tumor.
IV. To design and develop an algorithm for inverse analysis of a cancerous tumor in a 2-D semicircular section of a breast.
V. To validate and extend the work to a 3-D realistic numerical model.
VI. To establish an equivalence of PBHE and Wulff continuum model (WCM) to relate blood perfusion rate and mean blood velocity.

2.3. Geometry

Consideration is given to a simple 1-D planar and 2-D rectangular geometry of a tissue as shown in Fig. 2.1. The 1-D homogeneous domain of tissue of length L (Fig. 2.1a) is considered along the depth of the tissue. Figure 2.1a shows isothermal condition $\left(T = T_L\right)$ at right boundary $\left(x = L\right)$ and adiabatic $\left(\left.\frac{\partial T}{\partial x}\right|_{x=0} = 0\right)$ at the left $\left(x = 0\right)$ boundary of the 1-D domain. Depending upon the problems considered, these boundary conditions are different.

For the 2-D the geometry, the schematic is shown in Fig. 2.1b. The dimensions of the homogenous medium of tissue are $2L \times L$. The bottom or south boundary

$(0 \le x \le 2L, y = 0)$ of the domain, being at core body temperature is considered isothermal $(T = T_a)$. The top or the north boundary $(0 \le x \le 2L, y = L)$ is considered to be the skin surface, and is exposed to the convective boundary condition $\left(-k\left.\frac{\partial T}{\partial y}\right|_{y=L} = h(T - T_\infty)\right)$. Considering no change in thermal condition across the east $(x = L, 0 \le y \le L)$ and the west $(x = 0, 0 \le y \le L)$ boundaries of the tissue, it is made adiabatic $\left(\left.\frac{\partial T}{\partial y}\right|_{x=0,\ x=L} = 0\right)$. An inhomogeneity in the form of a 2-D square tumor of size $L_t \times L_t$ is imbedded in the tissue at a depth of $(L - \mathrm{Y})$ on the line of symmetry.

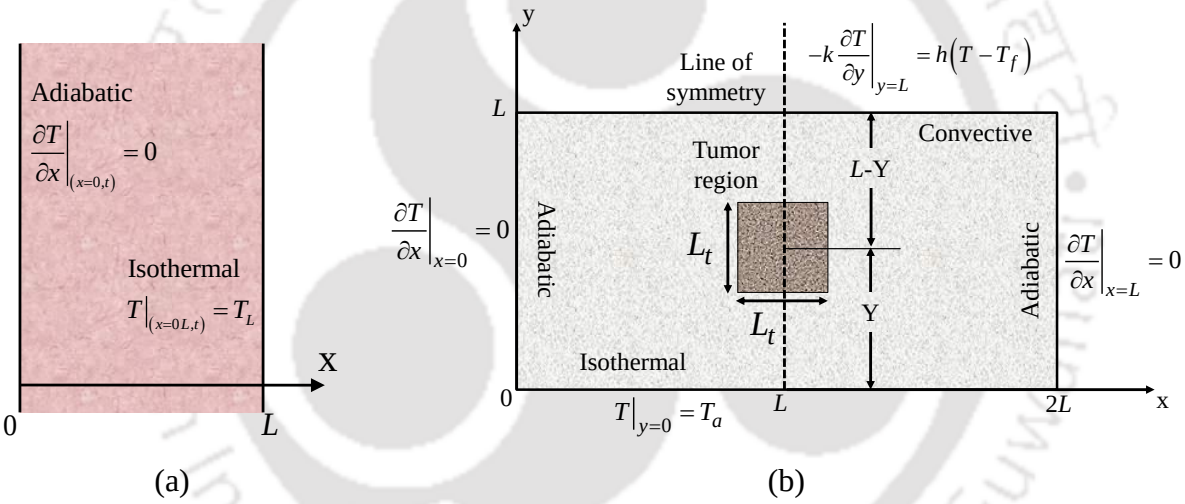

Figure 2.1 Schematics of (a) 1-D and (b) 2-D geometry of tissue.

A breast is a female mammary gland. A schematic of the same embedded with a tumor is shown in Fig. 2.2a. Consideration is given to a simplified 3-D hemispherical model of the breast of radius R with a tumor of radius r_t present in it (Fig. 2.2b), at a radial location r_o. In order to simulate a realistic condition, the skin surface (R, ϕ, θ) of the breast is exposed to a convective condition $\left(-\left(\hat{n} \cdot k \nabla T|_{r=R}\right) = h\left(T - T_f\right)\right)$ at room temperature T_f, where $\hat{n}$ is the outward normal, k is thermal conductivity of the skin and h is the heat transfer coefficient. The base of the hemisphere or the core body $(r, \phi = 0 \text{ and } \pi, \theta = 0 \text{ and } \pi)$ is at adiabatic condition $(\hat{n} \cdot \nabla T = 0)$. A 3-D hemispherical

model can be reduced to its 2-D semicircular section of the breast. Consideration is given to the breast contained in the 2-D *xy*-plane (Fig. 2.2c). Being far away from the skin surface, the base of the semicircle $(r, \phi = 0 \text{ and } \pi)$ and the hemisphere $(r, \phi = 0 \text{ and } \pi, \theta = 0 \text{ and } \pi)$ is considered to be at adiabatic $(\hat{n} \cdot \nabla T = 0)$, while the skin surface $(r = R)$ is exposed to a convective environment $\left(-\left(\hat{n} \cdot k \nabla T\big|_{r=R}\right) = h\left(T - T_f\right)\right)$. Realistic values of thermo-physical properties are considered for all the cases of the study.

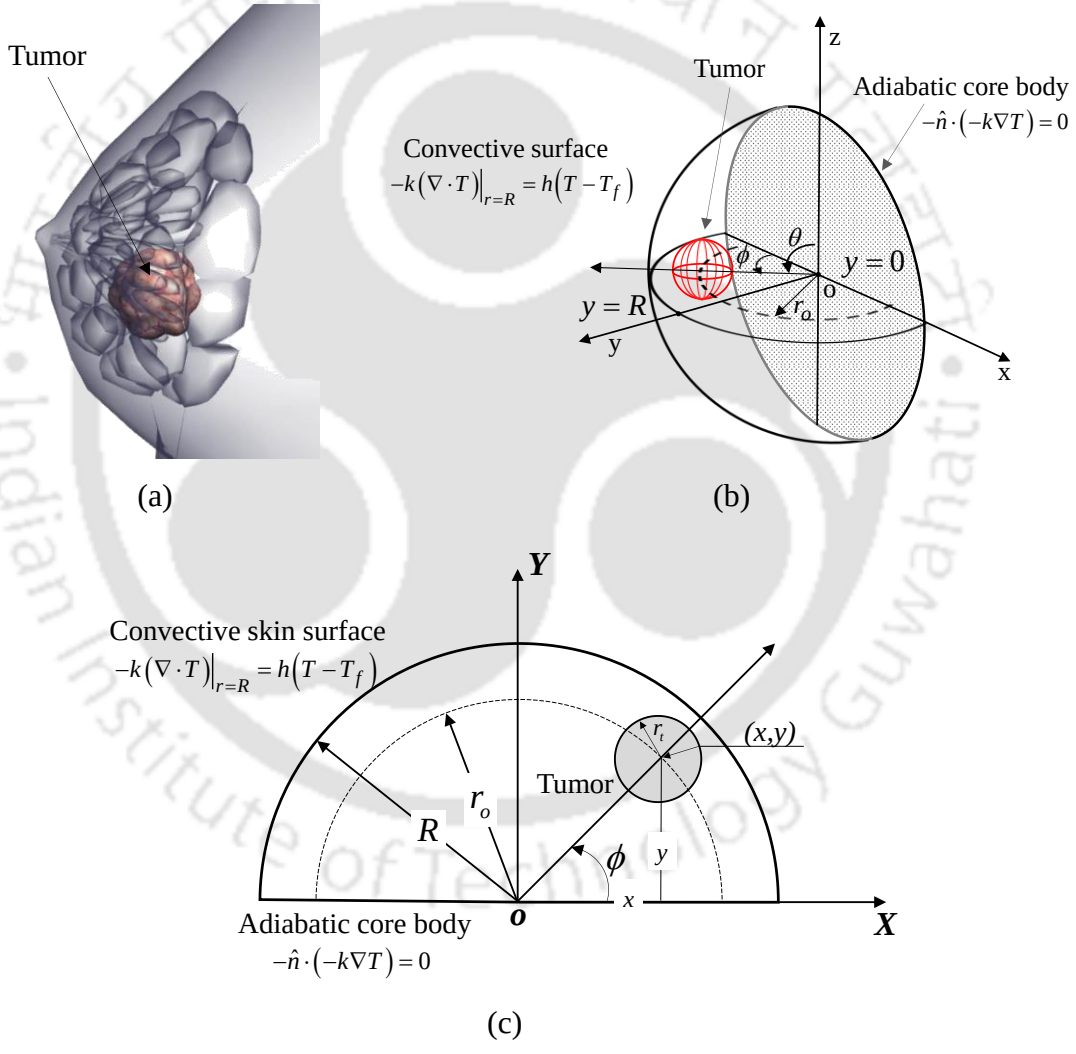

Figure 2.2 Schematic of (a) human breast affected by a malignant tumor (b) 3-D model of hemispherical human breast and its simplified representation in the form of (c) 2-D semicircular planar tissue with tumor.

2.4. Summary

This work is an effort to demonstrate that the thermal means can also be used as a potential diagnosis tool for cancer detection. Hence, a 2-D rectangular, a 2-D semicircular and a 3-D hemispherical geometry are considered for the current study and these are described in this chapter. The problems that are solved during the work are also discussed in detail. The main motive of the work is to retrieve different attribute related to a cancerous tumor situated inside a tissue. For the same, PBHE is solved. Genetic algorithm (GA) and a proposed method based on curve fitting are employed for the inverse analysis. These are discussed in subsequent chapters.

CHAPTER

3

METHODOLOGY AND FORMULATIONS

Nothing is devoid of temperature. Everything in this universe has some finite temperature. Temperature quantifies the thermal energy content of a body. Temperature difference between two bodies is responsible for flow of thermal energy by means of conduction and/or convection and/or radiation. Apart from the initial thermal condition and the boundary conditions, thermal field in any system depends on its thermophysical and optical properties. In order to understand the thermal response of a system, following the conservation principles, the physical problem is represented in mathematical forms. For a given geometry, its solution provides the knowledge about the influences of thermophysical and optical properties, and initial and boundary conditions on spatial and temporal temperature and heat flux distributions. In the present work, following the PBHE and the WCM, relations between the temperature gradient and the heat flux is utilized to analyze a biological system.

The physical quantity, heat flow rate Q, according to thermodynamics, is recognized at the boundary of a system. It is the quantity which flows normal to an isothermal surface, and being a vector quantity, can be resolved along the coordinate directions. The relation between the heat flux $q\left(=Q/A\right)$ and the temperature gradient ∇T is called the constitutive relation of heat flux, which is given by Fourier's law heat conduction. The bioheat equation is a modified form of the heat conduction equation with heat generation

term to account for the metabolic heat generation rate and blood perfusion. In this chapter, with background of a heat conduction heat equation based on Fourier's law, PBHE and WCM are discussed.

3.1. Fourier's Law of Heat Conduction

Fourier's law is the first constitutive relation of heat flux proposed by Joseph Fourier in 1807 based on his experimental investigation (Wang, 1994). For a homogeneous isotropic medium, Fourier's law of heat conduction is given by

$$q(r,t) = -k\nabla T(r,t) \tag{3.1}$$

where r is the coordinate point in the material, t is the time, T is the temperature and k is the thermal conductivity of the material, which depends on temperature and pressure (Cengel and Boles, 2006). In many engineering applications, thermal conductivity k is taken to be constant, because its variations with pressure and temperature are normally sufficiently small. The value of k is material dependent. The ∇ operator in Cartesian and spherical coordinate systems are given by

$$\nabla = \hat{i}\frac{\partial}{\partial x} + \hat{j}\frac{\partial}{\partial y} + \hat{k}\frac{\partial}{\partial z} \tag{3.2a}$$

$$\nabla = \hat{r}\frac{\partial}{\partial r} + \hat{\theta}\frac{1}{r}\frac{\partial}{\partial \theta} + \hat{\phi}\frac{1}{r\sin\theta}\frac{\partial}{\partial \phi} \tag{3.2b}$$

Applying conservation of energy principle for a small element of a material and combining it with Fourier's law of heat conduction, the coordinate independent form of the energy equation is given by

$$\rho c_p \frac{\partial T}{\partial t} = k\nabla^2 T + \dot{Q}_g \tag{3.3}$$

where $\dot{Q}_g$ is the volumetric heat generation rate.

Dividing both sides of Eq. (3.3) by k, we have,

$$\frac{1}{\alpha}\frac{\partial T}{\partial t} = \nabla^2 T + \frac{\dot{Q}_g}{k} \tag{3.4}$$

where $\alpha = \frac{k}{\rho c_p}$, and is the thermal diffusivity of the material. In Eqs. (3.3) and (3.4), ∇^2 in Cartesian system is given by

$$\nabla^2 = \frac{\partial}{\partial x^2} + \frac{\partial}{\partial y^2} + \frac{\partial}{\partial z^2} \tag{3.5}$$

Heat is the flow of energy through a medium due to temperature difference. i.e., temperature gradient is the cause of heat transfer (effect). In real practice, there is always a finite delay between the occurrence of cause and its effect. But, Fourier's law (Eq. 3.1) shows no time lag between the cause and the effect. It says that, the moment when temperature gradient appears, the disturbance in the system instantly propagates in all direction with infinite speed, which is not true in actual practice. Although, it is physically unrealistic, it has been confirmed from experiments, that the Fourier's law of heat conduction holds good for many media under usual range of heat flux and temperature gradient. In the present work, heat transfer by conduction is governed by Fourier's law (Eq. 3.1).

3.2. Bioheat Transfer

Bioheat transfer refers to the heat transfer in a biological system due to various metabolic activities, environmental conditions and flow of blood inside it. In the last decade, there were many contributions in the area of bioheat transfer. Application of hyperthermia to cancer treatment is a huge success. It lead to intense study of heat transfer inside a living tissue by the scientific and engineering community.

The experimental study by Bernard in 1876 is the beginning of heat transfer analysis in a living tissue due to blood flow (Cho, 1992). Since that time, development of mathematical model of thermal interaction inside a blood perfused tissue has been an area of interest for many researchers. The first continuum model on bioheat transfer in a blood perfused tissue was proposed by Pennes in 1948. Since then, scientists and researchers have proposed numerous bioheat models; and experiments were carried away to check

the validaty of these models (Bhowmik et al., 2013). Pennes bioheat equation is the first most widely used model in the area of bioheat transfer, and most of the models that evolved later, are more or less based on it.

Bioheat transfer is a very complex phenomenon. The complexity arises due to variable thermal properties, anisotropy in the tissue geometry and flow of blood, presence of lymphatic system, complex vascular architecture, etc. Moreover, the presence of the thermoregulatory mechanism of the living tissue makes the system even more complicated to analyze.

3.2.1. Pennes bio-heat equation

Heat transfer modeling in biological tissues is difficult due to convective effects of the blood flow. Among existing bioheat models, that of Pennes is widely used mathematical model. This is a continuum model in which the effects of the blood flow are treated as a temperature dependent heat source term. It has been proved that the PBHE is valid for a region far from large blood vessels (Bellil and Bennaoum, 2013). In a generalized form, the PBHE is given by (Zhang, 2008),

$$\rho c_{\mathrm{p}} \frac{\partial T}{\partial t} = k\nabla^2 T + \eta_{\mathrm{b}} \rho_{\mathrm{b}} c_{\mathrm{pb}} (T_{\mathrm{a}} - T) + Q_{\mathrm{m}} \tag{3.6}$$

where T is the temperature, t is the time; k, ρ and c_{p} are the thermal conductivity, the density and the specific heat of the tissue, respectively; ρ_{b} and c_{pb} are the density and the specific heat of the blood; η_b and Q_m are the blood perfusion and the metabolic heat generation rate of the tissue, and T_{a} is the temperature of the artery. In this equation, perfusion term (the second term on the right-hand-side of Eq. (3.6)) is considered as the heat source proportional to the temperature difference between the artery and the local tissue.

Equation (3.6) can be written as,

$$\rho c_{\mathrm{p}} \frac{\partial T}{\partial t} = k\nabla^2 T + \dot{Q}_g \tag{3.7}$$

where generalized source term $\dot{Q}_g$ and effective local heat source temperature T_e are defined as,

$$\dot{Q}_g = \eta_b \rho_b c_{pb} (T_e - T) \tag{3.8}$$

$$T_e = T_a + \frac{Q_m}{\rho_b \eta_b c_{pb}} \tag{3.9}$$

Using the solution of Eq. (3.7), the distribution of temperature in a blood perfused tissue can be estimated.

3.2.2. Wulff continuum model

In the year 1974, with an attempt to relax the assumptions of Pennes, Wulff (1974) proposed an alternate bioheat model called Wulff Continuum Model. Instead of blood perfusion rate η_b, consideration was given to blood velocity v in the tissue. With T as the temperature, t as the time; k, ρ and c_p as the thermal conductivity, the density and the specific heat of the tissue, respectively; ρ_b and c_{pb} as the density and the specific heat of the blood, and Q_m as the metabolic heat generation of the tissue, mathematically, the WCM can be expressed as,

$$k\nabla^2 T - \rho_b c_{pb} v \nabla T + Q_m = \rho c_p \frac{\partial T}{\partial t} \tag{3.10}$$

Apart from the common thermo-physical properties of tissue, in the PBHE (Eq. 3.6) and WCM (Eq. 3.10), the blood perfusion rate η_b is the governing parameter for the solution of Eq. (3.6), whereas the blood velocity v is required for the solution of Eq. (3.10).

3.3. Normalized Form of Governing Bioheat Equations

For generality, solutions of the bioheat models given by Eq. (3.6) and (3.10), for the problem statement VI: Equivalence of PBHE and WCM (section 2.2), needs normalization; which has been performed using the following non-dimensional parameters for length, time and temperature, respectively.

$$X = \frac{x}{L} \qquad \tau = \frac{\alpha t}{L^2} \qquad \theta = \frac{T - T_a}{T_f - T_a}$$

The normalized form of the PBHE and the WCM for a 1-D geometry are given by Eqs. (3.11) and (3.12), respectively

$$\frac{\partial \theta}{\partial \tau} = \frac{\partial^2 \theta}{\partial X^2} - A_p \theta + B_p \tag{3.11}$$

$$\frac{\partial \theta}{\partial \tau} = \frac{\partial^2 \theta}{\partial X^2} - A_w \frac{\partial \theta}{\partial X} + B_w \tag{3.12}$$

where in Eqs. (3.11) and (3.12), the non-dimensional coefficients A_p, A_w, B_p and B_w are the following:

$$A_p = \frac{\eta_b \rho_b c_{pb} L^2}{k} \tag{3.13}$$

$$A_w = \frac{\rho_b c_{pb} V L}{k} \tag{3.14}$$

$$B_p = B_w = \frac{Q_m L^2}{k\left(T_f - T_a\right)} \tag{3.15}$$

In the present work, Eqs. (3.6), (3.10), (3.11) and (3.12) are solved numerically for the SS condition to obtain temperature distribution in a tissue. In the numerical solution, the approach of the FVM (Versteeg and Malalasekera, 1995) is followed.

3.4. Finite Volume Method

In the thermal analysis of biological tissues, Eqs. (3.6) and (3.10) are numerically solved using the FVM (Versteeg and Malalasekera, 1995) for 1-D and 2-D planar tissue for various conditions. For the case of a 2-D tissue, in the FVM approach, Eq. (3.6) is first integrated over the discrete time Δt and the control volume $\Delta V = \Delta x \times \Delta y$.

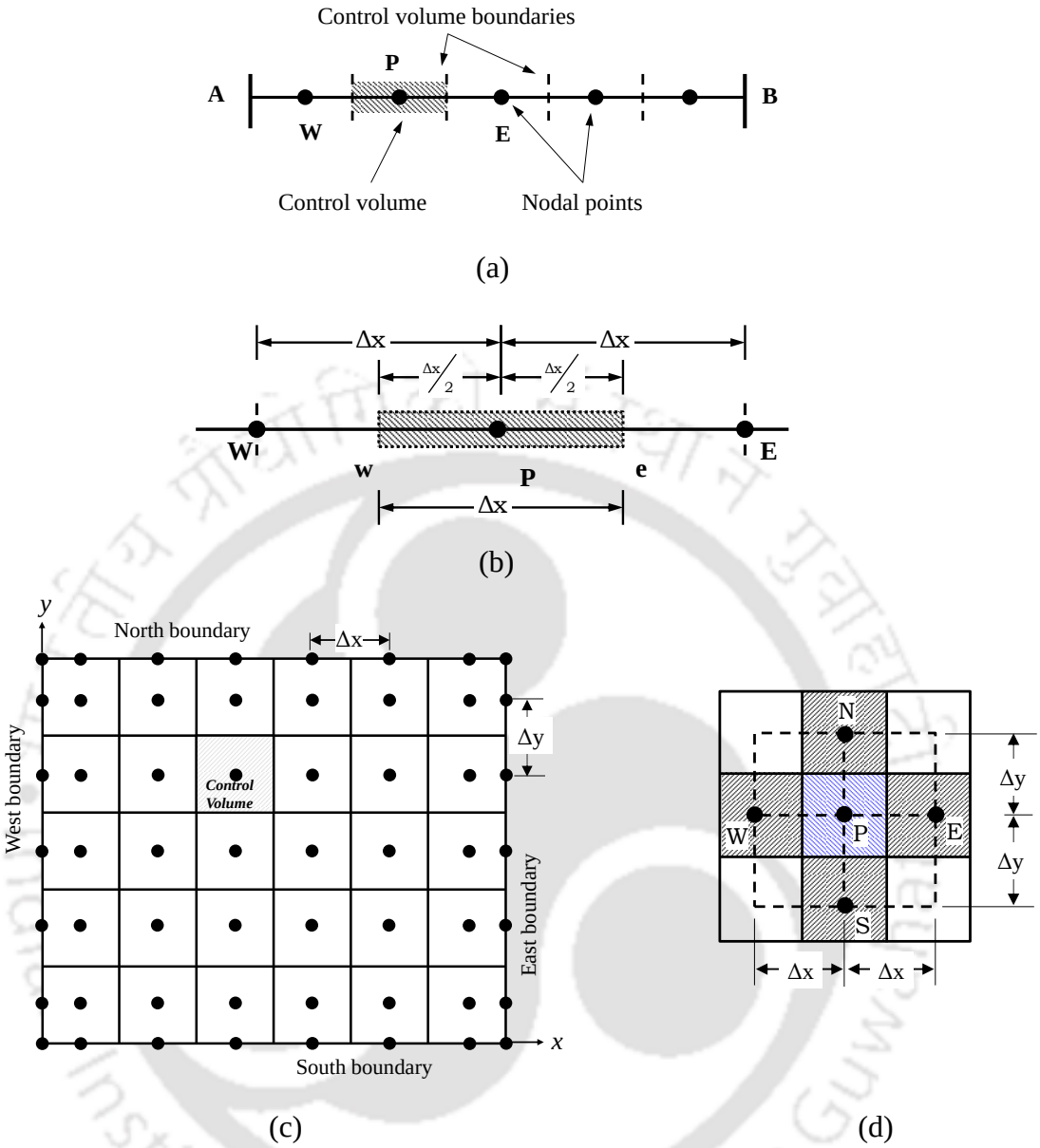

Figure 3.1 Schematics of (a) the 1-D and (b) the 2-D discretized solution space with nomenclatures of the control volume nodal points and description of the (c) 1-D and (d) 2-D FVM control volume.

$$\int_t^{t+\Delta t}\left(\int_{\Delta V}\rho c_p\frac{\partial T}{\partial t}dV\right)dt=\int_t^{t+\Delta t}\left(\int_{\Delta V}\frac{\partial\left(k\frac{\partial T}{\partial x}\right)}{\partial x}dV\right)dt+\int_t^{t+\Delta t}\left(\int_{\Delta V}\frac{\partial\left(k\frac{\partial T}{\partial y}\right)}{\partial y}dV\right)dt$$
$$+\int_t^{t+\Delta t}\left(\int_{\Delta V}\left(\eta_b\rho_b c_{pb}\left(T_a-T\right)+Q_m\right)dV\right)dt \qquad (3.16)$$

With reference to Figs. 3.1a-d, in discrete form, Eq. (3.16) is written as

$$T_P^{n+1} = T_P^n + \frac{\Delta t\, k}{\rho c_p (\Delta x)^2}\left(T_E^n - 2T_P^n + T_W^n\right) + \frac{\Delta t\, k}{\rho c_p (\Delta y)^2}\left(T_N^n - 2T_P^n + T_S^n\right) + \frac{\Delta t}{\rho c_p}\left[\eta_b \rho_b c_{pb}\left(T_a^n - T_P^n\right) + Q_m\right] \tag{3.17}$$

where temperature T with suffix P is the volume averaged value at the center of the discrete control volume (Fig. 3.1d), and those with suffixes *E*, *W*, *N* and *S* are the same at its east, west, north and south neighboring nodes. In Eq. (3.17), n represents the time level. The used scheme in the above discretization is an explicit one, the stability criterion for the same is

$$\Delta t \le \left[\frac{2\alpha}{(\Delta x)^2} + \frac{2\alpha}{(\Delta y)^2} + \eta_b \frac{\rho_b c_{pb}}{\rho c_p}\right]^{-1} \tag{3.18}$$

For the case of 1-D geometry (Fig. 3.1a), when the equivalence of two bioheat models are considered, Eq. (3.11) and (3.12) are discretized for the solution space as shown in Figs. 3.1a and 3.1b using the FVM approach. For numerical solution of both the bioheat equations, consideration is given to discretization of non-dimensional form of governing equations (Eq. 3.11 and 3.12). Following the procedure of the FVM, integrating the Eq. (3.11) and (3.12) over normalized discrete time and discrete space, $\Delta\tau$ and $\Delta\overline{V}(=\Delta X)$, respectively, we get,

PBHE, $$\theta_P^{n+1} = \theta_P^n + (\Delta\tau)\frac{\theta_E^n - 2\theta_P^n + \theta_W^n}{(\Delta X)^2} - \Delta\tau A_p \theta_P^n + \Delta\tau B_p \tag{3.19}$$

WCM, $$\theta_P^{n+1} = \theta_P^n + (\Delta\tau)\frac{\theta_E^n - 2\theta_P^n + \theta_W^n}{(\Delta X)^2} - \Delta\tau A_w \frac{\theta_E^n - \theta_W^n}{(2\Delta X)} + \Delta\tau B_w \tag{3.20}$$

Before development of the solvers for the discretized equations (Eq. 3.19 and 3.20), the stability criteria are evaluated and the obtained condition for the PBHE (Eq. 3.19) and WCM (Eq. 3.20), respectively, are $\Delta\tau \le \left(\frac{2}{(\Delta X)^2} + A_p\right)^{-1}$ and $\Delta\tau \le \frac{(\Delta X)^2}{2}$.

3.5. Finite Element Method

Consideration of a human breast in the form of a semicircular and a hemispherical geometry requires discretization of the solution space using triangular (Fig. 3.2a) or tetrahedral (Fig. 3.2b) grid elements. Finite element method is used in such cases to solve the governing bioheat models (Eqs. 3.6 and 3.10). COMSOL 4.3a, the FEM based commercial solver is used in the present cases. Considering a circular and a spherical tumor in 2-D and 3-D models of the breast, temperature distribution inside the computational domain is obtained. A tumor in a breast can be characterized using the size, the depth and the angular positions. With an aim to estimate these attributes of the malignancy (tumor), the circumferential skin surface temperature of the breast is analyzed. Inverse analysis is performed using the skin surface temperature of the breast. Numerical tools like GA and a newly proposed curve fitting method (CFM) is utilized in the present study. The details are discussed in the subsequent sections.

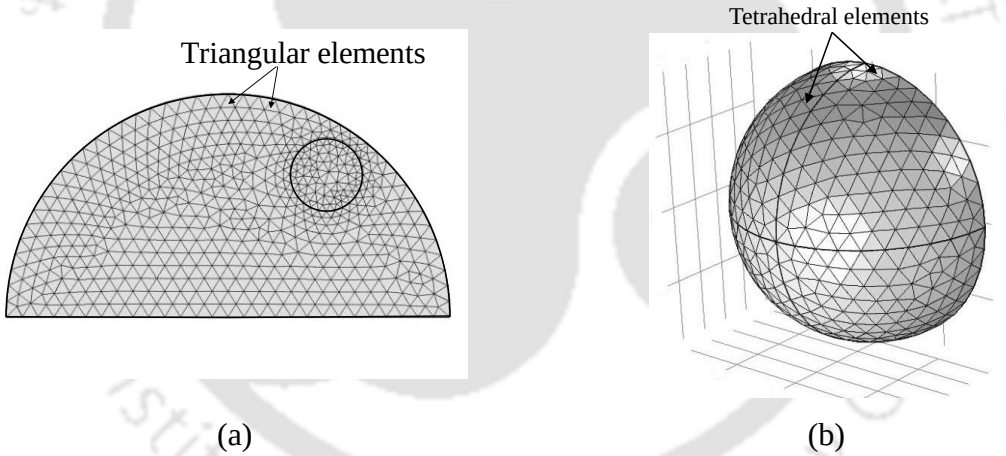

Figure 3.2 Schematics of the (a) 2-D and (b) 3-D FEM discretized solution space.

3.6. Inverse Analysis

An inverse heat transfer problem is one in which on the basis of the known temperature and/or heat flux distributions, thermophysical and/or optical properties and/or initial or boundary conditions that provided the temperature and/or heat flux distributions are estimated using an optimization tool. In the present work, skin surface temperature profiles of a human breast are optimized to retrieve the size and the location of a tumor, if present. The GA is utilized for

simple cases like 2-D rectangular domain of the tissue. The GA has been found computationally expensive, and therefore a method based on curve fitting has been proposed. The method (CFM) has been found applicable to 2-D semicircular and 3-D hemispherical geometry too. The details are as follows.

3.6.1. Genetic algorithm

Subjected to the initial and the boundary conditions stated in section 2.3, with thermo-physical properties known, solution of Eq. (3.6) yields the temperature distribution in the tissue. In the present work, with the temperature of the top surface of the breast tissue, i.e., the outer layer of the skin known through measurement, estimation is done to ascertain the presence of a tumor. This requires inverse analysis and thus minimization of an objective function. For the problem under consideration, the objective function is given by

$$J = \sum_{i=1}^{N_x} \left(T_{i,N_y}^{\text{ref}} - T_{i,N_y} \right)^2 \tag{3.21}$$

where T_{i,N_y}^{ref} is the temperature of the surface (x, L) of the breast skin obtained from any high precision temperature measurement technique. In the present work, to demonstrate the feasibility of the approach, it is the temperature obtained from the solution of Eq. (3.6). In Eq. (3.21), T_{i,N_y} is the temperature obtained using the process of optimization. This also requires solution of Eq. (3.6) using the evolving values of the estimated parameters. The optimization starts with some guess values of the estimated parameters from the assigned ranges. The process continues until the desired accuracy is obtained.

Among the available optimization methods, genetic algorithm (GA) has found wide applications in science and engineering (Das et al., 2008; Golovkin et al., 2002; Das et al., 2009). It is a population-based stochastic technique which works like Darwin's principle of natural selection. In the present work, the objective function (Eq. 3.21) has been optimized using the GA. A brief description of the GA with its schematic (Fig. 3.3) is given below.

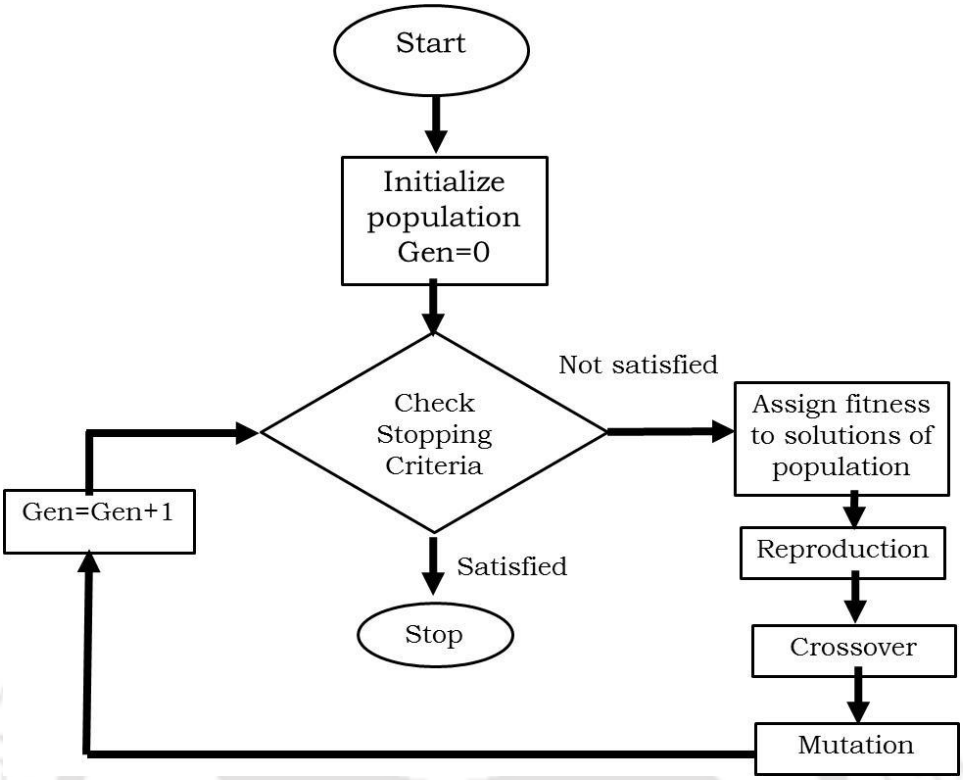

Figure 3.3 Flow chart showing optimization steps in GA.

The GA is an iterative tool. It successively geneates and refines the population like the biological evolution of any species in which successive generations are conceived, born and raised until they themselves are ready for reproduction. The reproduction starts after the fitness of the population is evaluated. In the next generation, population with good fitness is replicated. Crossover starts next, in which pairs from new strings mate to produce new offsprings. In order to capture the global minima or maxima, the mutation is introduced in the population. This gives new generation. This process is repeated until the objective function/the fitness value reaches the desired value.Apart from optimization using an evolutionary algorithm, the present work also proposes an inverse algorithm based on curve fitting technique. With thermo-physical properties known, and the initial and the boundary conditions as stated, Eq. (3.6) is solved for breast tissue to obtain the SS temperature distribution, with and without a tumor. In the present work, the tissue has been considered to be a mathematically 2-D one and the spatial temperature profiles of the skin are obtained for different sizes and locations of the tumor. The similar temperature profiles are the basis of estimation of the size and locations of the tumor in the inverse analysis. A technique based on curve fitting is proposed from the observed spatial distribution of temperature.

3.6.2. Curve fitting technique

A breast in presence of tumor yields a temperature profile that is different from a normal tissue. In malignant condition, these thermal profiles are similar in nature for different locations and sizes of the tumor. With similarity of skin surface temperature profiles as the foundation, the size and the location of malignancy inside the breast is estimated in the current work. From the study of effect of various configurations of tumor in the breast, it has been observed that all the skin surface temperature profiles have Gaussian distribution. Considering T_o as the base temperature, w as the width, A as the amplitude and the $\bar{x}_c$ as the location of the peak, a general Gaussian temperature profile (Fig. 3.4) can be expressed as,

$$T = T_o + Ae^{-(x-\bar{x}_c)^2/2w^2} \tag{3.22}$$

For a particular size and location of the tumor inside the breast, uniqueness of the profiles has been observed. A study of the *Area* and amplitude *A* of the Gaussian temperature profiles reveals the uniqueness of the distribution. The value of the amplitude (*A*) and the *Area* under such profiles are found specific for a particular size $(r_t \text{ or } L_t)$ and location $(r_o \text{ or } \mathrm{Y})$ of a tumor. Hence, for a particular set of (r_t, r_o, θ, ϕ) or (L_t, Y) of tissue-tumor configuration, a unique set of $(A, Area)$ has been obtained. Taking into account this uniqueness, the proposed inverse methodology utilizes curve fitting in the current inverse method. The details of the algorithm are described in the subsequent chapters.

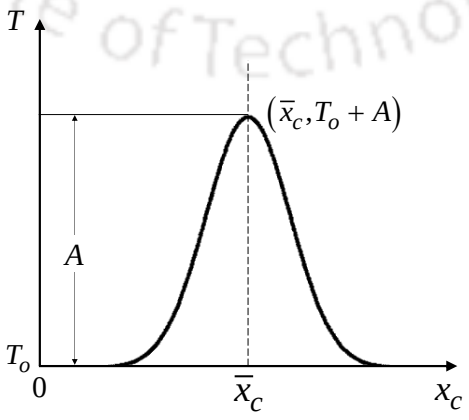

Figure 3.4 Schematic of a Gaussian distribution.

3.7. Summary

In this chapter, the formulations and the methodology used during the numerical analysis of a biological system are discussed in detail. PBHE which governs heat transfer in a biological tissue is considered and formulated using the FVM. It will help in studying the temperature profiles of tissues with different attributes of tumor located inside it. Inverse analysis of the obtained temperature profiles can be done using the GA, and a proposed method based on curve fitting to retrieve different parameters associated with tissues under normal and malignant conditions. Another bioheat model called WCM is also discussed under the formulations to develop a mathematical relation between blood velocity and blood perfusion rate.

CHAPTER 4

THERMAL MODELING OF A 2-D TISSUE

Following the formulations, numerical solution of the governing equations yields different thermal outputs of a tissue under the influence of various internal and external conditions. Prior to simulation of the defined problems, the developed solver is validated with the available literature.

4.1. Validation

4.1.1. Validation of the numerical solver

In the following, the formulation of the numerical scheme is validated by solving Eq. (3.6) for both 1-D planar (Fig. 3.1a) and 2-D rectangular (Fig. 3.1c) tissues with the results available in the literature (Zhang, 2008). Spatial temperature distributions at different instants for the 1-D planar tissue (Fig. 3.1a) with thickness L = 4.0 cm are compared with the results of Zhang (2008) (Fig. 4.1a). Due to the presence of metabolic generation of heat (Q_m) in the 1-D tissue, a higher initial value of temperature have been observed. With time, the thermal diffusion inside the tissue reduces the temperature along its length and after sometime, it reaches SS condition. For two grades of the centrally located tumor in a 2-D tissue (Fig. 3.1c), the SS temperature distributions on the skin surface (x, L) and along the centerline (L, y) are compared against the results of Zhang (2008) in Figs. 4.1b and 4.1c, respectively. For these validations, with L = 5 cm, a tissue

with boundary conditions as mentioned in previous chapter is considered. A tumor of size $\frac{L}{4}\times\frac{L}{4}$ is located at the center of the domain (Fig. 3.1c). The thermo-physical properties used are (Zhang, 2008): thermal conductivity $k=0.5\,\mathrm{Wm^{-1}K^{-1}}$, densities of the tissue and the blood $\rho=\rho_b=1052\,\mathrm{kg\cdot m^{-3}}$, the specific heats of the tissue and the blood, $c_p=c_{pb}=3800\,\mathrm{J\,kg^{-1}K^{-1}}$, for the normal tissue blood perfusion rate $\eta_b=1\times10^{-4}\,\mathrm{s^{-1}}$ and the metabolic heat generation rate, $Q_m=400\,\mathrm{W\,m^{-3}}$. Blood perfusion rate and the metabolic heat generation rates are: tumor I- $\left(\eta_b=1\times10^{-3}\,\mathrm{s^{-1}},Q_m=4000\,\mathrm{W\,m^{-3}}\right)$ and tumor II- $\left(\eta_b=1\times10^{-2}\,\mathrm{s^{-1}},Q_m=40000\,\mathrm{W\,m^{-3}}\right)$. Distributed volumetric heat source due to spatial heating Q_S is considered absent.

As the geometry (Fig. 3.1c) is symmetric about the line $x=L$, for the purpose of computation, consideration is given to the right hand part of it. The left hand boundary of the computational domain, hence have a symmetry boundary condition i.e., adiabatic. In order to obtain a grid independent solution, the computational domain $\left(L\le x\le 2L,0\le y\le L\right)$ is divided into 50×50 control volumes, with time step Δt as 0.01 sec. SS skin surface $\left(y=L\right)$ and centerline $\left(x=L\right)$ temperature distributions are compared against the results of Zhang (2008) in Figs. 4.1b and 4.1c, respectively obtained using the lattice Boltzmann method. The results are further compared against that obtained by solving the same problem using the FEM based-solver, COMSOL 4.3a. For the tissue, with and without tumors, temperature distributions (Fig. 4.1) obtained using the FVM and the FEM show a good match with the results of Zhang (2008). In the absence of the tumor, at the SS, temperature (27.77 °C) along the skin surface is constant (Fig. 4.1b), while, in the presence of a tumor, throughout the skin surface, temperature rises. Temperature rise is the maximum in the center $\left(L,L\right)$ of the skin, and it continuously decreases away from it.

Temperature rise at any location on the skin is more for the tumor II for which the blood perfusion rate and metabolic heat generation rates are higher than that for the tumor I. With increase in blood perfusion rate, more heat is taken away from the tumor region, and this causes reduction in temperature. On the other hand, with increase in metabolic

heat generation rate, more heat is generated, and this increases the temperature. As the tumor advances, the metabolic heat generation rate becomes very high, and it not only nullifies the effect of blood perfusion, but also contributes further to the temperature rise.

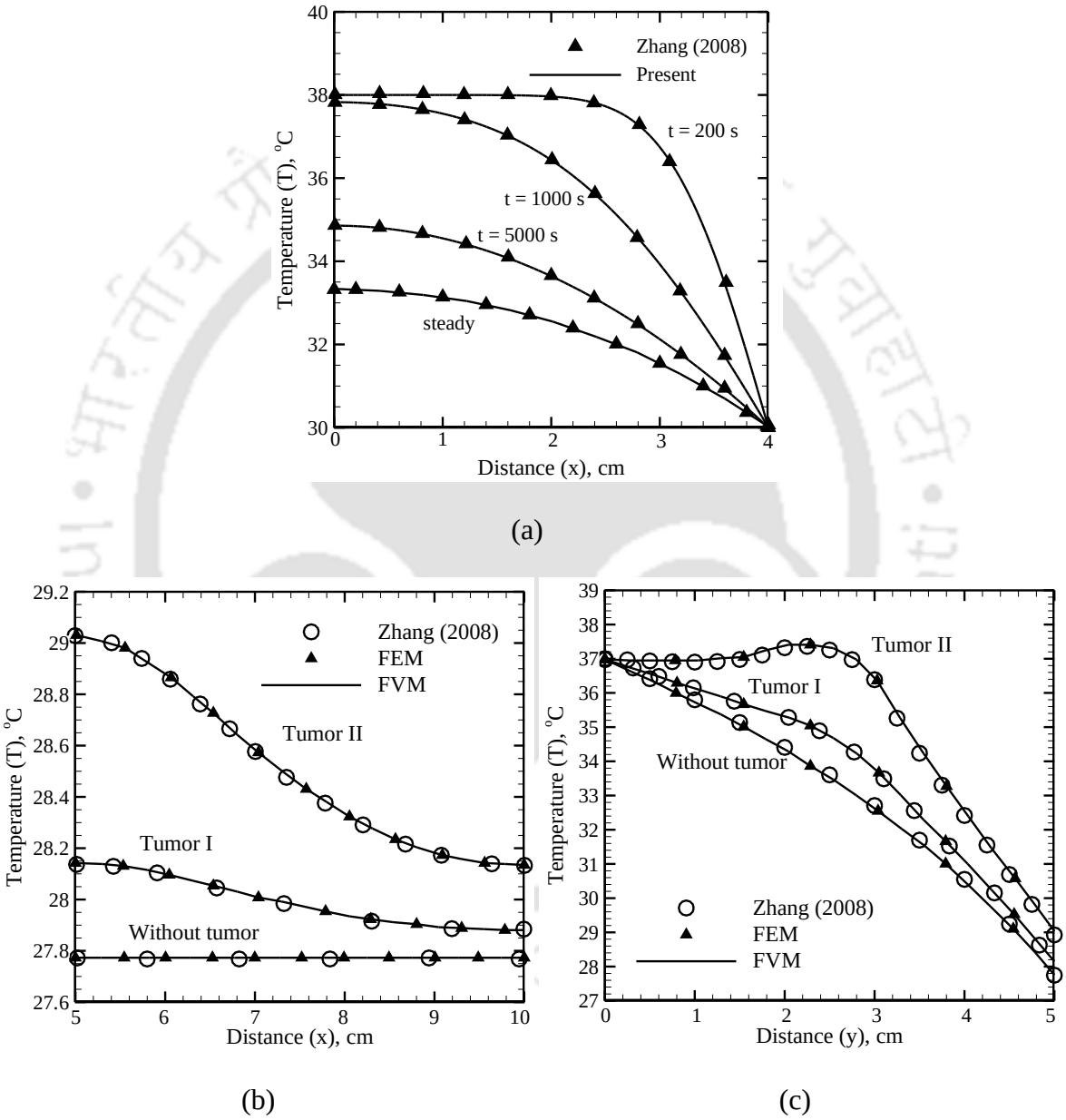

Figure 4.1 Comparison of (a) transient spatial distribution of temperature in 1-D tissue and SS temperature distribution in 2-D tissue along (b) the skin surface (x, L) and (c) the centerline (L, y) with Zhang (2008).

4.1.2. Equivalence of 2-D and 3-D numerical simulation of human breast

Consideration of a 2-D rectangular domain in the present work is a numerical simplification to a realistic 3-D human breast. In order to find out the extent of closeness of the simplification, a hemispherical model of the breast as shown in Fig. 4.2a is considered. The hemisphere of radius $r = 10.0$ cm is having a spherical tumor of radius (r_t) 1.5 cm, which is located at a depth of 5 cm from the skin along the negative *y*-direction (Fig. 4.2a). The two important properties of a living tissue, the blood perfusion rate (η_b) and metabolic heat generation rate (Q_m) are selected for the human breast from available literature, and considered as shown in Table 4.1.

For a healthy breast tissue, the blood perfusion rate and the metabolic heat generation rate are with reference to Gautherie (1980): $\eta_b = 0.92\times10^{-3}\,\mathrm{s}^{-1}$ and $Q_m = 450\,\mathrm{Wm}^{-3}$, respectively; while, in cancerous condition, the value of the blood perfusion rate lies in the range of $1.22\times10^{-3} - 14.5\times10^{-3}\,\mathrm{s}^{-1}$ with a mean of $4.9\times10^{-3}\,\mathrm{s}^{-1}$ (Gautherie, 1980). Other properties of the tissue and the blood taken are: thermal conductivity $k = 0.42\,\mathrm{Wm}^{-1}\,\mathrm{K}^{-1}$ density of the tissue $\rho = 920\,\mathrm{kg\,m}^{-3}$, density of the blood $\rho = 1052\,\mathrm{kg\,m}^{-3}$, specific heat of the tissue $c_p = 3000\,\mathrm{J\,kg}^{-1}\mathrm{K}^{-1}$, and the specific heat of the blood $c_p = 3800\,\mathrm{J\,kg}^{-1}\mathrm{K}^{-1}$ (Zhang, 2008). The flat surface ($xz-$plane) of the hemisphere is at isothermal core body temperature of 37°C, whereas the curved skin surface is exposed to a convective environment with $h = 20\,\mathrm{Wm}^{-2}\mathrm{K}^{-1}$ and $T_f = 20\,^{\circ}\mathrm{C}$. These core body and convective conditions are the same as that for the case considered for the validation (Fig. 4.1).

Table 4.1: Value of blood perfusion rate (η_b) and metabolic heat generation rate (Q_m) of human breast with reference to different literatures.

	Property	Gonz´alez (2007)	Gautherie (1980)
Normal tissue	Blood perfusion rate (η_b), s^{-1}	0.00018	0.92×10^{-3}
	Metabolic heat generation rate (Q_m), Wm^{-3}	450	———
Cancerous tissue	Blood perfusion rate (η_b), s^{-1}	0.009	$1.22\times10^{-3} - 14.5\times10^{-3}$
	Metabolic heat generation rate (Q_m), Wm^{-3}	29000	29000

The 2-D counterpart of the 3-D model (Fig. 4.2a) of the breast with a tumor is mathematically taken as a rectangular domain with a square shaped tumor (Fig. 4.2b). The 2-D domain is considered to be on the *xy*-plane (Fig. 4.2b) with a length of 10 cm and a width of 20 cm. *y*-axis is the line of symmetry. The spherical tumor is reduced to a 2-D square shaped tumor of size L_t located at 5 cm from the surface. Considering equal area covered by both the geometries of the tumor on the *xy*-plane, the value of L_t is found from the relation $L_t^2 = \pi r_t^2$.

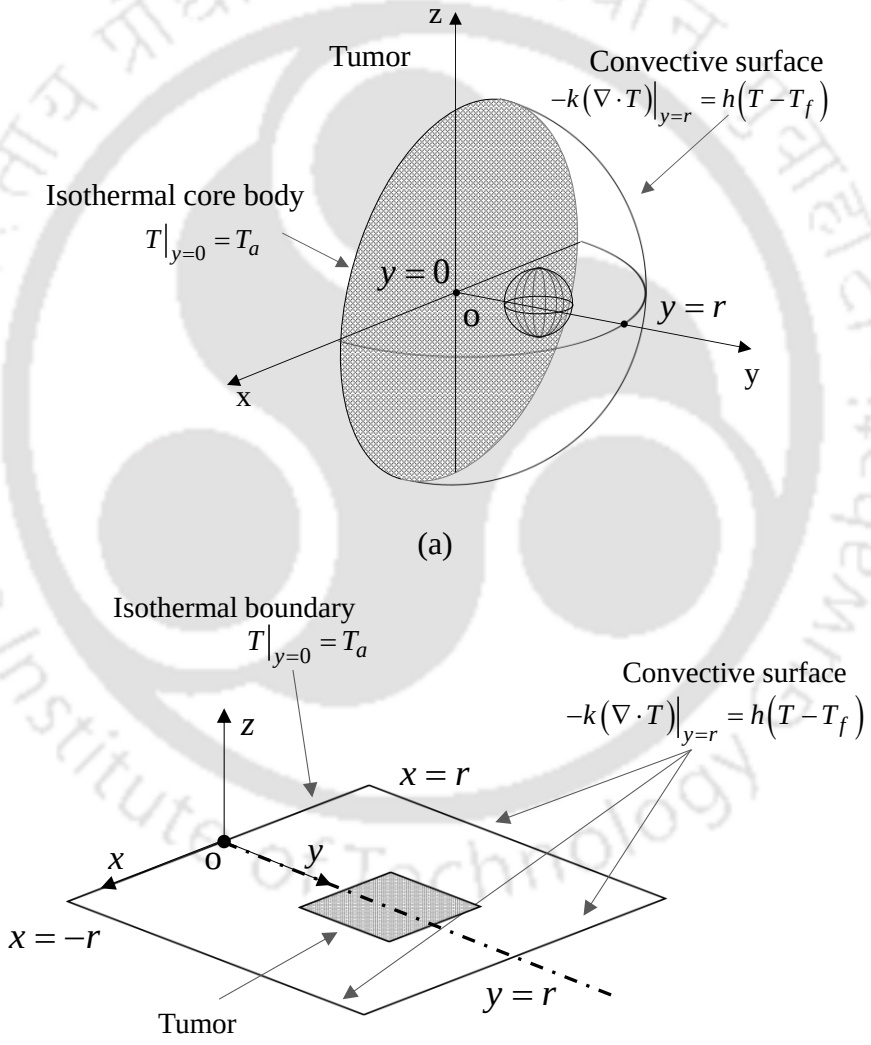

Figure 4.2 Schematic of (a) a 3-D hemispherical breast with an imbedded tumor and (b) a 2-D equivalent system of the 3-D model

The boundary of the 2-D domain lying over the *x*- axis is considered at isothermal condition of 37 °C, and all the three boundaries are kept at the same convective condition as that for the 3-D case. With all the system properties and the boundary conditions provided, PBHE is solved numerically using the FEM for the 3-D domain (Fig.4.2a), and the FVM is used for the 2-D domain (Fig.4.2b) of the breast tissue. Figure 4.3 shows the comparison of the SS temperature distribution along the *y*-axis in a breast tissue with and without tumor for 2-D and 3-D models. The results from the 3-D and the simplified 2-D models obtained using different methods compare exceedingly well, thus justifies the use of the simplified geometry. Hence, validation of the developed solver and the closeness of the simplified 2-D rectangular geometry with the 3-D one make it appropriate for application to the realistic breast.

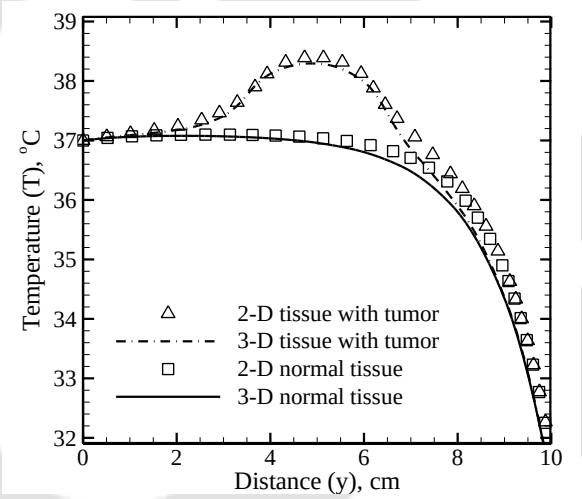

(c)

Figure 4.3 A comparison of SS centerline (L, y) temperature distribution for the breast with and without tumor

4.2. Thermal Analysis of a Tissue

4.2.1. Based on properties given by Gonz´alez (2007)

For a breast tissue of size $(5\,\text{cm}\times 10\,\text{cm})$, with and without malignancy, properties as given by Gonz´alez (2007) are considered, and a thermal analysis is done. With thermal conductivity, $k = 0.42\,\text{Wm}^{-1}\text{K}^{-1}$, density of the tissue, $\rho = 920\,\text{kg m}^{-3}$, and the specific

heat of the tissue, $c_p = 3000\,\mathrm{J\,kg^{-1}K^{-1}}$, the thermo-physical properties of blood are as considered earlier.

Surface temperature profiles with a tumor of size $\left(L/4 \times L/4\right)$ located at three different locations viz., bottom $\left(0.125L \le y \le 0.375L\right)$, middle $\left(0.375L \le y \le 0.625L\right)$ and top $\left(0.625L \le y \le 0.875L\right)$ are shown in Figs. 4.4a-c, respectively. Because of the symmetry, in the analysis, the tumor size is $\left(L/8 \times L/4\right) = 0.625\,\mathrm{cm} \times 1.25\,\mathrm{cm}$. An observation of Figs. 4.4a-c shows that surface temperature changes with the presence of a tumor.

The tumor at the top position gives the maximum temperature rise $\left(0.56\,^{\circ}\mathrm{C}\right)$ (Fig. 4.4a). These values for tumor located in the middle and at the bottom are 0.05°C and0.0075 °C, respectively. The observed temperature rise is attributed to increased blood perfusion rate $\eta_b = 0.009\,\mathrm{s^{-1}}$ and metabolic heat generation rates $Q_m = 29000\,\mathrm{Wm^{-3}}$ of the breast tumor. Tumor in a tissue is thermally a heat generation source, and skin surface temperature will thus as observed is maximum when it is located close to the top surface. After a tumor manifests, its size grows with time. Metabolic heat generation in a breast tumor is about 65 times more than that of the normal tissue, whereas the blood perfusion rate is 50 times more. Both these contribute to the net heat generation in the tumor. With increase in the size (volume) of the tumor, thus temperature will increase in the tissue. For three sizes, i.e., $\frac{L}{8} \times \frac{L}{4}, \frac{L}{8} \times \frac{L}{2}$, and $\frac{L}{8} \times \frac{3L}{8}$ of a centrally located tumor, surface temperature profiles are shown in Figs. 4.5a-c, respectively.

With *x*-length $\left(\frac{L}{8} = 1.25\,\mathrm{cm}\right)$ of the tumor unchanged, these thicknesses correspond to 1.25 cm, 2.5 cm and 3.75 cm, respectively. It is to be noted that size of a tumor in the breast can go up to 5.0 cm (Fisher et al., 1969). An observation of Figs. 4.5a-c shows that when the size of the tumor increases from $L/4$ to $3L/4$, the maximum skin surface temperature increases from 32.85ºC to 33.35ºC. Further, on the surface of the skin, in the vicinity of the tumor, temperature varies sharply (Figs. 4.5a-c).

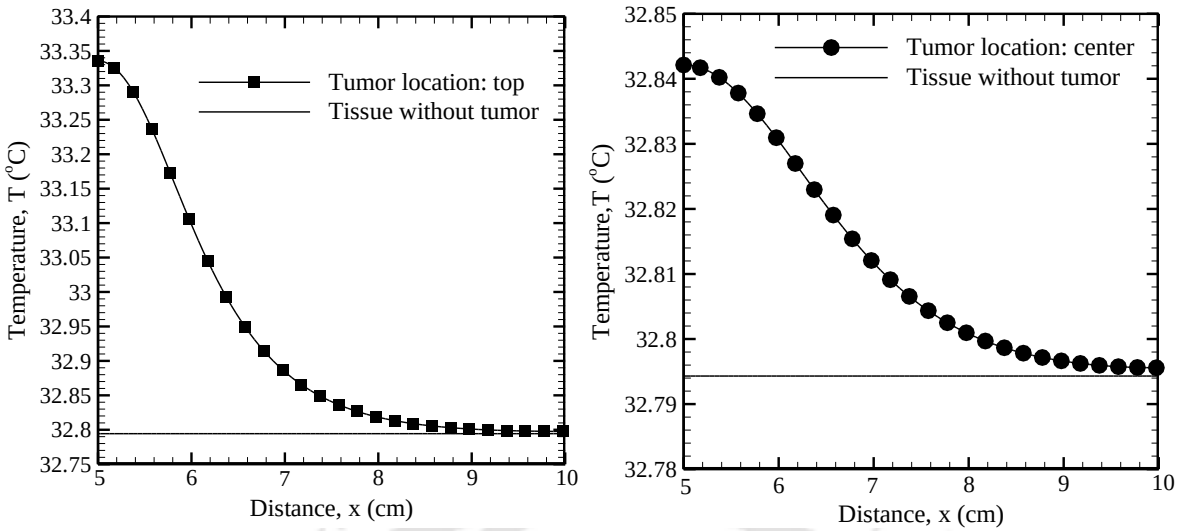

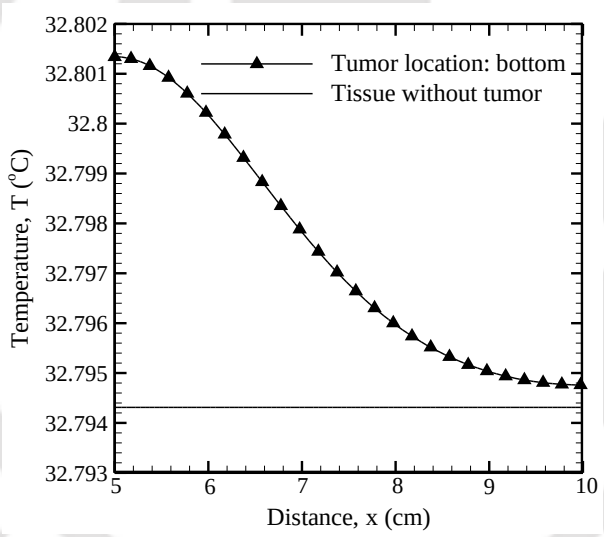

Figure 4.4 Steady-state temperature distributions along the skin surface (x, L) of the breast tissue imbedded with a tumor $(\text{size:}1.25\,\text{cm}\times 1.25\,\text{cm})$ at position (a) top: $(0.625L \le y \le 0.875L)$ (b) center: $(0.375L \le y \le 0.625L)$ and (c) bottom $(0.125L \le y \le 0.375L)$.

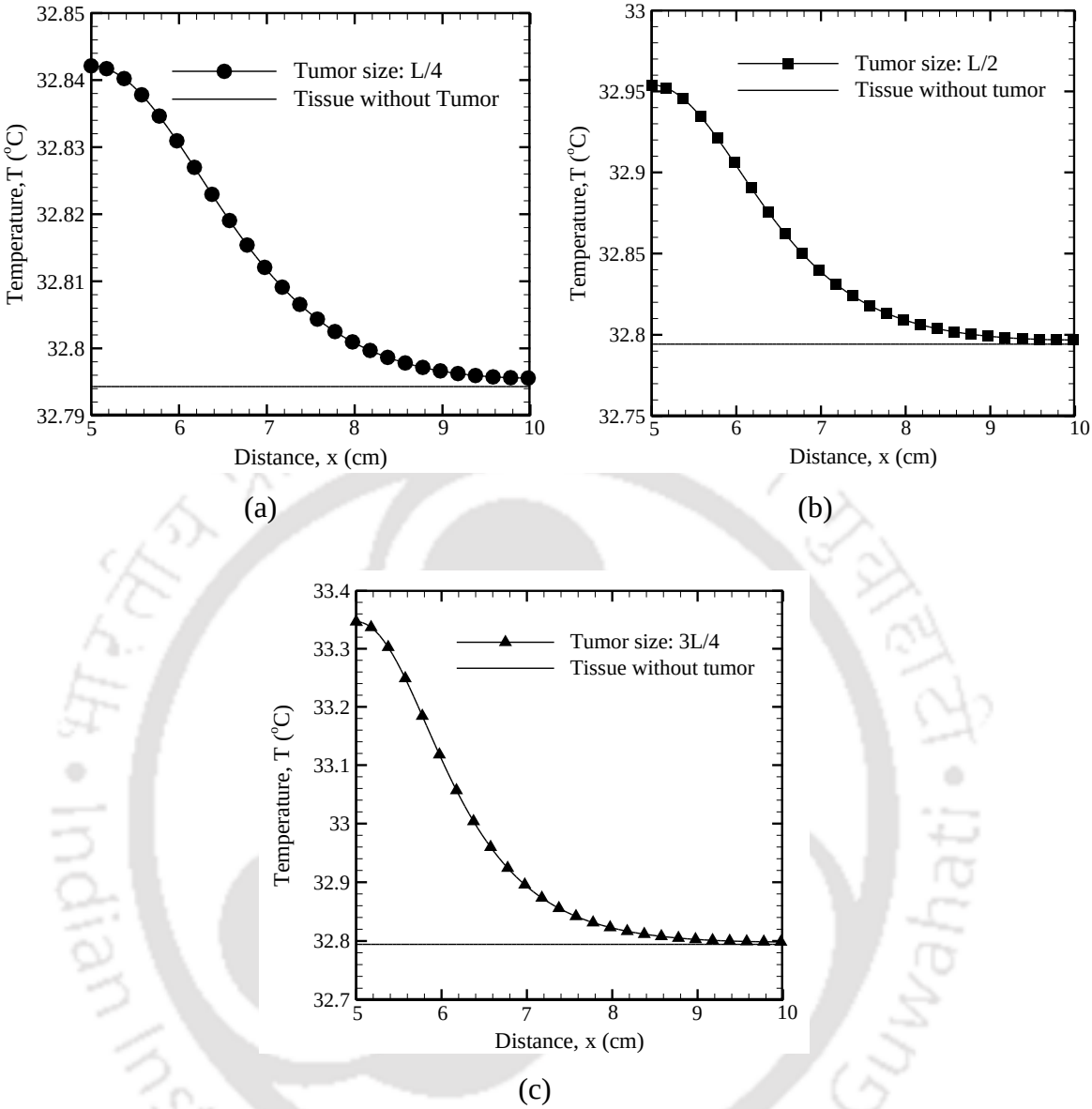

Figure 4.5 Steady-state temperature distributions along the skin surface (x, L) of the breast tissue with a centrally imbedded tumor of thickness (a) $L/4$, (b) $L/2$ and (c) $3L/4$.

4.2.2. Based on properties given by Gautherie (1980)

Considering the properties obtained by Gautherie (1980), for a healthy breast tissue, the blood perfusion rate and the metabolic heat generation rates are $\eta_b = 0.92\times10^{-3}\,\mathrm{s}^{-1}$ and $Q_m = 450\,\mathrm{Wm}^{-3}$, respectively (Table 4.1); while, in cancerous condition, the value of the blood perfusion rate lies in the range of $\eta_b = 1.22\times10^{-3} - 14.5\times10^{-3}\,\mathrm{s}^{-1}$ (Gautherie, 1980) with a mean of $\eta_b = 4.9\times10^{-3}\,\mathrm{s}^{-1}$. A high value of the metabolic heat generation rate of

$29000\,\mathrm{Wm}^{-3}$ (Gonz´alez, 2007) is observed for a cancerous tumor of breast. With other thermo-physical properties of tissue and blood, considered the same as Gonz´alez (2007), the effect of location (Y) of different sizes of the tumor on the temperature profile is studied as the earlier case.

For a centrally located tumor of size 0.5 cm and 2.5 cm, effect of location $(\mathrm{L}-\mathrm{Y})$ of the tumor on the SS skin surface temperature distributions are shown in Fig. 4.6a and 4.6b, respectively. For these and subsequent results, computations are done for the entire domain keeping in mind the inverse methodology proposed by the author in the next section. At the SS, in absence of a tumor, a healthy tissue yields uniform skin surface temperature of 31.34°C. When a tumor is present, the skin surface temperature increases, and the uniformity is lost. For any location or any size, the skin surface temperature profiles are similar, and their spatial distribution is Gaussian in nature.

An observation of Fig. 4.6a and 4.6b reveals that when the distance $(L-\mathrm{Y})$ of the tumor from the skin surface decreases, temperature of the skin increases. For a tumor of size $0.5\mathrm{cm}\times 0.5\mathrm{cm}$, when the distance $(L-\mathrm{Y})$ of the center of the tumor are 4.5 cm, 1.75 cm and 0.75 cm, the increase in the peak temperature at (L,L) are 0.001, 0.09 and 0.56 °C, respectively (Fig. 4.6a). While for the tumor with 2.5 cm, when the distances $(L-\mathrm{Y})$ of the center of the tumor are 3.25 cm, 2.75 cm, 2.25 and 1.75 cm, the increase in peak temperature at (L,L) are 0.18, 0.365, 0.77 and 1.7°C, respectively (Fig. 4.6b).

Another important observation from the skin surface temperature distributions shown in Figs.4.5a and 4.5b is that, when the distance $(L-\mathrm{Y})$ of the tumor from the skin surface decreases, the peak magnitude (amplitude *A*) of the skin surface temperature profile increases. When $(L-\mathrm{Y})\to L$, i.e., the tumor is far away from the skin surface, the amplitude $A\to 0$. Similarly, with increase in the size of the tumor, both amplitude *A* and area under the curve increase (Fig. 4.6c). This increase is for the fact, when the size of the tumor increases, the heat generation rate also increases. The effect is clearly visible from a comparative plot of the SS temperature distributions for various sizes of the tumor located at $(L-\mathrm{Y})$ = 2.75 cm (Fig. 4.6c). Having observed the effect of various attributes

of the tumor, the skin surface temperature profiles are optimized to retrieve the unknown size and location of the tumor. The details are as follows.

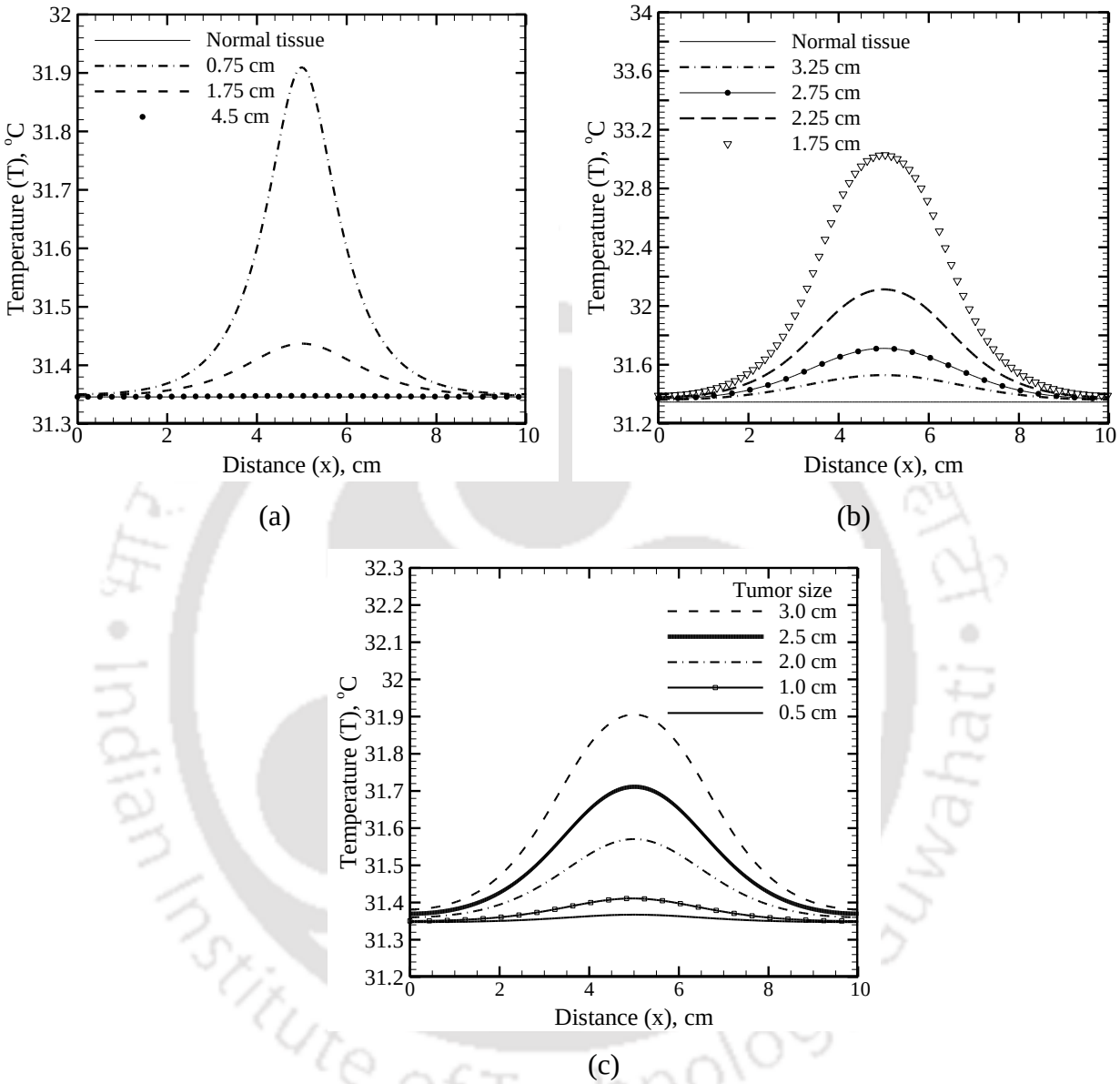

Figure 4.6 Steady-state skin surface (x, L) temperature distribution: Effect of locations $(L-\mathrm{Y})$ of tumor for tumor of size (a) 0.5 cm and (b) 2.5 cm, (c) effect of sizes of the tumor located at $(L-\mathrm{Y}) = 2.75$ cm.

4.3. Inverse Analysis

Present work estimates the attributes of a tumor in a human breast. With an aim to detect a tumor non-invasively, inverse analysis of the skin surface temperature

profiles are performed using the GA. With certain limitations of GA, a newly proposed CFM is employed, and the results are presented for various cases.

4.3.1. Genetic algorithm

With an assumption that, the skin surface temperature profiles are known from measurement, we next estimate various attributes of the tumor, viz., the blood perfusion rate η_b, location and size. In estimating these attributes, in the GA, for a population size of 1000, the stopping criteria was the minimum value of the objective function 10^{-10} or 1000 generations whichever was reached first. Results of estimations are shown in Tables 4.2-4.4.

Table 4.2: Estimated values of blood perfusion rate η_b of a healthy and malignant breast tissue.

Breast tissue	**Blood perfusion rate** $\eta_b \left(\mathrm{s}^{-1}\right)$		**% Error**
	Actual value	**Estimated value**	
Healthy	0.00018	0.00018009	0.05
Malignant	0.009	0.009	0.0

Table 4.2 shows the estimated values of the blood perfusion rate η_b for a healthy tissue and a tissue with a centrally located tumor of size $\frac{L}{4}$. It is observed that the blood perfusion rate η_b is estimated exactly. With one of the properties of the tumor estimated exactly, next we simultaneously estimate the location (distance from the top boundary) of the tumor in the tissue and its thickness. Results are shown in Table 4.3. With y_{top} and y_{bottom} as the distance of the top and bottom face of the tumor from the skin surface, non-dimensional lengths defined as $y^*_{top} = \frac{y_{top}}{L}$, $y^*_{bottom} = \frac{y_{bottom}}{L}$ and $\text{size} = \frac{y_{bottom} - y_{top}}{L}$, in Table 4.3, results are shown for 6 cases. These 6 cases correspond to 3 different thicknesses of

Table 4.3: Estimation of location of the top y_t^* and the bottom y_b^* surfaces of the tumor in a breast tissue.

Actual value		**Estimated value**		**% error in**	
y^*_{top}	y^*_{bottom}	y^*_{top}	y^*_{bottom}	y^*_{top}	y^*_{bottom}
0.2	0.325	0.198	0.33	1.0	1.538
0.5	0.625	0.4896	0.6161	2.08	1.44
0.25	0.5	0.2478	0.5024	0.88	0.48
0.3	0.55	0.3009	0.5493	0.3	0.127
0.2	0.7	0.2051	0.7004	2.55	0.057
0.4	0.9	0.408	0.893	2.0	0.78

Table 4.4: Simultaneous estimation of blood perfusion rate η_b and location $\left(y_t^*, y_b^*\right)$ of a tumor in breast tissue.

Actual value			**Estimated value**			**% error in**		
η_b	y^*_{top}	y^*_{bottom}	η_b	y^*_{top}	y^*_{bottom}	η_b	y^*_{top}	y^*_{bottom}
			0.0091	0.3935	0.6474	1.11	4.93	3.60
0.0090	0.375	0.625	0.0091	0.3809	0.6488	1.11	1.57	3.80
			0.0090	0.3757	0.6383	0.0	0.18	2.12
			0.0091	0.2518	0.4973	1.11	0.72	0.54
0.0090	0.25	0.5	0.0090	0.2426	0.4945	0.0	2.96	1.1
			0.0091	0.2577	0.509	1.11	3.08	1.8
			0.0090	0.189	0.604	0.0	5.5	0.67
0.0090	0.20	0.6	0.0090	0.1901	0.6088	0.0	4.95	1.46
			0.0090	0.20	0.6106	0.0	0.0	1.76

the tumor, viz. size $= \dfrac{y_{bottom} - y_{top}}{L} = 0.125, 0.25$ and 0.50, and 6 locations, viz., $\left(y^*_{top}, y^*_{bottom}\right) = (0.20, 0.325)$, (0.50, 0.625), (0.25, 0.50), (0.30, 0.55), (0.20, 0.70) and

(0.40, 0.90). It is to be noted that for these cases, the measured surface temperature profiles were obtained by solving the direct problem. An observation of Table 4.3 shows that errors in the estimations of the positions are within 3%.

Results for the simultaneous estimation of three parameters, viz., blood perfusion rate η_b, y^*_{top} and y^*_{bottom} are shown in Table 4.4. It is observed that the η_b is estimated almost exactly, and the maximum % error in estimations of y^*_{top} and y^*_{bottom} are within acceptable limit.

4.3.2. Curve fitting technique

For a centrally $(x = L)$ located tumor, irrespective of its size and location, it is observed from Figs. 4.6a – 4.6c that the spatial distribution of the skin surface temperature is Gaussian (Fig. 4.7a). The characteristics of the Gaussian profile such as the amplitude A, full width at half maximum (FWHM) and width w (Fig. 4.7a) are functions of tumor size and location. With T_o as the reference (base) temperature, in terms of amplitude A, distance L and width w, it can be expressed as

$$T = T_o + Ae^{-(x-L)^2/2w^2} \tag{4.1}$$

A tissue with a tumor of particular size and location yields a skin surface temperature profile which remains unique to that particular size and location. Hence, the amplitude, width and the area under the curve also remain unique. In the present work, this feature is used in the proposed inverse technique to estimate the size and the location of a tumor in a tissue.

The inverse estimation of the size and the location of the tumor in a breast tissue using this method of curve fitting starts with building a database of amplitude *A* vs. location Y, and area vs. location Y for different sizes of the tumor. For an unknown condition of the tissue, the obtained surface temperature profile is fitted with a curve fitting tool using a Gaussian fit. The amplitude of the curve so obtained is searched in the stored database of A vs. Y and its corresponding size and location are noted down. Any unavailable data is interpolated from the known values. Now, from the database of area vs. Y, for that

particular size, at that location, the area is found out. The match of the found area below 10% confirms the presence of a tumor of that size at that particular location. In case of any mismatch (>10%), the search process continues till the end of the database. The developed solver performs different operations such as search, interpolation and matching of values, etc.

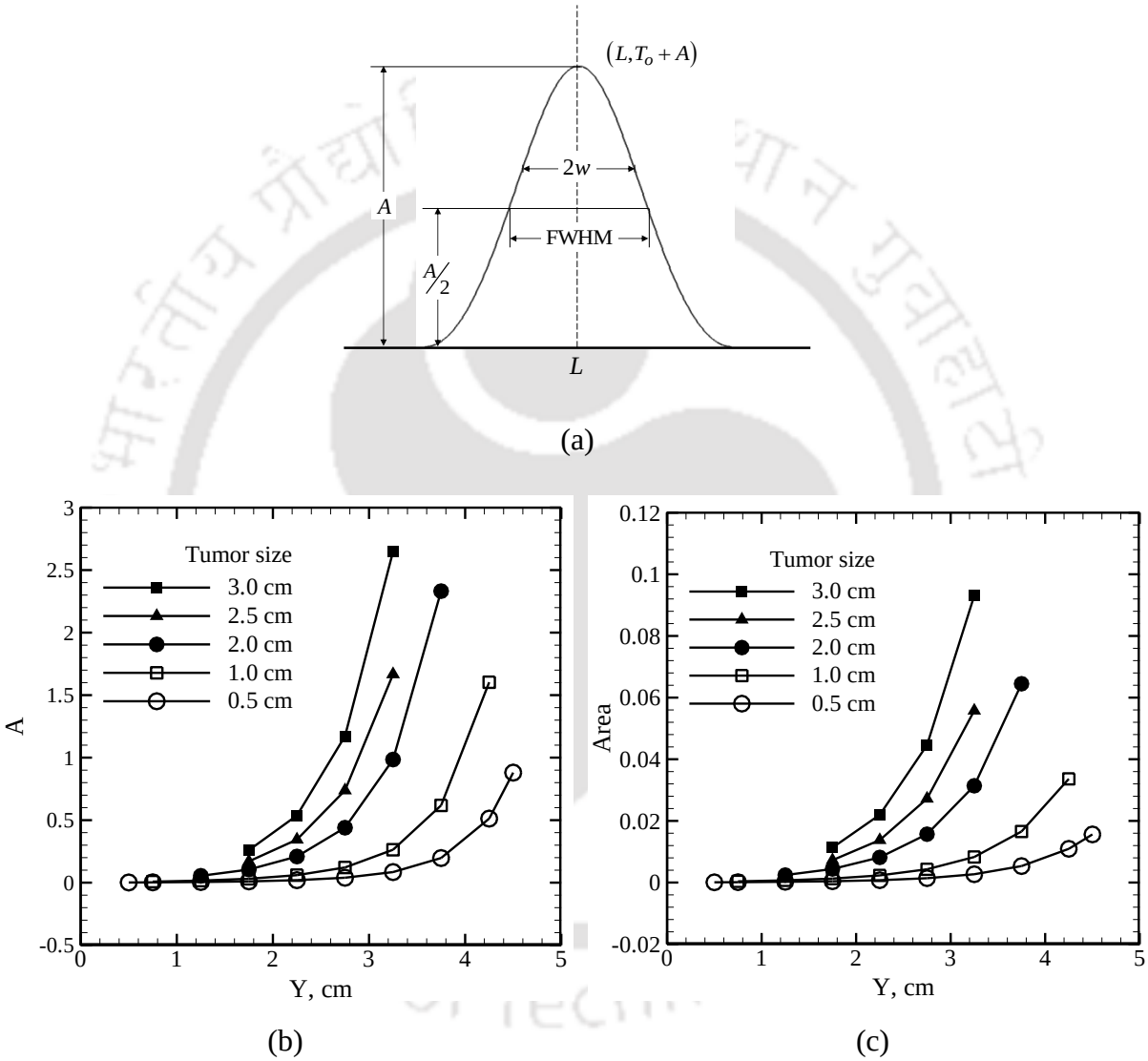

Figure 4.7 (a) Schematic of a Gaussian profile, and variation of its (b) amplitude and (c) area for different sizes of tumors at its different locations *Y* in a 2-D tissue.

With the proposed technique, a database of amplitude *A* vs. location Y is made for 0.5 cm, 1.0 cm, 2.0 cm, 2.5 cm and 3.0 cm of the tumors with the mean value of blood perfusion rate. For the given size of the tumor, another database of the values of area vs. location (Y) is made. The uniqueness of the skin surface temperature profiles can be

made clear from the profiles of area and amplitude against the location Y, for different sizes of the tumor as shown in Fig. 4.7b and 4.7c, respectively.

As the blood perfusion rate of a breast tumor varies over a small range of $1.22\times10^{-3} - 14.5\times10^{-3}\text{s}^{-1}$ (Gautherie, 1980), very minor change in the SS temperature profile is observed even for the limiting values of η_b (Fig. 4.8). Hence, the database can be made using any value of η_b within the range. In this case, the mean value of blood perfusion rate $4.9\times10^{-3}\text{s}^{-1}$, as reported in the literature (Gautherie, 1980), is considered for the purpose.

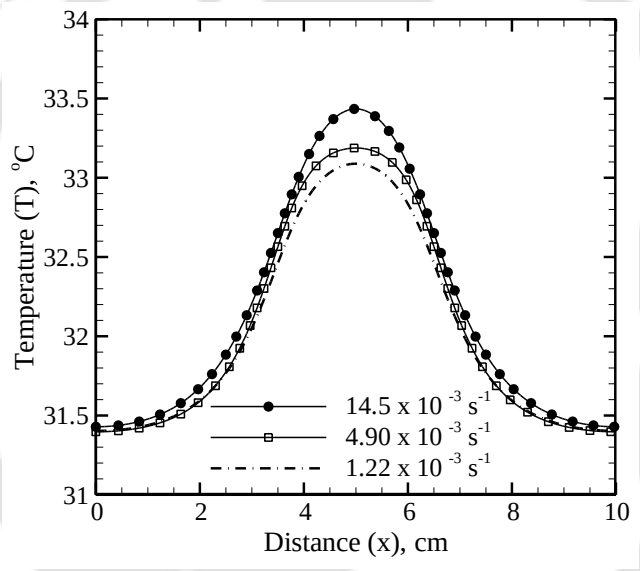

Figure 4.8 Effect of change of blood perfusion rate (η_b) on SS skin surface (x,L) temperature distribution for a tumor of size 3 cm located at *Y*= 3.0 cm.

Steady-state skin surface temperature profile of a breast with and without a tumor obtained from measurement serves as the reference temperature profile. In the present case, however, numerically computed skin surface temperature profile obtained by solving the PBHE serves this purpose. This temperature profile is fitted in a curve fitting tool using Gaussian fit, and the values of its amplitude and area are obtained, and these are fed to the solver. After going through the series of operations as stated before, when the match is within the set value (≤10%), the estimation of the size and location of the tumor is assumed to be complete.

Table 4.5 shows the results of simultaneous estimation of size and location of 25 different sizes and locations of the tumors. In practice, in the proposed approach, during the estimation nothing else but the skin surface temperature profile is needed that gives its amplitude and area. Knowledge about the thermo-physical properties, the blood perfusion rate and the metabolic heat generation rate are not needed. An observation of results in Table 4.5 shows that in most of the cases, size and location are exactly estimated. In some cases, the maximum error in estimation of the size is 4.167%, while the same in location is 7.7%. Though this accuracy in estimation is accepted, it can further be refined by making the database comprehensive by considering wide ranges of sizes and locations of the tumor.

Table 4.5. Inverse estimated value of location and size of a tumor in 2-D breast tissue.

Sl No.	Blood Perfusion Rate $\times 10^3$	Actual value		Estimated value		Error (%)	
		Size, L_t (cm)	Location, Y (cm)	Size, L_t (cm)	Location, Y (cm)	Size, L_t	Location, Y
1	4.9	0.48	4.25	0.50	4.25	4.167	0.000
2	4.9	0.49	4	0.5	3.9328	2.041	1.680
3	4.9	0.50	1.250	0.50	1.250	0.000	0.000
4	4.9	0.50	3.816	0.50	3.779	0.000	0.962
5	2	0.50	1.250	0.50	1.328	0.000	6.232
6	10	0.50	4.000	0.50	4.102	0.000	2.557
7	14.5	0.51	3.250	0.50	3.335	1.961	2.604
8	10.5	0.52	3.250	0.50	3.315	3.846	1.988
9	4	0.98	3.500	1.00	3.403	2.041	2.766
10	4	0.99	4.000	1.00	3.889	1.010	2.788
11	4.9	1.00	1.750	1.00	1.784	0.000	1.949
12	4.9	1.00	2.790	1.00	2.783	0.000	0.251
13	3.5	1.00	4.000	1.00	3.895	0.000	2.620
14	5.67	1.00	1.000	1.00	0.922	0.000	7.770
15	4.9	2.00	2.750	2.00	2.750	0.000	0.000
16	4.9	2.00	1.260	2.00	1.250	0.000	0.762
17	3.55	2.00	3.750	2.00	3.718	0.000	0.843
18	7.58	2.00	3.000	2.00	2.932	0.000	2.277
19	4.9	2.50	1.750	2.50	1.750	0.000	0.000
20	4.9	2.50	3.000	2.50	2.946	0.000	1.787
21	6.8	2.50	2.800	2.50	2.772	0.000	0.993
22	4.9	3.00	3.250	3.00	3.250	0.000	0.000
23	4.9	3.00	1.800	3.00	1.784	0.000	0.883
24	5.5	3.00	2.100	3.00	2.034	0.000	3.167
25	3.95	3.00	3.000	3.00	2.949	0.000	1.697

The optimization tools like the genetic algorithm, etc., used in the inverse analysis are time consuming. The inverse analysis using these methods also requires solution of the direct problem. However, in the proposed approach, no such thing is needed, and the computation is exceedingly fast. For the present geometry, with 100×100 control volumes, the genetic algorithm with population size 1000 on 32 bit-2.10 GHz processor with 2 GB RAM took almost 16 hours, while the proposed approach, the estimation has been instantaneous. It took less than 0.1 seconds.

4.4. Summary

The size and the location of a tumor inside a breast were simultaneously estimated. Estimation was based on the skin surface temperature distribution. Solution of the Pennes bioheat equation provided the skin surface temperature distribution. Use of the mathematically 2-D rectangular geometry instead of a 3-D hemispherical geometry was justified. For different sizes and locations of the tumors, the skin surface temperature distributions had Gaussian profile. The obtained Gaussian temperature profile was specific for the specific size and location of the tumor. The characteristics of the Gaussian temperature profile, viz., the amplitude and the area were the basis of estimation using the proposed curve fitting technique. Estimations were done for a wide range of values of size and locations. The size and the location of the tumor were estimated with good accuracy. The analysis of the estimation was not only simple; the required computational time was almost insignificant compared to estimation of the same parameters using the genetic algorithm.

CHAPTER 5

THERMAL MODELING AND INVERSE ANALYSIS OF A REALISTIC BREAST GEOMETRY

Consideration of a 2-D rectangular domain of tissue is one of the simple way to analyze a human breast. In realistic scenario, one can imagine it in the form of a hemisphere. The tissue consists of multiple layers of skin tissues, blood vessels, adipose tissues, milk ducts and lobules. In the following, a numerical model of breast is analyzed thermally, considering a homogenous medium of tissue and an embedded tumor. The realistic model is validated with the experimental data available in the literature. The newly proposed curve fitting algorithm is also implemented to simultaneously estimate tumor size and location.

5.1. Geometry

A human breast can be well approximated in the form of a hemisphere as shown in Fig. 5.1a. To show that even the analysis of a 2-D semicircular section provides correct estimates, first the consideration is given to the breast contained in the 2-D *xy*-plane (Fig. 5.1b). Being far away from the skin surface, the base of the semicircle $(r, \phi = 0 \text{ and } \pi)$ and the hemisphere $(r, \phi = 0 \text{ and } \pi, \theta = 0 \text{ and } \pi)$ are considered to be at adiabatic

$\left(\hat{n}\cdot\nabla T=0\right)$, while the skin surface $\left(r=R\right)$is exposed to a convective environment $\left(-\left(\hat{n}\cdot k\nabla T\big|_{r=R}\right)=h\left(T-T_f\right)\right)$. The FEM is employed in the solution of Eq. (3.6) for both 2-D (Fig. 5.1b) and 3-D (Fig. 5.1a) geometry of the breast. Figures 5.2a and 5.2b show schematic of the FEM triangular and tetrahedral grids considered for both the geometries of the breast.

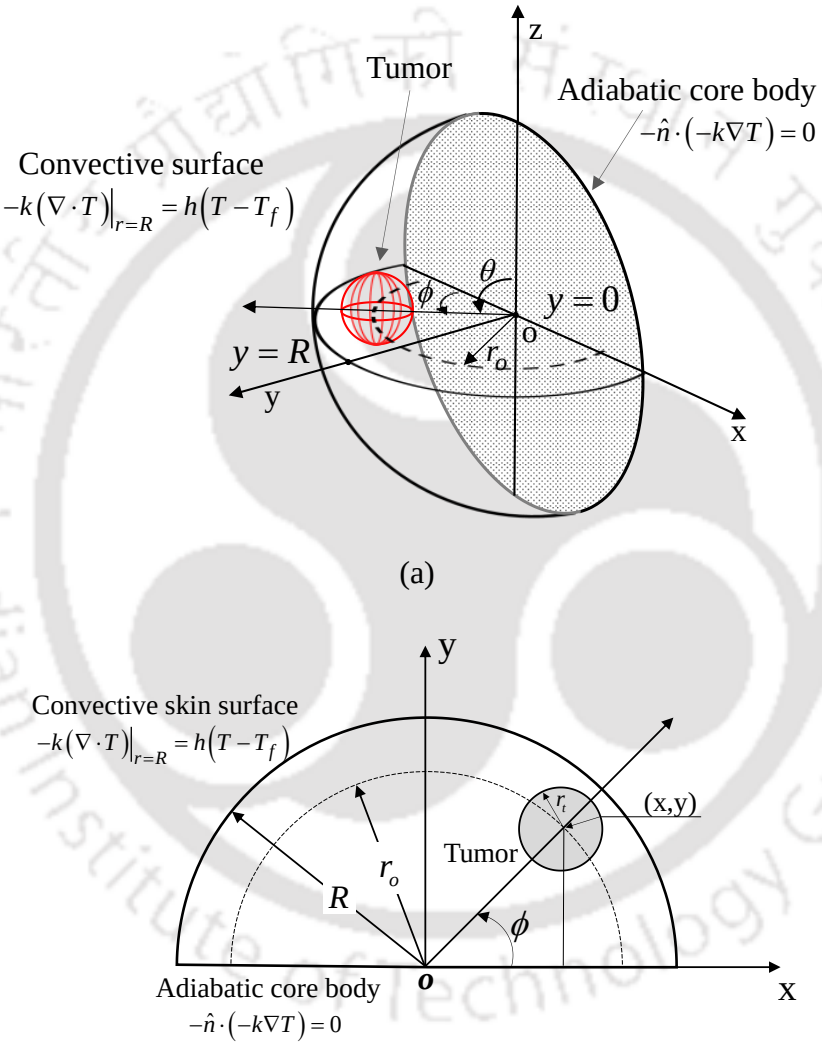

Figure 5.1 Schematic of (a) 3-D model of hemispherical human breast and its simplified representation in the form of (b) 2-D semicircular planar tissue with tumor.

With thermophysical properties known, subjected to the initial and the boundary conditions, numerical solution of Eq. (3.6) yields the temperature distribution in the tissue. As mentioned before, first consideration is given to a 2-D semicircular section

(Figs. 5.1b, 5.2b). Consideration of the 2-D semicircular section instead of a full scale 3-D hemispherical model will be justified by comparing the temperature profiles along the surface and the centerline for cases with and without a tumor.

Similar to the 2-D rectangular domain of tissue, presence of a tumor shows a particular pattern of Gaussian temperature profiles along the skin surface of the breast and these profiles are similar in nature for various cases of tumor positions and sizes. Taking similarity of these temperature profiles along the skin surface, current work estimates the size and the location of malignancy inside the 2-D semicircular section of the breast.

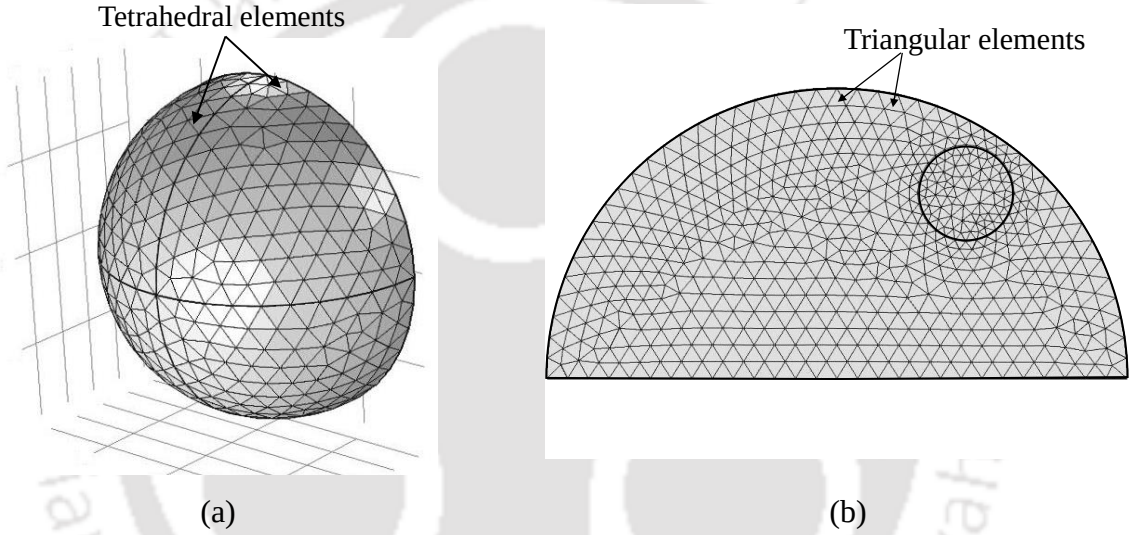

Figure 5.2 Schematics of the (a) 3-D and (b) 2-D FEM discretized solution space.

5.2. Validation

5.2.1. Closeness of 2-D semicircular and 3-D hemispherical model of breast

To check the viability of the assumption that the analysis of a 2-D breast tissue is as good as a 3-D tissue, temperature profiles for the two geometry are compared. Consideration is given to a 3-D hemispherical model (Fig. 5.1a) with reference to Gautherie (1980). Following Gautherie (1980), the diameter of the breast is taken to be 18 cm. With convective condition on the skin surface $\left(T_f = 21^{\circ}\mathrm{C}, h = 5\,\mathrm{W/m^2K}\right)$ and an adiabatic core, the breast is embedded with a spherical tumor of size (r_t) 2.5 cm, located at a depth of 3 cm on the *y*-axis. With thermophysical properties of breast tissue and the tumor

(Gonz´alez, 2007) as, $\rho = 920\,\mathrm{kg/m^3}$, $c_p = 3000\,\mathrm{J/kg\cdot K}$, and $k = 0.42\,\mathrm{W/m\cdot K}$; and that for blood as $\rho_b = 1052\,\mathrm{kg/m^3}$, $c_{pb} = 3800\,\mathrm{J/kg\cdot K}$, the PBHE (Eq. 3.6) has been solved for the 3-D model (Fig. 5.1a) using COMSOL 4.3a. A tetrahedral grid (Fig. 5.2a) of element size, minimum 0.027 cm and maximum 0.63 cm are used for the current geometry.

In a human breast, when a tumor manifests, compared to normal tissue, a large increase in metabolic heat generation rate (Q_m) and blood perfusion rate (η_b) have been observed. A cancerous breast tumor shows a metabolic heat generation rate of $29000\,\mathrm{W/m^3}$ (Gautherie, 1980) and a range of blood perfusion rate of $1.22\times10^{-3} - 14.5\times10^{-3}\,\mathrm{s^{-1}}$ (Mankoff et al., 2002), against its normal values of $450\,\mathrm{W/m^3}$ (Gautherie, 1980) and $0.92\times10^{-3}\,\mathrm{s^{-1}}$ (Mankoff et al., 2002), respectively. For the 2-D semicircular domain (Fig. 5.1b) contained in the *xy*-plane, thermophysical properties and the boundary conditions remain the same as for the 3-D model (Fig. 5.1a). With a triangular FEM grid (Fig. 5.2b) of size: $3.6\times10^{-4}\,\mathrm{cm}$ (minimum) and $0.18\,\mathrm{cm}$ (maximum), Figs. 5.3a and 5.3b show SS temperature profiles along the centerline $\left(\text{3-D:}(r,\theta=\pi/2,\phi=\pi/2);\ \text{2-D:}\ (r,\phi=\pi/2)\right)$ and the surface $\left(\text{3-D:}(R,\theta=\pi/2,\phi);\ \text{2-D:}\ (R,\phi)\right)$ of the breast. Following the similar pattern of the temperature profiles in the breast, with and without a tumor, a maximum over estimation of 0.6°C by the 2-D geometry has been observed, justifying the applicability of the assumption.

Having shown that the centerline (Fig. 5.3a) and the skin surface (Fig. 5.3b) temperature profiles of the 2-D semicircular geometry closely match with that of the 3-D hemispherical geometry, in the following, effects of tumor size and location on the temperature profiles are presented for the 2-D geometry.

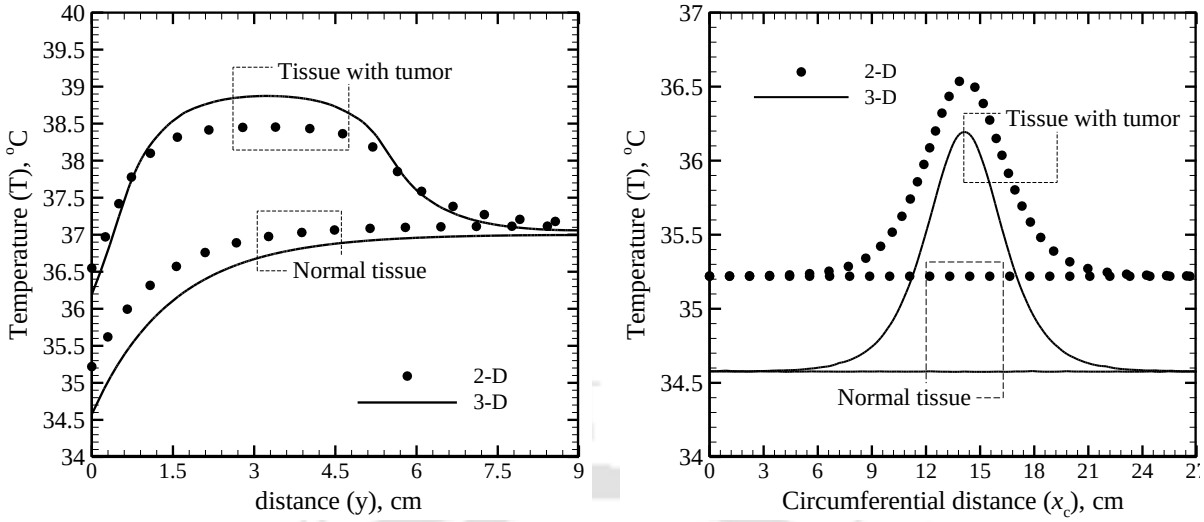

(a) (b)

Figure 5.3 Comparison of SS (a) centerline $\left(r,\pi/2\right)$ and (b) skin surface $\left(R,\phi\right)$ temperature distribution of 3-D hemispherical model with 2-D section of human breast with tumor of size 2.5 cm located at a depth of 3 cm on *y*- axis.

5.2.2. Validation with experimental data

Prior to the numerical simulations and the use, the model, the solver and the considered initial and boundary conditions are validated with the experimental data available in the literature (Gautherie, 1980). With a tumor of radius r_t = 1.15 cm located at a depth of 2 cm, the size of the breast (Fig. 5.1a and 5.1b) is considered as 18 cm in diameter $\left(2r_b\right)$ (Gautherie, 1980). Considering convective condition on the skin surface, with an ambient at $T_f = 21^{\circ}\mathrm{C}$ and $h = 5\,\mathrm{W/m^2\cdot K}$, the thermophysical properties of breast tissue (Gonz´alez, 2007) are taken as: $\rho = 920\,\mathrm{kg/m^3}$, $c_p = 3000\,\mathrm{J/kg\cdot K}$, $k = 0.42\,\mathrm{W/m\cdot K}$; and that for blood as $\rho_b = 1052\,\mathrm{kg/m^3}$ and $c_{pb} = 3800\,\mathrm{J/kg\cdot K}$. A large elevation in metabolic heat generation rate Q_m and blood perfusion rate η_b is observed in case of malignant condition of the breast. Metabolic heat generation rate of $29000\,\mathrm{W/m^3}$ (Gautherie, 1980) and blood perfusion rate of $0.009\,\mathrm{s^{-1}}$ (Gonz´alez, 2007) for a breast tumor are much higher than that of the healthy tissue ($450\,\mathrm{W/m^3}$ (Gautherie, 1980) and $0.00018\,\mathrm{s^{-1}}$ (Gonz´alez, 2007)). With a tetrahedral grid (Fig. 5.2a) of element size: 0.027 cm (minimum) and 0.63 cm (maximum) as in the earlier study, the PBHE is solved for the

geometry of the breast. Figure 5.4a shows SS temperature profiles along the centerline $(r_b, \theta = 0, \phi = \pi/2)$ of the breast, and the results are compared with the experimental data presented by Gautherie (1980). A good agreement is observed for both normal and malignant condition of the breast. With and without a tumor, Fig. 5.4b shows the skin surface temperature. In the absence of a tumor, the temperature at the skin surface is uniform (Fig. 5.4b). In the presence of a tumor, though a higher value of blood perfusion rate is observed, due to a very high value (65 times more than the healthy tissue) of metabolic heat generation rate, a significant change in the skin surface temperature is observed.

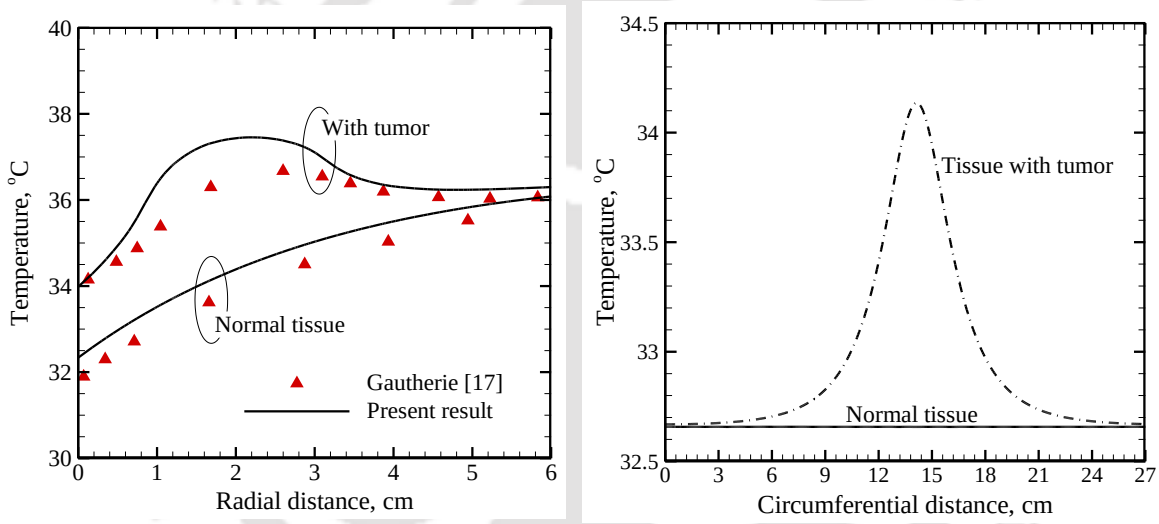

(a) (b)

Figure 5.4 Steady-state temperature distribution along (a) the centerline $(r, \theta = 0, \phi = \pi/2)$ and (b) the skin surface $(r_b, \theta = 0, \phi)$ of the 3-D breast validating the results with experimental data (Gautherie, 1980).

5.3. Effects of Tumor Size and Location on the Skin Surface Temperature

5.3.1. 2-D semicircular breast

Tumors of sizes 1 cm and 2.5 cm are considered at different locations. Figures 5.5a-d show distributions of SS temperature profiles along the centerline $(r, \phi = \pi/2)$ and the

skin surface (R,ϕ). In every case, temperature distribution for the breast without a tumor is also plotted. Without a tumor in a tissue, the value of blood perfusion rate and metabolic heat generation rate are uniformly distributed over the domain, which results in uniform skin surface temperature profile along the circumferential distance of the breast (Fig. 4a-b). On the other hand, in presence of a malignancy due to high value of localized metabolic heat generation, the tumor acts as a heat source, and a rise in temperature is observed.

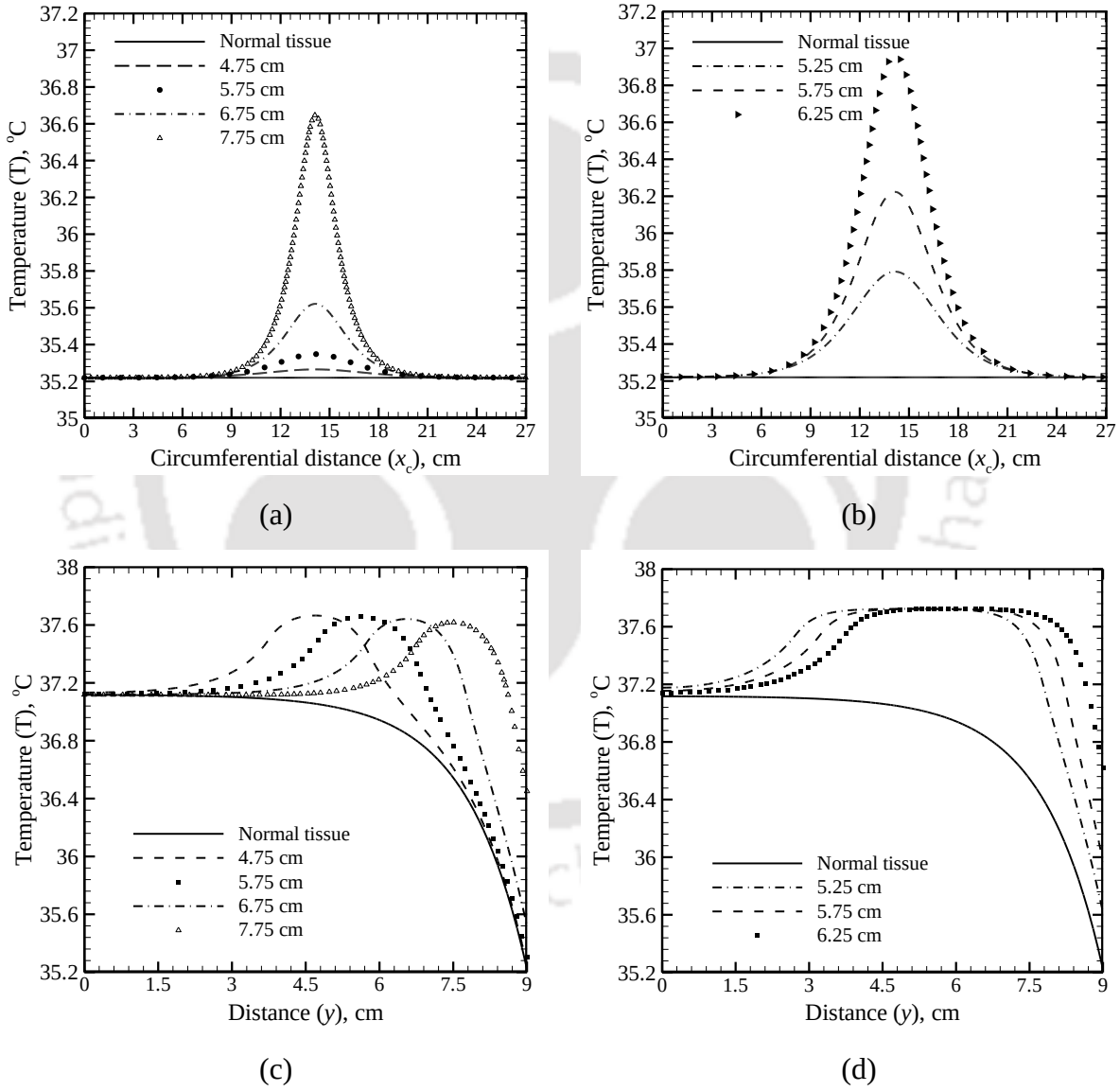

Figure 5.5 Steady-state temperature distribution of (a, b) surface (R,ϕ) and (c, d) centerline $(r,\pi/2)$ of the 2-D breast tissue with tumor of size 1.0 cm (a, c) and 2.5 cm (b,

d) located on the centerline $\left(\phi = \pi/2\right)$ at different *r*.

The blood perfusion rate in the PBHE (Eq. 3.6) is a convective parameter, and is combined with negative of the temperature at a particular point. Hence, the second term on the RHS of Eq. (3.6) is responsible for carrying away the heat generated due metabolic activities. Inside a tumor, as the perfusion of blood is not sufficiently high to compensate the metabolically generated heat, the sole result is an increase in temperature at the core of the tumor (Fig. 5.5c and 5.5d). From the temperature profiles along the skin surface for different sizes of the tumor (Fig. 5.5a and 5.5b), it is observed that, closer is the tumor to the skin surface, higher is the temperature of the skin and vice versa.

Once a tumor manifests, it progresses with time, and the size increases. Figure 5.6 shows a comparison of SS temperature distribution along the skin surface $\left(R,\phi\right)$ and the centerline $\left(r,\phi = \pi/2\right)$ of the breast for various sizes of the tumor located at a radius of 4.5 cm on the *y*-axis. When size of a tumor increases from 1 cm to 3 cm, the net amount of volumetric heat generation also increases, and the effect is increase in temperature of the skin surface of the breast (Fig. 5.6a). On the other hand, owing to its homogeneity, the peak temperatures of the tumor for all sizes do not vary much (Fig. 5.6b).

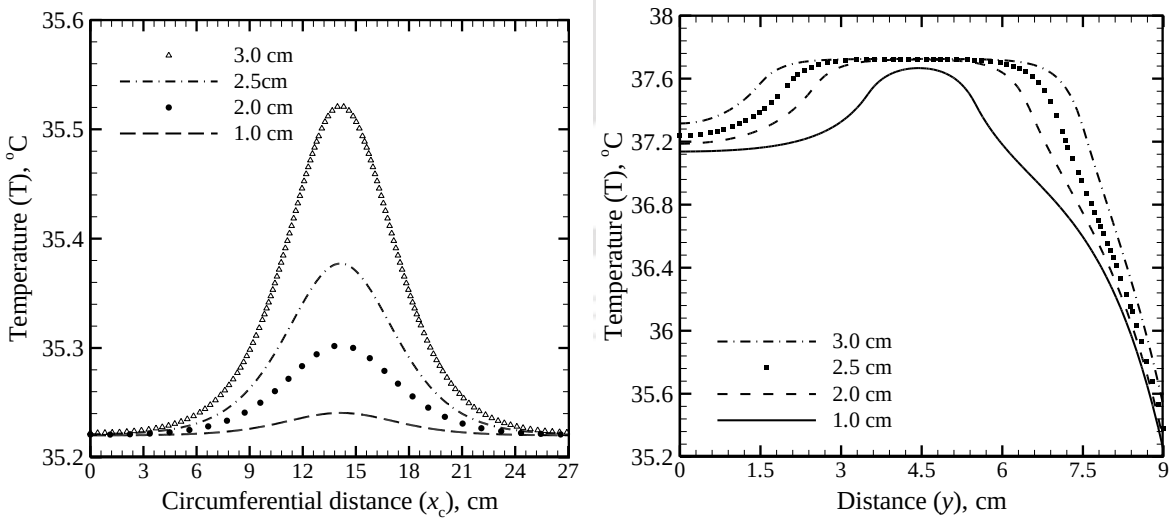

(a) (b)

Figure 5.6 Variation of SS temperature distributions along (a) the skin surface $\left(R,\phi\right)$ and (b) centerline $\left(r,\pi/2\right)$ of the 2-D breast tissue with tumors of different sizes located at

$(r_o = 4.5\,\text{cm})$.

In reality, a tumor can be located anywhere in the breast. With reference to Fig. 5.1b, its angular location ϕ could be anything. To study the effect of the angular locations, 4 cases are considered (Fig. 5.7). From the skin surface, in all cases, the tumors are located at the same depth (Fig. 5.7). The motive for this study is to view the effect of angle ϕ on the SS skin surface temperature profile, which forms the basis of inverse analysis to estimate the size and the location of the tumor. With thermophysical properties, geometrical parameters (sizes of the breast) and the boundary conditions the same as before, for a tumor of size 1 cm, effects of the angular locations of the tumor on skin surface temperature distributions are shown in Figs. 5.8a and 5.8b for the tumor located at a radius 7 cm and 6.5 cm, respectively. For the results shown in Fig. 5.8a, the tumor angular locations are ϕ = 90°, 106.6°, 124.8° and 148.9°, whereas tumor angular locations are ϕ = 90°, 72°, 52° and 22.6° for results in Fig. 5.8b. It is observed from Figs. 5.8a and 5.8b that for a given size of the tumor, not only the peak of the temperature profile remains unchanged, for all angular locations of the tumor, temperature profiles remain identical. It is further observed that the peak of the skin surface temperature profile appears exactly along the centerline of the tumor.

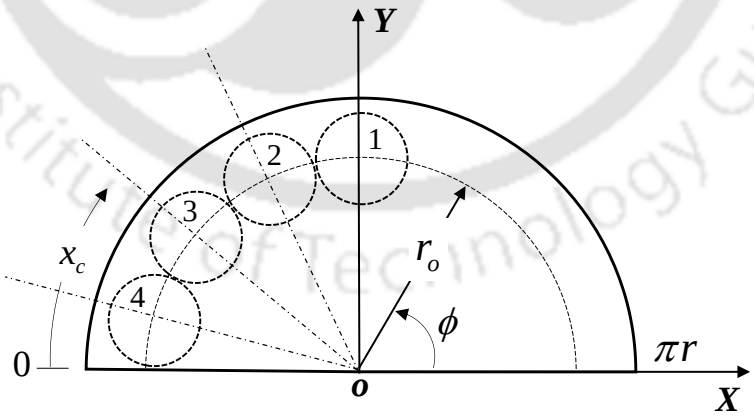

Figure 5.7 Schematic of 2-D semicircular tissue with tumors at same depths from skin and with different offset from Y-axis.

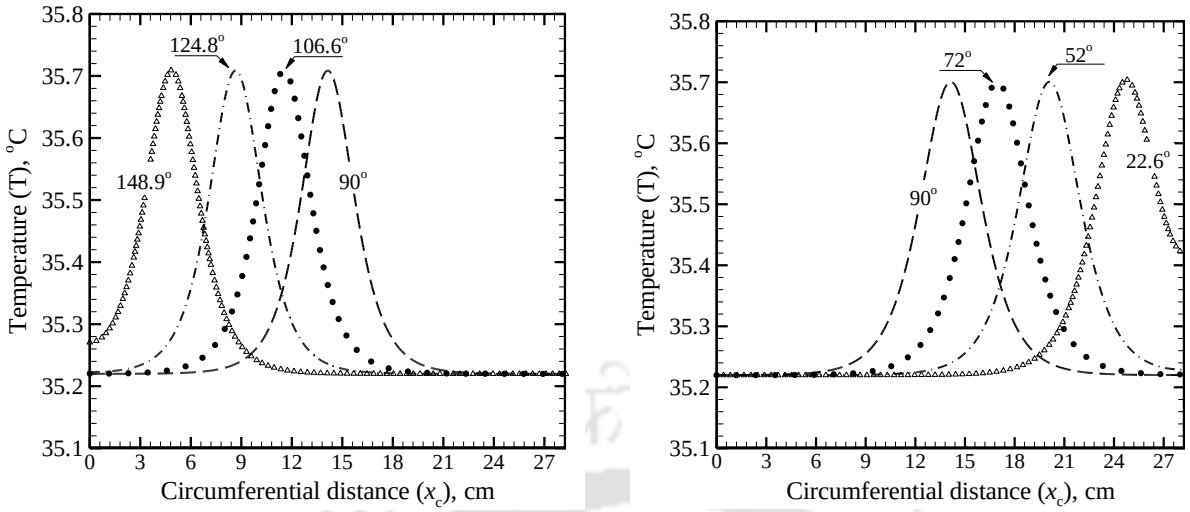

(a) (b)

Figure 5.8 Variation of SS temperature distributions along the skin surface of the breast having tumor of size 1 cm with different angular positions, located on radius (a) $r_o = 7.0\,\text{cm}$ and (b) $r_o = 6.5\,\text{cm}$.

5.3.2. 3-D hemispherical breast

A tumor in a breast in 3-D can be characterized by its size, radius r_t, radial location r_o and angular location (θ,ϕ) (Figs. 5.1a and 5.1b). Similar to the 2-D semicircular case, a study has been done to capture the effect of these attributes of tumor on the skin surface temperature. For these studies, to accommodate large variation of breast sizes in a group of population, an average breast of 18 cm diameter has been considered (Gautherie, 1980). In order to analyze the effect of growing tumor size over time, a SS temperature distribution along the skin surface $(R,\theta=0,\phi)$ of the breast is plotted (Fig. 5.9a) for various sizes (r_t) of the tumor located on the centerline $(\theta=0,\phi=\pi/2)$ at r_o = 4.75 cm. With realistic thermophysical properties of the breast tissue, compared to a normal condition, with tumor of sizes 1.5 cm, 2.0 cm, 2.5 cm and 3.0 cm, a maximum rise of 0.038°C, 0.092°C, 0.206°C and 0.44°C, of the tissue has been observed, respectively. Due to higher value of metabolic heat generation rate and blood perfusion rate of a tumor than that of a normal breast tissue, the net amount of volumetric generated heat inside the tissue increases significantly. The increased value of blood perfusion rate is unable to compensate the rise, leading to rise in temperature of the entire breast along with the skin surface.

In a practical scenario, a tumor in a breast is located at any depth, mostly in the lobules. To see the effect of tumor depth, a thermal analysis has been done by varying the depth of a tumor of size $r_t =$ 1.5 cm. Figure 5.9b shows the SS spatial variation of skin surface temperature of the breast, for various depths $(R - r_o)$ of 2.25 cm, 2.75 cm, 3.75 cm and 4.25 cm. Being malignant, the tumor generates heat due to higher value of metabolic activities, and raises the temperature of its nearby tissue regions. Closer the tumor to the skin surface, more is the rise in temperature of the breast skin. With a 1.5 cm tumor located at a depth of 2.25 cm from the skin, the maximum rise in temperature of 0.597°C has been observed than the normal tissue; whereas, 0.038°C of temperature rise has been observed by the same tumor is located at a depth of 4.25 cm.

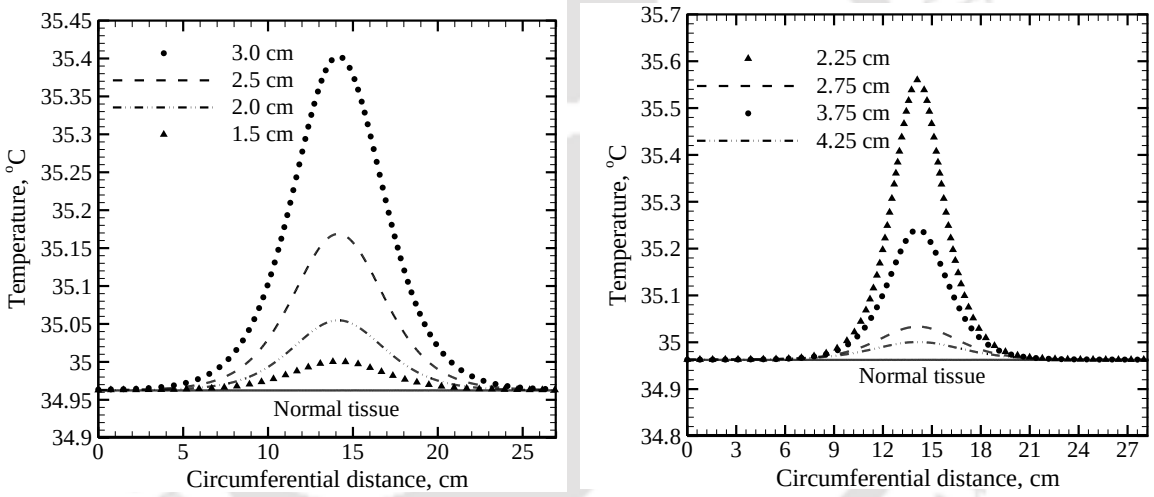

(a) (b)

Figure 5.9 Steady-state temperature distribution of surface $(R, \theta = 0, \phi)$ of the breast with tumor (a) of various sizes, at $r_t = 4.75\,\text{cm}$ and (b) at various depths $(R - r_o)$ with tumor radius (r_t) 1.5 cm, located on the centerline $\left(\theta = 0, \phi = \pi/2\right)$.

In the current study, skin surface temperature profile of the breast is the basis of the inverse analysis to estimate different attributes of a tumor. After analyzing the effect of the size (r_t) and the depth $(R - r_o)$ on the skin surface of the breast, next the effect of the

angular location (θ,ϕ) of the tumor is checked. Figure 5.10a shows the SS temperature distribution of the breast skin along the circumference of the semicircle passing through the center of the tumor at different θ for $(R-r_o)=6.25\text{cm}$ and $\phi=\pi/2$. For all the values of θ $(=0,\ \pi/12,\ \pi/6 \text{ and } \pi/4)$, the temperature profiles coincide with each other with equal value of temperature along the skin surface. Similarly, for the tumor at the same depth, the variation of $\phi-$location of the tumor at $\theta=0$ has been shown in Fig. 5.10b. The effect on the temperature profiles are clearly visible from the shifting of the temperature dome. However, with constant peak temperature of 35.24ºC, the temperature profiles maintain the similarity of shapes.

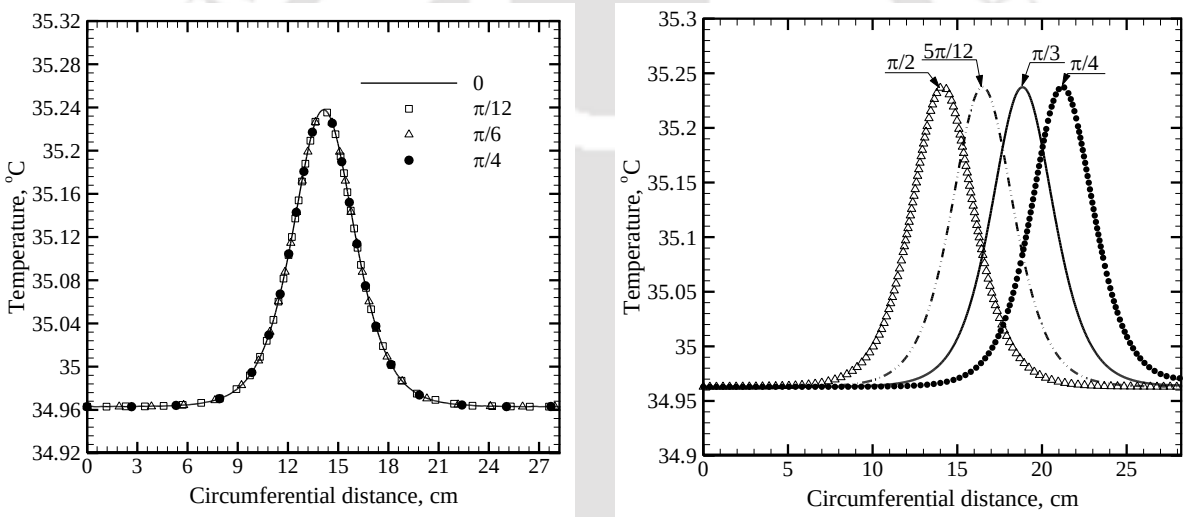

Figure 5.10 Variation of SS temperature distributions along the skin surface of the breast with tumor of size 1.5 cm located at various (a) θ-position with $\phi=\pi/2$ and (b) ϕ-position with $\theta=0$ at $r_o=6.25\text{cm}$.

5.4. Inverse Analysis

5.4.1. 2-D semicircular breast

From Figs. 5.5 and 5.6, it is observed that irrespective of the tumor size and its angular and radial locations, the skin surface temperature profiles in a 2-D section of the breast

are similar. Temperature profiles have a Gaussian distribution as in the earlier 2-D rectangular geometry. With T_o as the base temperature, w as the width and A as the amplitude, the Gaussian temperature profile (Fig. 5.11) can be expressed as,

$$T = T_o + Ae^{-(x-\bar{x}_c)^2/2w^2} \tag{5.1}$$

Though Gaussian in nature, the skin surface temperature profile is specific to specific tumor (size, radial and angular location). This uniqueness is revealed when various attributes of a Gaussian temperature profiles are analyzed. These attributes are the amplitude (A) and area $(Area)$ Gaussian temperature profile. For a tumor size ranging from 0.5 cm to 3 cm, and various locations along the *y*-axis (Fig. 5.1b), Figs. 5.12a and 5.12b show the variations of the amplitude A and *Area* of skin surface temperature profile. For a specific size and location of a tumor, it is observed that the amplitude and the area are also specific. Hence, for a particular tissue-tumor configuration, a unique sets of $(A, Area)$ is observed. Taking this as the basis, current work proposes an inverse methodology based on the curve fitting technique. In the following, the same is described.

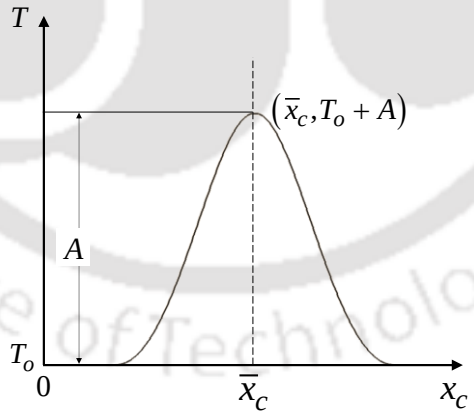

Figure 5.11 Schematic of a general Gaussian profile.

The algorithm starts with building of a database of amplitude A vs. *r* and *Area* vs. *r* for different sizes of the tumor, as was done for the 2-D rectangular domain of the tissue. In the previous section it has been stated that, irrespective of the angular position ϕ of the tumor, the skin surface temperature profiles yield the same value of the peak temperature (Fig. 5.8) i.e., the amplitude, *A*. For a given tumor and its radial location, as the skin

surface temperature profiles are identical, their areas and amplitudes are the same. Hence, for a given radial location of the tumor, with the knowledge of center $(\bar{x}_c)$, a single database of A vs. *r* and *Area* vs. *r* works well for tumors located at different angles.

Using tumors of sizes: 0.5 cm, 1.0 cm, 1.5 cm, 2.0 cm, 2.5 cm and 3.0 cm, the required database is made for all possible radial locations of the tumor using mean value of the blood perfusion rate $\left(\eta_b = 4.9\times10^{-3}\,\mathrm{s}^{-1}\right)$. Considering temperature profiles obtained from numerical simulation as the measured temperature, various cases of breast tissue with tumor are studied for simultaneous estimation of size and location of a tumor, and the results are presented in Table 5.1. The presented results show a maximum error of 2.33% in the simultaneous estimation of location of the tumor; and the size is estimated exactly. Although, the percentage of error in location of the tumor is well within the acceptable range, the accuracy can be further increased by refining the database. In all the cases considered in Table 5.1, the measured (simulated) temperature profiles are corresponding to tumor with blood perfusion rate of $4.9\times10^{-3}\,\mathrm{s}^{-1}$.

As the blood perfusion rate for a malignant breast tissue varies over a range of $1.22\times10^{-3} - 14.5\times10^{-3}\,\mathrm{s}^{-1}$, the effect of blood perfusion rate on the estimated value is also evaluated and the results are shown in Table 5.2. In almost all the cases, results are well within accuracy of 5%, except for case with value of $\eta_b = 10.0\times10^{-3}\,\mathrm{s}^{-1}$, where a large deviation from its mean value of η_b is there, and the size is estimated 0.5 cm smaller than the actual one.

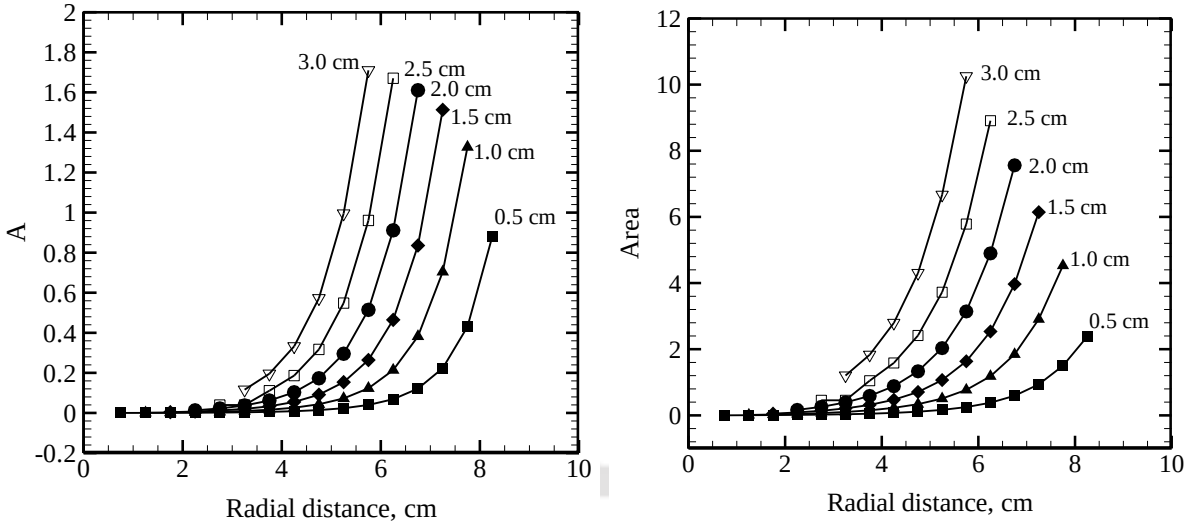

(a) (b)

Figure 5.12 Variation of (a) amplitude (*A*) and (b) *Area* of SS Gaussian temperature profile for wide range of locations and sizes of tumor in 2-D semicircular tissue.

Table 5.1. . Inverse estimated value of location and size of a tumor in 2-D semicircular human breast.

Case No.	Actual			Estimated			Error (%)		
	Size (cm)	Location		Size (cm)	Location		Size	Location	
		r_o (cm)	ϕ (degree)		r_o (cm)	ϕ (degree)		r_o	ϕ
1	1.00	7.00000	90.00000	1.00	6.87796	90.00004	0.00	1.74349	0.00005
2	1.00	7.00000	106.60156	1.00	6.87794	106.60162	0.00	1.74366	0.00006
3	1.00	7.00000	124.84990	1.00	6.87793	124.85065	0.00	1.74393	0.00060
4	1.00	7.00000	148.99728	1.00	6.87619	149.09937	0.00	1.76876	0.06852
5	0.50	3.60555	56.30993	0.50	3.592233	55.33438	0.00	0.36938	1.73247
6	2.00	5.83095	30.96376	2.00	5.81212	30.23985	0.00	0.32290	2.33793
7	3.00	3.64005	74.05460	3.00	3.61751	73.95061	0.00	0.61949	0.14044
8	1.50	4.93356	107.70043	1.50	4.90233	107.71240	0.00	0.63290	0.01111
9	2.50	4.31856	137.81556	2.50	4.27866	138.92943	0.00	0.92398	0.80823
10	0.50	8.15414	113.10633	0.50	8.12061	113.10635	0.00	0.41119	0.00002

Table 5.2. Effect of blood perfusion rate on estimation of size and location of tumor in breast.

Blood perfusion rate $\eta_b\ (s^{-1})$	Actual			Estimated			Error (%)		
	Size (cm)	Location		Size (cm)	Location		Size	Location	
		r_o (cm)	ϕ (degree)		r_o (cm)	ϕ (degree)		r_o	ϕ
3.50×10^{-3}	1.00	7.0000	148.9972	1.00	7.0708	149.1624	0.00	1.01160	0.11082
6.70×10^{-3}	1.00	5.8309	30.9637	1.00	5.6439	30.07617	0.00	3.20658	2.86653
6.70×10^{-3}	2.00	5.8309	30.9637	2.00	5.6662	30.30555	0.00	2.82497	2.12575
8.90×10^{-3}	0.50	5.9363	57.3807	0.50	5.6843	57.36889	0.00	4.24486	0.02068
10.0×10^{-3}	2.50	5.6568	45.00	2.00	5.9281	44.92947	20.0	4.79536	0.15674

5.4.2. 3-D hemispherical breast

For a particular size and location of the tumor inside the breast, uniqueness of the temperature profiles has been observed for the 3-D case too. A study of various parameters of the Gaussian temperature profiles reveals the uniqueness of the distribution. Figure 5.13a and 5.13b, show the variation of *Area* and amplitude A of the Gaussian skin surface temperature distribution for different sizes of the tumor ranging from 0.5 cm to 3.0 cm, located at various radial distances on the centerline $(\theta = 0, \phi = \pi/2)$ of the 3-D breast. The value of the amplitude A and the *Area* under such profiles are found specific for a particular size r_t and location r_o of a tumor. Hence, for a particular set of (r_t, r_T, θ, ϕ) of tissue-tumor configuration, a unique set of $(A, Area)$ has been obtained. Taking into account this uniqueness, similar inverse curve fitting methodology has been used.

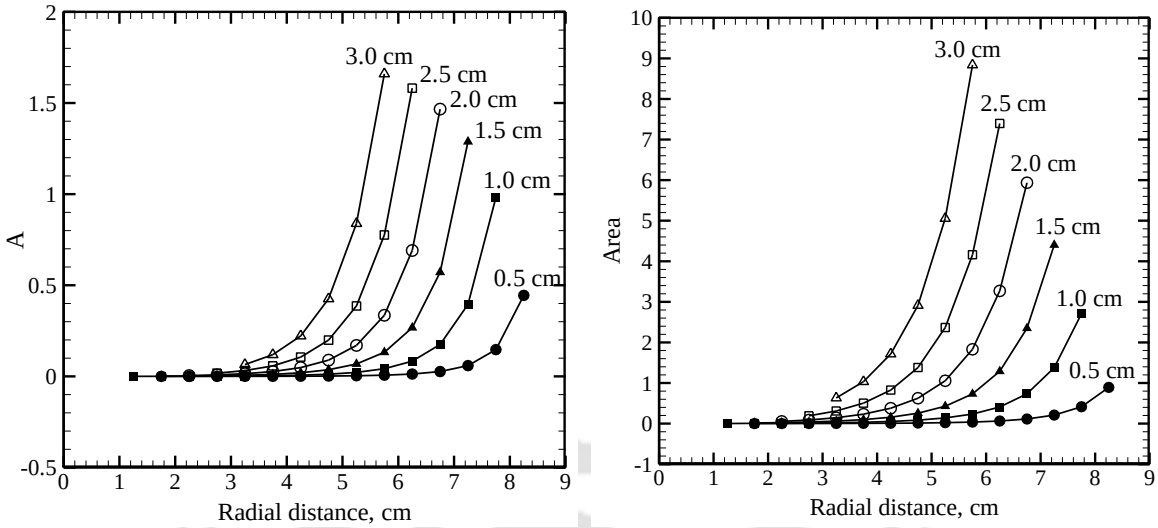

(a) (b)

Figure 5.13 Variation of (a) amplitude, *A* and (b) Area of the Gaussian distribution of temperature for different sizes of the tumor at various radial locations.

The proposed algorithm is based on searching and sorting of the characteristics of the Gaussian skin surface temperature profile of the breast. Therefore, the work starts with building of a database of *Area* and amplitude *A* for various sizes r_t of the tumor, corresponding to particular radial position r_o, located on the centerline $(\theta = 0, \phi = \pi/2)$ of the breast (Fig 5.1a). Study shows that the variation of *A* and *Area* with radial location r_o of the tumor is independent of θ and $\phi-$position of the tumor (Fig. 5.10a and 5.10b). Therefore, a single database works well for all the θ and $\phi-$positions of the tumor.

Skin surface temperature distribution of the breast of any suspected patient is obtained using any state-of-art measurement technique. A Gaussian temperature distribution of the skin surface so obtained, ensures presence of a tumor inside the breast. Figure 5.14a shows a numerically simulated skin surface temperature profile of a breast infected with a tumor, whose size and location are considered unknown. An analysis of the temperature contour of the skin provides the location of maximum temperature on the skin. For the present case, the value of the maximum temperature is 33.61°C, and is found to be located at an angle $\theta =$ 29.74°. Retrieval of the $\theta-$position of the tumor reveals the position of the semicircular plane passing through the center of the tumor (Fig. 5.14b and 5.14c) and the problem is dissolved down to a 2-D semicircular case. Using the

temperature distribution along the circumference of the semicircle (Fig. 5.14c), a Gaussian curve is obtained. An analysis of this curve, using a curve fitting tool is able to give the values of the *Area* and *A* of the plot. Using the developed curve fitting algorithm for the 2-D semicircular case, the values of r_o and r_t have been retrieved. The value of the location of the peak of the temperature profile $\bar{x}_c$ (Fig. 5.11) provides the $\phi-$location of the tumor from the geometrical configuration of the breast (Fig. 5.1b),

$$\phi = \frac{(\pi r_b - \bar{x}_c)\times 180^o}{\pi r_b} \tag{5.2}$$

With a tumor of sizes 0.5 cm, 1.0 cm, 1.5 cm, 2.0 cm, 2.5 cm and 3.0 cm, the database is made for all possible radial locations r_o of the tumor at $\theta = 0$ and $\phi = \pi/2$. Considering, numerically obtained skin surface temperature profiles as the measured temperature, breast tissue with various tumor attributes are studied for estimation of size and location of a tumor, and the results are presented in Table 5.3. With a maximum error of 5.5% in the estimation of location of the tumor, the size of the tumor is estimated with good accuracy (3.45%).

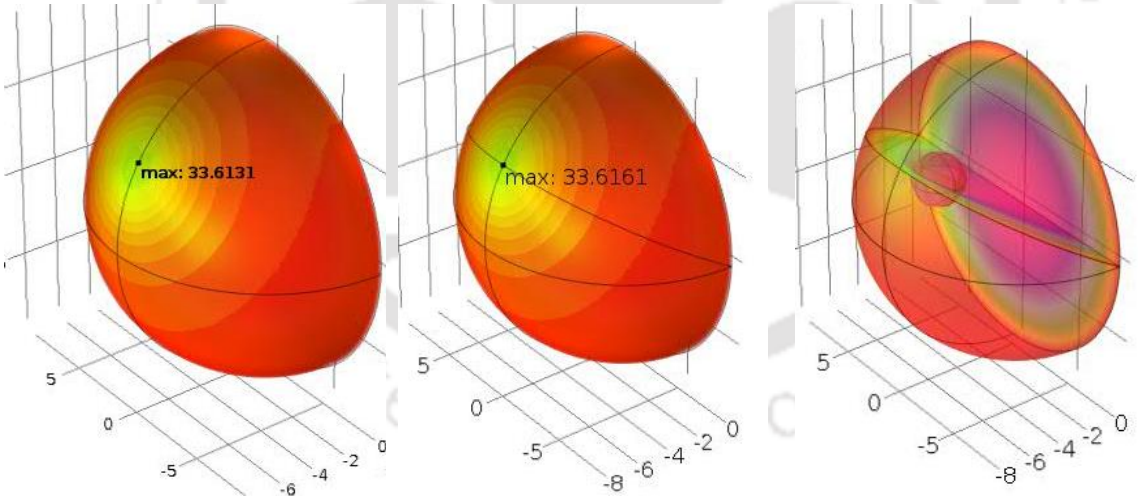

(a) (b) (c)

Figure 5.14 Steady-state temperature contours of the skin surface of the breast with 1.5 cm tumor located at a depth of 3.75 showing (a) the point of maximum surface temperature, (b) the circumferential curve passing through the point of maximum temprature and (c) the virtual semicircular plan subtended on the curve passing through the center of the tumor.

Table 5.3. Inverse estimated values of size (r_t) and location (r_T, θ, ϕ) of a tumor in a breast

Case No.	Actual value				Estimated value				Error (%)			
	r_t	r_T	θ	ϕ	r_t	r_T	θ	ϕ	r_t	r_T	θ	ϕ
1.	1.50	5.25	0.00	90.00	1.50	5.25	0.25	90.00	0.00	0.02	--	0.00
2.	0.51	7.50	-15.95	104.42	0.50	7.65	-16.60	103.89	0.99	1.95	4.10	0.51
3.	1.50	6.05	29.74	90.00	1.50	6.00	30.13	90.02	0.00	0.81	1.31	0.02
4.	1.50	6.37	29.74	69.15	1.50	6.33	30.13	71.64	0.00	0.54	1.31	3.61
5.	2.50	5.77	33.69	66.04	2.50	5.76	35.18	69.67	0.00	0.18	4.42	5.51
6.	2.00	5.77	-23.96	123.69	2.00	5.76	-24.36	121.34	0.00	0.11	1.64	1.90
7.	1.00	7.14	11.31	45.00	1.00	6.82	11.00	44.98	0.00	4.43	2.76	0.03
8.	2.05	6.39	19.03	72.76	2.00	6.40	19.15	73.65	2.44	0.03	0.65	1.22
9.	3.00	4.58	14.04	63.43	3.00	4.34	14.99	63.30	0.00	5.20	6.81	0.21
10.	1.45	6.63	18.43	71.57	1.50	6.50	19.16	72.45	3.45	1.97	3.93	1.24

5.5. Effect of Measurement Error on Inverse Analysis

In the above study, the estimation of tumor attributes are based on the numerically simulated temperature of the skin surface of the breast. It assumes an accurate measurement of temperature, which is slightly difficult in actual practice. With the state-of-art surface measurement techniques it is possible now a days to achieve an accuracy within ±0.75% (National Instruments). Therefore, the study has been extended to introduce a random error of maximum ±1.0% in the simulated temperature, and using it in the estimation of size and location of the tumor inside the human breast.

5.5.1. 2-D semicircular breast

Steady-state temperature distribution of the skin surface of the breast has been shown in figure 5.15 with a random error within ±1%, for the cases as in table 5.1. Using the curve fitting technique, the fitted temperature profile has also been observed to be of Gaussian nature. The analysis of the obtained profiles, using the developed database and the algorithm yields the estimated values of the size and the location of the tumor. Table 5.4 shows the estimated values of all the cases as considered in the table 5.1 with an accuracy in temperature within ±1%. It has been observed that for a smaller size of the tumor (r_t =

0.5 cm), the deviation of the temperature profile is very small. Therefore, the curve fitting tool could not generate a Gaussian profile from the error introduced temperature data. That has made it difficult with the current database to estimate the size and location for a tumor of radius (r_t) less than 1 cm. Similar to the earlier case, the effect of blood perfusion on the estimation of tumor attributes are evaluated. Table 5.5 shows the estimation of size and location of a tumor for different values of blood perfusion rate of the malignancy, as in table 5.2. In all the cases the accuracy of the estimation is well within the acceptable limit and a maximum error of 20% has been observed.

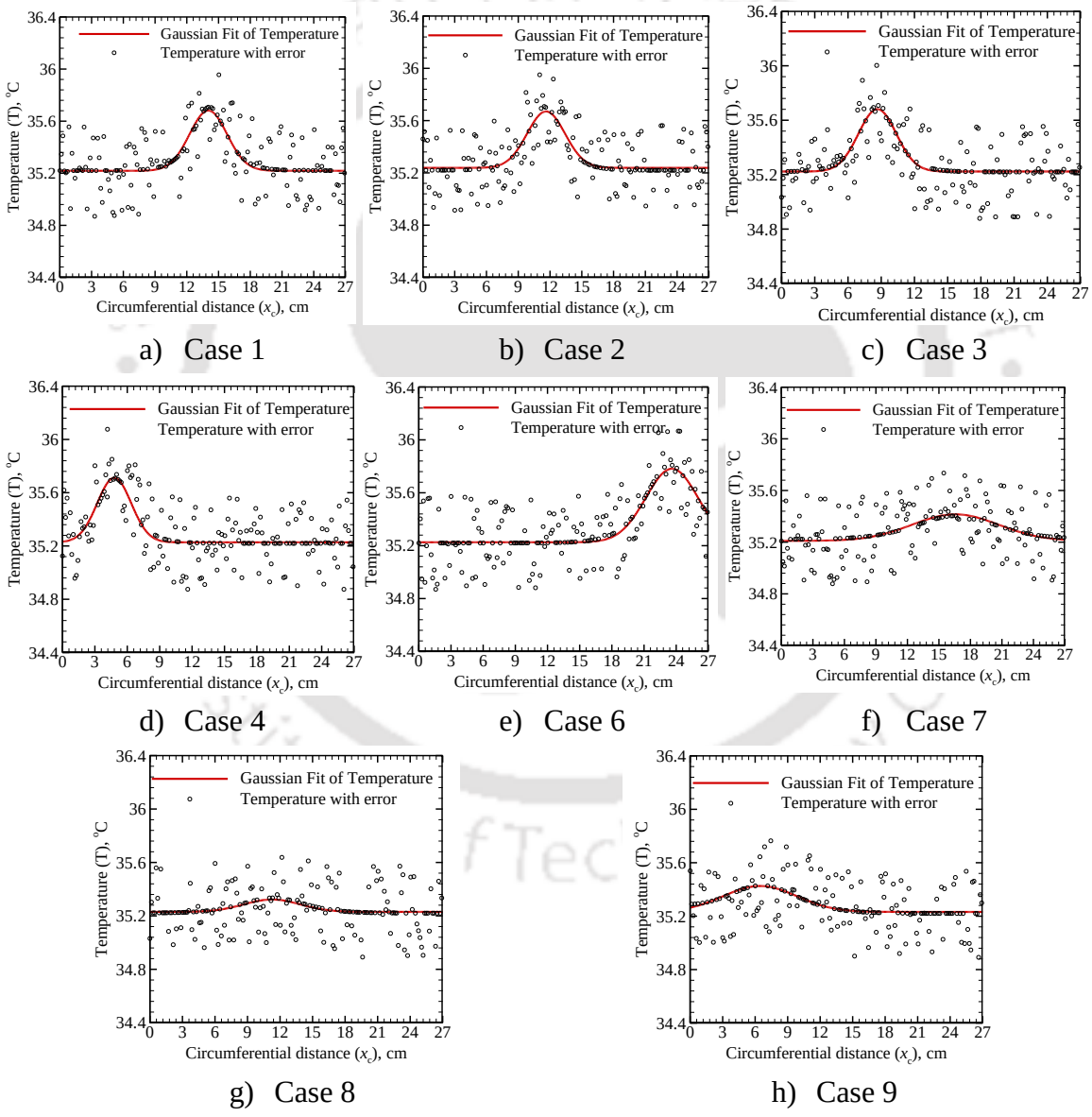

Figure 5.15: Steady-state distributions of temperature along the skin surface of the breast with an accuracy of ±1% for the tissue-tumor configuration as shown in table 5.1.

Table 5.4. Inverse estimated value of location and size of a tumor using skin surface temperature of 2-D human breast with an accuracy of ±1%.

Case No.	Actual			Estimated			Error (%)		
	Size (cm)	Location		Size (cm)	Location		Size	Location	
		r_o (cm)	ϕ (degree)		r_o (cm)	ϕ (degree)		r_o	ϕ
1	1.000	7.000	90.000	1.000	0.079	6.875	0.000	1.783	0.734
2	1.000	7.000	106.602	1.000	1.880	6.563	0.000	2.474	0.575
3	1.000	7.000	124.850	1.000	3.931	5.632	0.000	1.883	0.050
4	1.000	7.000	148.997	0.500	6.728	3.966	50.000	11.571	0.324
5	0.500	3.606	56.310	Could not be estimated					
6	2.000	5.831	30.964	1.500	5.534	3.163	25.000	9.309	3.927
7	3.000	3.640	74.055	2.500	1.151	4.165	16.667	18.722	0.669
8	1.500	4.934	107.700	1.000	1.709	5.173	33.333	10.430	0.537
9	2.500	4.319	137.816	2.500	3.242	2.850	0.000	0.038	0.626
10	0.500	8.154	113.106	Could not be estimated					

Table 5.5. Effect of blood perfusion rate on estimation of size and location of tumor in a breast using skin surface temperature of ±1% accuracy.

Blood Perfusion rate (s^{-1})	Actual			Estimated			Error (%)		
	Size (cm)	Location		Size (cm)	Location		Size	Location	
		r_o (cm)	ϕ (degree)		r_o (cm)	ϕ (degree)		r_o (cm)	ϕ (degree)
3.50×10^{-3}	1.000	7.000	148.997	1.000	7.066	148.977	0.000	0.945	0.014
6.70×10^{-3}	1.000	5.831	30.964	1.000	5.742	27.972	0.000	1.534	9.662
6.70×10^{-3}	2.000	5.831	30.964	2.000	5.751	31.191	0.000	1.372	0.735
8.90×10^{-3}	0.500	5.936	57.381	Could not be estimated					
10.0×10^{-3}	2.500	5.657	45.000	2.000	5.932	45.666	20.000	4.862	1.480

5.5.2. 3-D hemispherical breast

Similar to the 2D case, in a 3-D hemispherical breast too, the accuracy of inverse estimated values parameters depends on the accuracy of the measured temperature profile. In real practice, measurement of any quantity with 100% accuracy is not possible. Same is the case with temperature too. Thus, the effect of temperature measurement error on the estimation of tumor attributes in a 3-D human breast is also evaluated. Figure 5.16

shows the steady state temperature distribution of the skin surface of the breast with a random error within ±0.75%, initially for the four cases as in table 5.3. Using the curve fitting technique, the fitted temperature profile has been found to be of Gaussian nature. The analysis of the obtained profiles, using the developed database and the algorithm yields the estimated values of the size and the location of the tumor. Considering an accuracy in temperature within ±0.75%, table 5.6 shows the estimated values for the cases 2, 4, 7 and 8 as considered in the table 5.3. With an accuracy of estimation of location well below 20%, the size of the tumor is estimated 0.5 cm lesser than the actual value for case 7 (table 5.6). It has been observed that introduction of an error deviates the temperature profiles from its ideal situation (0% error), especially for a smaller size of the tumor (r_t = 0.51 cm). Therefore, even after obtaining Gaussian profile from the curve fitting, the solver could not estimate the attributes of the tumor. That has made it difficult with the current database to estimate the size and location for a tumor of radius (r_t) less than 1 cm.

The analysis has also been carried out with a measurement error of ±1% (Fig. 5.17) for the cases 1, 3, 5 and 6. The obtained estimation of location of the tumors for these cases are well below 11% and the sizes are estimated accurately (table 5.7). The accuracy of the estimation can be further improved by considering more sizes of tumor while making the database. Only with the knowledge of the skin surface temperature profile, the proposed CFM simultaneously estimates size and location with good accuracy. The method is found remarkably fast in terms of computation, and a single run of the proposed method can estimate size and location of the tumor in a breast within 0.1 s on a 32 bit intel processor with 1.6 GHz clock speed and 2GB RAM.

In the current approach, using the breast skin surface temperature profile, the size and the location are estimated without the knowledge of any thermophysical property of the tissue and the tumor. Unlike the GA (Das and Mishra, 2013), in the present approach of the CFM do not require solution of the governing equation (Eq. 3.6). Hence, the method is exceedingly fast in terms of computation.

Table 5.6. Inverse estimated value of location (r_T, θ, ϕ) and size (r_t) of a tumor using skin surface temperature of 3-D human breast with an accuracy of ±0.75%.

Case No.	Actual				Estimated				Error (%)			
	Size	Location			Size	Location			Size	Location		
	(r_t)	r_T	θ	ϕ	(r_t)	r_T	θ	ϕ	(r_t)	r_T	θ	ϕ
2	0.51	7.50	-15.95	104.42	Could not be estimate							
4	1.50	6.37	29.74	69.15	2.000	5.591	30.133	71.977	33.33	12.210	1.306	4.095
7	1.00	7.14	11.31	45.00	0.500	7.981	10.998	45.082	50.00	11.761	2.757	0.183
8	3.00	4.58	14.04	63.43	3.000	4.359	14.992	65.616	0.00	4.872	6.812	3.439

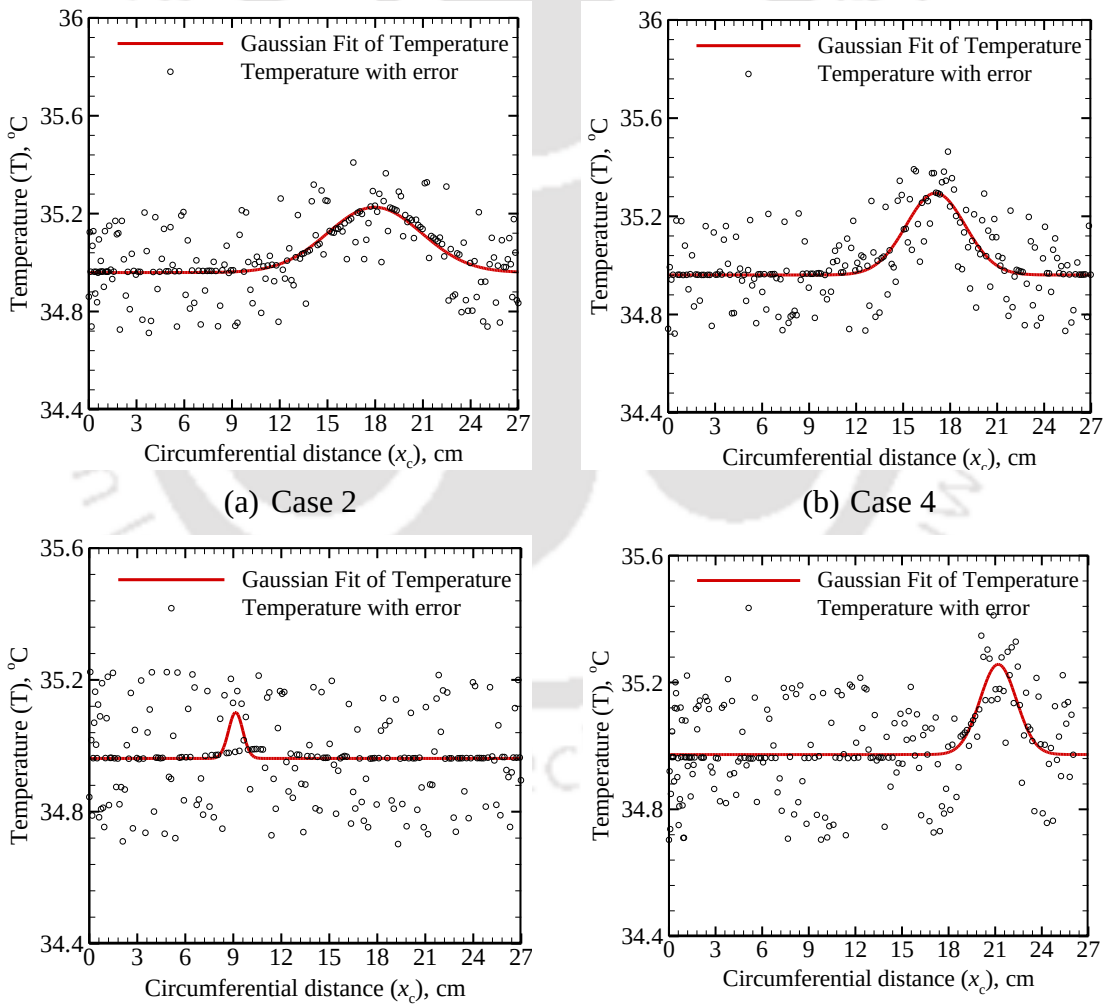

Figure 5.16: Steady-state distributions of temperature along the skin surface of the breast with an accuracy of ±0.75% for the tissue-tumor configuration as shown in table 5.3.

Table 5.7. Inverse estimated value of location (r_T, θ, ϕ) and size (r_t) of a tumor using skin surface temperature of 3-D human breast with an accuracy of ±1%.

Case No.	Actual				Estimated				Error (%)			
	Size	Location			Size	Location			Size	Location		
	(r_t)	r_T	θ	ϕ	(r_t)	r_T	θ	ϕ	(r_t)	r_T	θ	ϕ
1	1.50	5.25	0.00	90.00	1.500	5.223	0.246	91.708	0.000	0.518	--	1.898
3	1.50	6.05	29.74	90.00	1.500	5.895	30.134	93.273	0.000	2.503	1.307	3.637
5	2.50	5.77	33.69	66.04	2.500	5.758	35.181	69.615	0.000	0.147	4.425	5.417
6	2.00	5.77	-23.96	123.69	2.000	5.184	-24.356	120.862	0.000	10.106	1.640	2.287

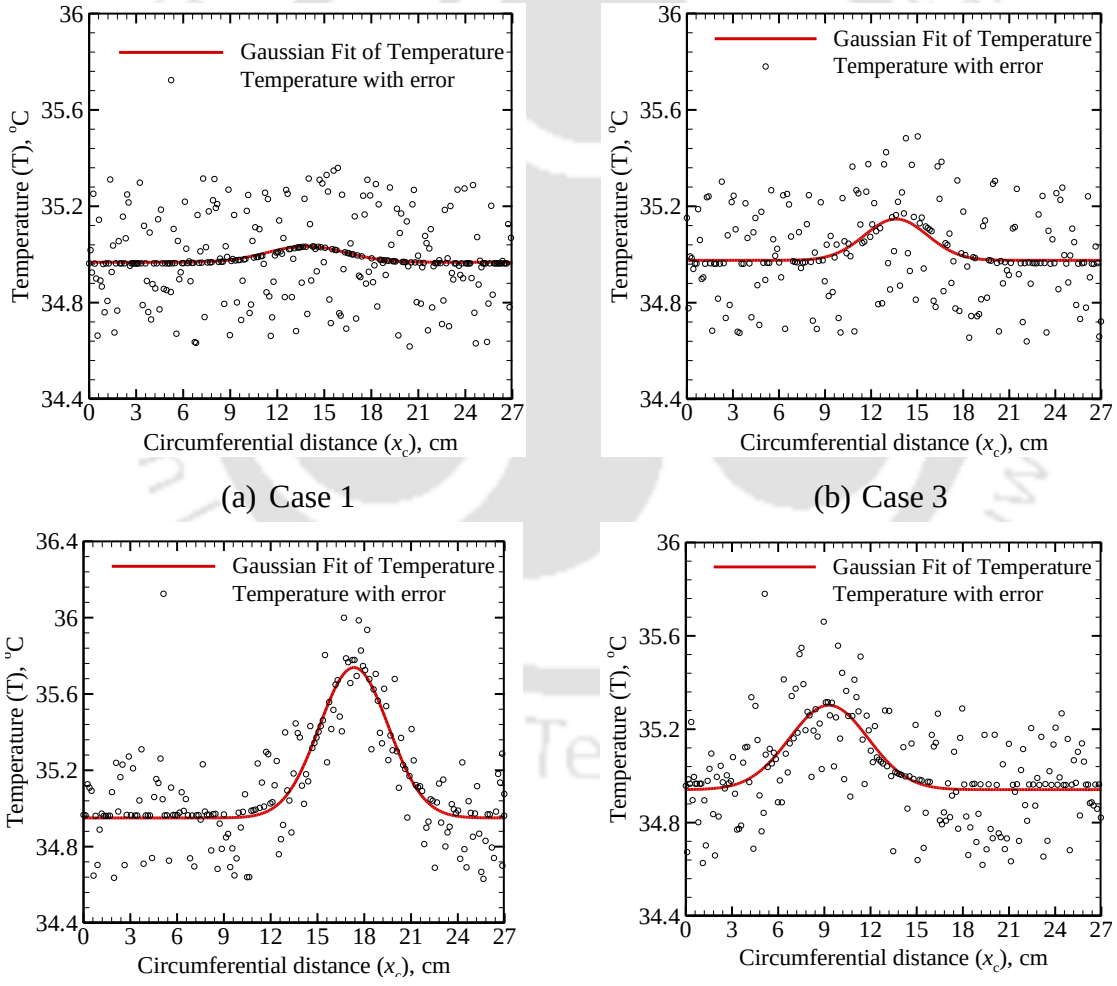

(a) Case 1 (b) Case 3

(c) Case 5 (d) Case 6

Figure 5.17: Steady-state distributions of temperature along the skin surface of the breast with an accuracy of ±1% for the tissue-tumor configuration as shown in table 5.3.

5.6. Summary

The size and the location of the tumor inside a human breast was estimated noninvasively considering a semicircular section of a breast as well as a 3-D hemispherical model. The PBHE was solved to study a numerically assumed semicircular and hemispherical geometry of breast. A good match of the SS temperature distributions along the centerline and the skin surface of the breast supported the simplification of a 3-D hemispherical model to a 2-D semicircular one. The results were also validated with experimental data. Irrespective of the size, angular and radial locations of the tumor, the skin surface temperature profiles were found to be Gaussian. In terms of the amplitude and the area, these profiles were specific to a particular combination of size and location of the tumor. A comprehensive database of amplitude (A) vs. radial location (r), and area $(Area)$ vs. radial location (r), became the basis of simultaneous estimation of size and location of the tumor using the curve fitting technique. An accurate estimation was obtained. Once the database was available, the proposed technique did not require solution of the governing energy bioheat equation, and thus, computationally, the approach was found very fast. The technique is also tested for any skin surface temperature with random measurement errors within ±0.75% and ±1%, for various cases. An estimation with good accuracy has been obtained.

CHAPTER 6

EQUIVALENCE OF PENNES AND WULFFS' MODELS

Human body is a complicated system, and that too when we talk of heat transfer in it, the analysis becomes complex. To relate blood flow and heat transfer in a living tissue, in 1948, Pennes proposed the first constitutive relationship between temperature and the blood flow rate. This relation is based on experimental analysis, and it has been assumed that, heat transfer between the tissue and the blood takes place only in the capillaries. To simplify his continuum approach, he neglected the effect of large blood vessels (Wissler, 1998; Shih et al., 2007).

In the year 1974, Wulff directly criticized the assumptions of Pennes, and provided an alternate model (1974). According to Wulff, the shortcomings in Pennes bioheat equation are (a) inappropriate combination of energy storage, heat diffusion and metabolic heat generation rate with convection term due to blood perfusion in a control system, (b) wrong consideration of three temperatures: tissue, inlet and outlet blood stream at the same point in the tissue, (c) ignorance of all intra- and extra- cellular bio-fluids in motion that are capable to convect heat in any direction and (d) assigning zero temperature difference between stationary tissue and bio-fluids. Wulff also argued that the isotropic perfusion term that appeared in the PBHE was unable to take care of the convective heat transfer by the flowing blood (Wulff, 1974). Hence, instead of blood perfusion rate in the PBHE, Wulff proposed a new bioheat model known as Wulff continuum model (WCM) which utilizes local mean blood velocity in a tissue in a particular direction.

Use of the PBHE and the WCM needs the knowledge of blood perfusion rate and blood velocity, respectively. Blood flow is a very important physiological parameter, and is also very difficult to measure without invasion. Positron emission tomography (PET) is one of the few techniques used for measurement of blood perfusion rate, which is popularly used now-a- days. Low resolution images and poor ability to detect small lesions in tissues are the main drawbacks of the standard PET. Hence, it is combined with computed tomography (CT) to have better accuracy (Griffeth, 2005).Use of Doppler ultrasound is one of the ways to measure the blood velocity in a particular blood vessel. This technique is again limited by phenomenon like aliasing etc. Direct measurement of these quantities is not possible due to complicated structure of living tissue without invading it, and needs instrumentation with state-of-the-art technology. In the present work, an effort has been made to derive a mathematical relation between the blood perfusion rate and the blood flow velocity in a 1-D tissue. Numerical analysis has also been done to substantiate the derived relation.

6.1. The $v-\eta_b$ Relation

In the present study, consideration is given to a 1-D planar tissue (Fig. 6.1a). Initially, the tissue is considered to be at the effective temperature $T(x,0)=T_e$. For time $t>0$, its inner $(x=0.0)$, i.e., its core body, and the outer $(x=L)$ boundaries, i.e., the skin surface, have isothermal conditions of $T(x=0,t)=T_a$ and $T(x=L,t)=T_f$, respectively. The boundary conditions considered are subjected to change for various cases. The thermo-physical properties, such as the density ρ, the specific heat c_p, the thermal conductivity k, the blood perfusion rate η_b, the volumetric metabolic heat generation rate Q_m are tissue and tumor specific. For any particular case, the temperature in the tissue is low, and it varies over a small range of 30°C - 40°C. Thus, the thermo-physical properties like ρ, c_p, k and η_b are considered independent of temperature. The volumetric metabolic heat generation rate Q_m is also independent of temperature. With ρ_b as density of the blood, c_{pb} as the specific heat of the blood, T_a as the temperature of the arterial blood, the heat transfer in the tissue governed by PBHE (Pennes, 1948) is given by

$$\rho c_p \frac{\partial T}{\partial t} = k \frac{\partial^2 T}{\partial x^2} + \eta_b \rho_b c_{pb} \left(T_a - T \right) + Q_m \tag{6.1}$$

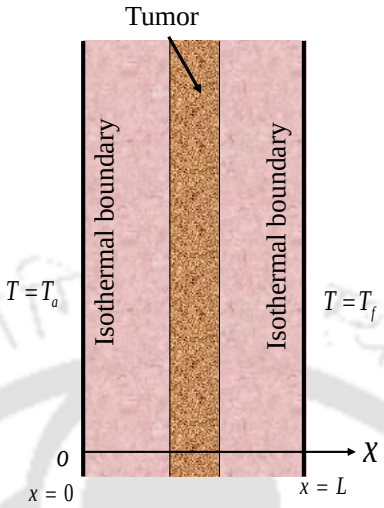

(a)

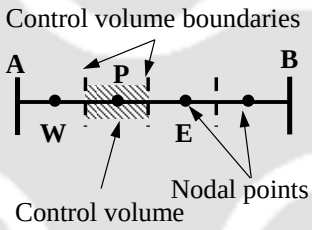

(b)

Figure 6.1 Schematic of 1-D (a) tissue with a tumor and (b) FVM grid used in the analysis.

Instead of blood perfusion rate, considering blood velocity in a tissue, in 1974, Wulff (1974) proposed a new bioheat model. This is given by

$$\rho c_p \frac{\partial T}{\partial t} = k \frac{\partial^2 T}{\partial x^2} - \rho_b c_{pb} v \frac{\partial T}{\partial x} + Q_m \tag{6.2}$$

Apart from the common thermo-physical properties in the PBHE (Eq. 6.1) and WCM (Eq. 6.2), the blood perfusion rate η_b is needed for the solution of Eq. (6.1), whereas the blood velocity v is required for the solution of Eq. (6.2). In order to solve the bioheat models given by Eq. (6.1) and Eq. (6.2), both the equations are normalized using the non-dimensional parameters for length X, time τ and temperature θ, ase mentioned in section 3.3.

The normalized form of the PBHE and the WCM are given by Eq. (6.3) and (6.4), respectively

$$\frac{\partial \theta}{\partial \tau} = \frac{\partial^2 \theta}{\partial X^2} - A_p \theta + B_p \tag{6.3}$$

$$\frac{\partial \theta}{\partial \tau} = \frac{\partial^2 \theta}{\partial X^2} - A_w \frac{\partial \theta}{\partial X} + B_w \tag{6.4}$$

wherein Eqs. (6.3) and (6.4), the non-dimensional coefficients A_p, A_w, B_p and B_w are the following:

$$A_p = \frac{\eta_b \rho_b c_{pb} L^2}{k} \tag{6.5}$$

$$A_w = \frac{\rho_b c_{pb} V L}{k} \tag{6.6}$$

$$B_p = B_w = \frac{Q_m L^2}{k\left(T_f - T_a\right)} \tag{6.7}$$

Thermally, a tissue has to always behave the same whether it follows PBHE or WCM. The main objective of the current work is to find out the equivalence between the PBHE and the WCM for 1-D planar tissue in order to relate blood perfusion rate and blood velocity. Hence, to have the same temperature profile, following Eq. (6.3) and Eq. (6.4), the second term in the RHS of the two equations must be equal. This equality leads to the following relationship:

$$A_w \frac{d\theta}{dX} = A_p \theta \tag{6.8}$$

Solution of Eq. (6.8) yields,

$$\theta = Ce^{X\left(A_p / A_w\right)} \tag{6.9}$$

where C is an arbitrary constant and can be found from the boundary condition.

With metabolic heat generation rate $Q_m = 0$, the terms B_p and B_w in Eq. (6.7) also become zero. In this case, substitution of temperature θ from Eq. (6.9) in Eq. (6.3) and Eq. (6.4) yields

$$A_p = A_w^2 \tag{6.10}$$

From Eqs. (6.5), (6.6) and (6.10), the blood perfusion rate η_b and blood velocity v can be related as

$$v = \sqrt{\frac{k\eta_b}{\rho_b c_{pb}}} \tag{6.11}$$

With $A_p = A_w^2$, the PBHE (Eq. 6.3) and WCM (Eq. 6.4) become equivalent. To prove this equivalence, Eqs. (6.3) and (6.4) are solved. These equations are solved for the SS condition. In the numerical solution, the approach of the FVM (Versteeg and Malalasekera, 1995) is adopted. The relation as shown in Eq. 6.11 is derived without taking into account the type of boundary conditions, to which the domain (Fig. 6.1a) is subjected. Hence, the equivalence is also shown for the cases with different boundary conditions. The computational grid is shown in Fig. 6.1b. Beyond 50 control volumes, no change in temperature profile was observed.

6.2. Comparison of Numerical Results with Experimental Data

Validation of the developed solver for solution of PBHE is done prior to numerical establishment of the relation given by Eq. (6.10) and Eq. (6.11), and has been shown in chapter 4. Use of the derived relation and its applicability in actual practice is also checked by numerically solving the governing equations (Eqs. 6.3 and 6.4). The effect of boundary conditions and the assumption taken while establishing the relations (Eq. 10) is justified, in this study.

Gautherie (1980) has carried out experiments on a good number of patients having breast cancer. The in-vivo analysis done on patients of different age groups resulted in estimation of thermal conductivity, blood flow rate and metabolic heat generation rate of healthy and cancerous breast tissues. The same work has reported measurement of local

temperature along the depth of the breast. The study was carried on 147 patients. In the present study, a numerical modeling of a 3-D breast is done in COMSOL 4.3a and the results are compared with the experimental data reported in the literature (Gautherie, 1980).

A 3-D model of human breast in the form of a hemisphere is considered as shown in Fig. 5.1a. A hemisphere of radius 9 cm is considered in order to accommodate breast sizes of most of the patients of different age groups, as reported in Gautherie (1980). A spherical tumor of size $(2r_t)$ 2.3 cm is placed at a distance of 2 cm from skin surface. The base of the hemisphere is considered adiabatic and the skin surface is exposed to environmental convective boundary condition with heat transfer coefficient of $h = 5\ \mathrm{Wm^2K^{-1}}$ and ambient temperature of $T_f = 21\,^{\circ}\mathrm{C}$ as maintained by Gautherie during his experiment. Various thermophysical properties of breast and blood considered in this validation are: $\rho = 920\,\mathrm{kg\,m^{-3}}$, $\rho_b = 1052\,\mathrm{kg\,m^{-3}}$, $k = 0.42\ \mathrm{Wm^{-1}K^{-1}}$, $c_p = 3000\ \mathrm{J\,kg^{-1}K^{-1}}$, $c_{pb} = 3800\ \mathrm{J\,kg^{-1}K^{-1}}$; for normal tissue $\eta_b = 0.00018\,\mathrm{s^{-1}}$ and for the tumor $\eta_b = 0.009\,\mathrm{s^{-1}}$ and the metabolic heat generation rate for both the cases are $Q_m = 450\ \mathrm{Wm^{-3}}$ and $Q_m = 29000\ \mathrm{Wm^{-3}}$, respectively (Gore, 2003).

A human breast is non-homogenous in nature. It comprises of different kinds of tissues, layers of fats, lymphatic glands, and blood capillaries. In the PBHE, the non-homogeneity of the breast tissues is neglected, and the tissue and the tumor are considered homogenous. Temperature along the centerline $(0, y, 0)$ of the hemispherical breast without and with a tumor are compared against the experimental data reported by Gautherie (1980) in Figs. 6.3a and 6.3b, respectively. In the absence of a tumor, results of the present work compare exceedingly well with the experimental results reported by Gautherie (1980).With a tumor inside the breast, expect near the tumor, the comparison is reasonably well.

Having validated the numerical results for the 1-D planar tissue without a tumor with 1-D results of Zhang (2008) and for a 3-D breast tissue with and without a tumor with Gautherie (1980), next it has been checked how closely the 1-D planar assumption matches with the actual case. It is to be noted that owing to the uniform thermal

condition along the skin surface and also along the core body, mathematically 3-D breast tissue (Fig. 5.1a) is in fact 1-D. In the planar tissue, the area is constant along the depth. However, in a 3-D hemispherical tissue (Fig. 5.1a), the area varies along the radial direction. With boundary conditions for 1-D planar tissue the same as that for the 3-D breast tissue geometry, temperature distributions obtained by solving PBHE (Eq. 6.1) with and without a tumor are compared against the experimental data for 3-D case in Figs. 6.2a and 6.2b, respectively. In the absence (Fig. 6.2a) and also in the presence of a tumor (Fig. 6.2b), results of the 1-D case follows the trend of the 3-D case. The maximum temperature difference is approximately $2\,^{o}$C. 1-D planar model overestimates the temperature. An observation of Figs. 6.2a and 6.2b shows that in the presence of a tumor, at any location, temperature is more. This is also well evident for the 1-D planar tissue.

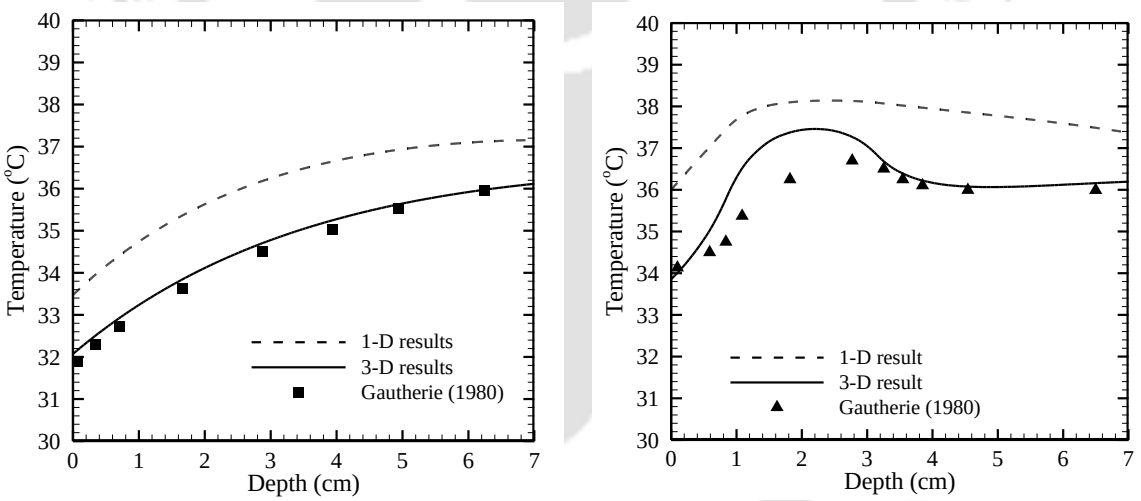

Figure 6.2 Comparison of 3-D numerical and experimental data for a human breast (a) without and (b) with tumor showing the closeness of the results with a 1-D planar geometry.

6.3. Numerical Validation of the $\nu - \eta_b$ Relation

With the numerical approach validated against the benchmark experimental results, next the equivalence of PBHE and WCM are establish. The non-dimensional temperature for the 1-D planar tissue (Fig. 6.1a) is calculated using PBHE and the WCM. Considering

different values of A_p and A_w, maintaining the relation $A_p = A_w^2$ leads to same temperature profile for the 1-D geometry of a healthy tissue (Fig. 6.3). Boundary conditions used are the same as mentioned in the formulation. Figure 6.3 shows the non-dimensional temperature profile of θ against normalized length X for values of A_w = 4, 5, 6 and 10. The corresponding values of A_p are 16, 25, 36 and 100, respectively. Results for these 4 cases are shown in Figs. 6.3a - d. A very a good match is observed between the PBHE and the WCM.

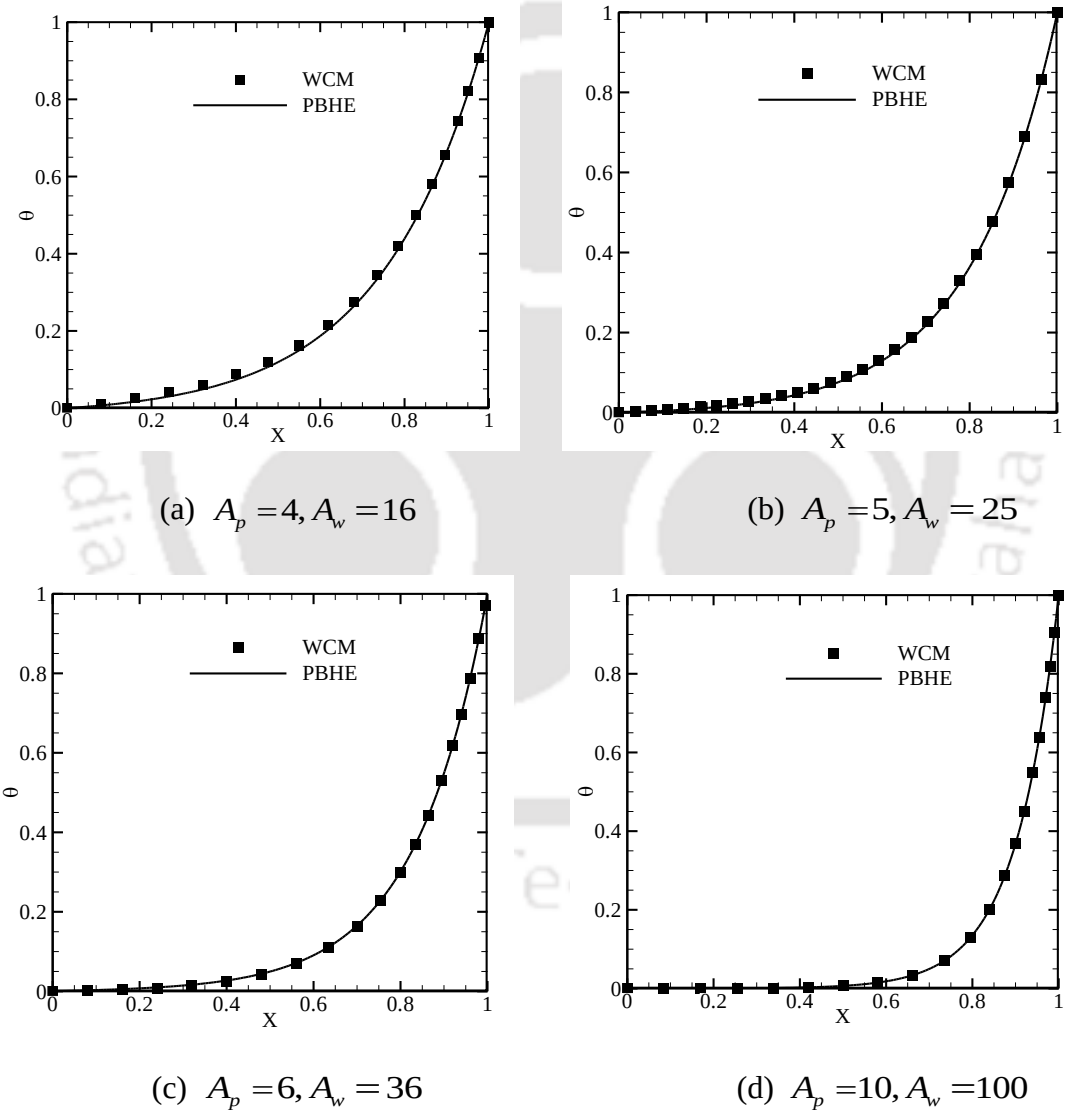

Figure 6.3 θ vs. X profile of 1-D geometry of tissue showing equivalence of PBHE and WCM.

6.4. Calculation of Local Mean Blood Velocity

The most important assumption in the derivation of the relation $A_p = A_w^2$ is that the metabolic heat generation rate $Q_m = 0$. Hence, to use this relation in practical cases, the calculation of the local mean blood velocities is questionable. In order to check the practicability of the assumption $Q_m = 0$, four different conditions of tissues are studied as mentioned below, and temperature *T* along the thickness of 1-D planar tissue is plotted. The four cases considered are shown in Table 6.1 (Gautherie, 1980).

Table 6.1. Values of blood perfusion rate and metabolic heat generation rate for different cases breast tissue (Gautherie, 1980).

Case	Blood perfusion rate $\eta_b\,(\mathrm{s}^{-1})$		Metabolic heat generation rate $Q_m\,(\mathrm{Wm}^{-3})$	
	Tissue	Tumor	Tissue	Tumor
1	0.00018	--	0.0	--
2		--	450.0	--
3		0.009	0.0	0.0
4		0.009	450.0	29000

For the four cases (Table 6.1), the PBHE is solved for the 1-D planar tissue (Fig. 6.1a). Temperature distribution profiles are shown in Fig. 6.4. The thickness of the tissue is 0.04 m, and both the boundaries are maintained at isothermal condition as mentioned in the formulation. For the case of a healthy tissue (cases 1 and 2), with and without metabolic heat generation, both the profiles remain almost the same. Hence, for a normal breast tissue, the relation $A_p = A_w^2$ can be used to relate the PBHE and the WCM. From the known blood perfusion rate, one can estimate the local mean blood velocity needed in the WCM. In the present work, with $\eta_b = 0.00018\,\mathrm{s}^{-1}$, the resulting local mean blood velocity is $4.744\times10^{-3}\ \mathrm{mm}\cdot\mathrm{s}^{-1}$. It is seen from the Fig.6.4 that the temperature profiles in the tissue

with a tumor with (Case 4) and without (Case 3) metabolic heat generation are also closely matching. Hence, in the tumor, the local mean blood velocity is found to be $0.0336\,\text{mm}\cdot\text{s}^{-1}$ from Eq. (6.11).

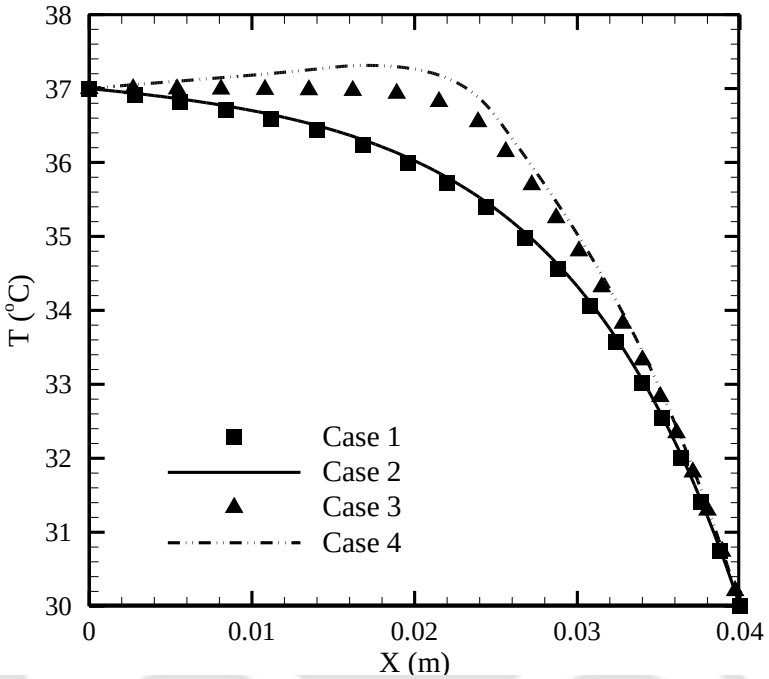

Figure 6.4 Temperature profile for 1-D tissue geometry for different cases of having tumor and no tumor condition with and without metabolic heat generation.

6.5. Effect of Boundary Conditions

The relation $A_p = A_w^2$, worked out to relate local mean blood velocity and the blood perfusion rate (Eq. 6.11) has been derived without taking into account of the type of boundary condition the domain is subjected to. Hence, the relationship is applicable to any condition at the boundaries. In order to establish the fact, the 1-D domain of the tissue is exposed to different boundary conditions of constant temperature and constant heat flux. Figure 6.3 has already explained equivalence of both the bioheat models for isothermal conditions at both the boundaries. Under constant heat flux at east boundary of the domain Figs. 6.5a and 6.5b shows equivalence of both the models for $q^* = 1$. Same is shown in Figs. 6.5c and 6.5d for $q^* = -1$ with different values of A_p and A_w.

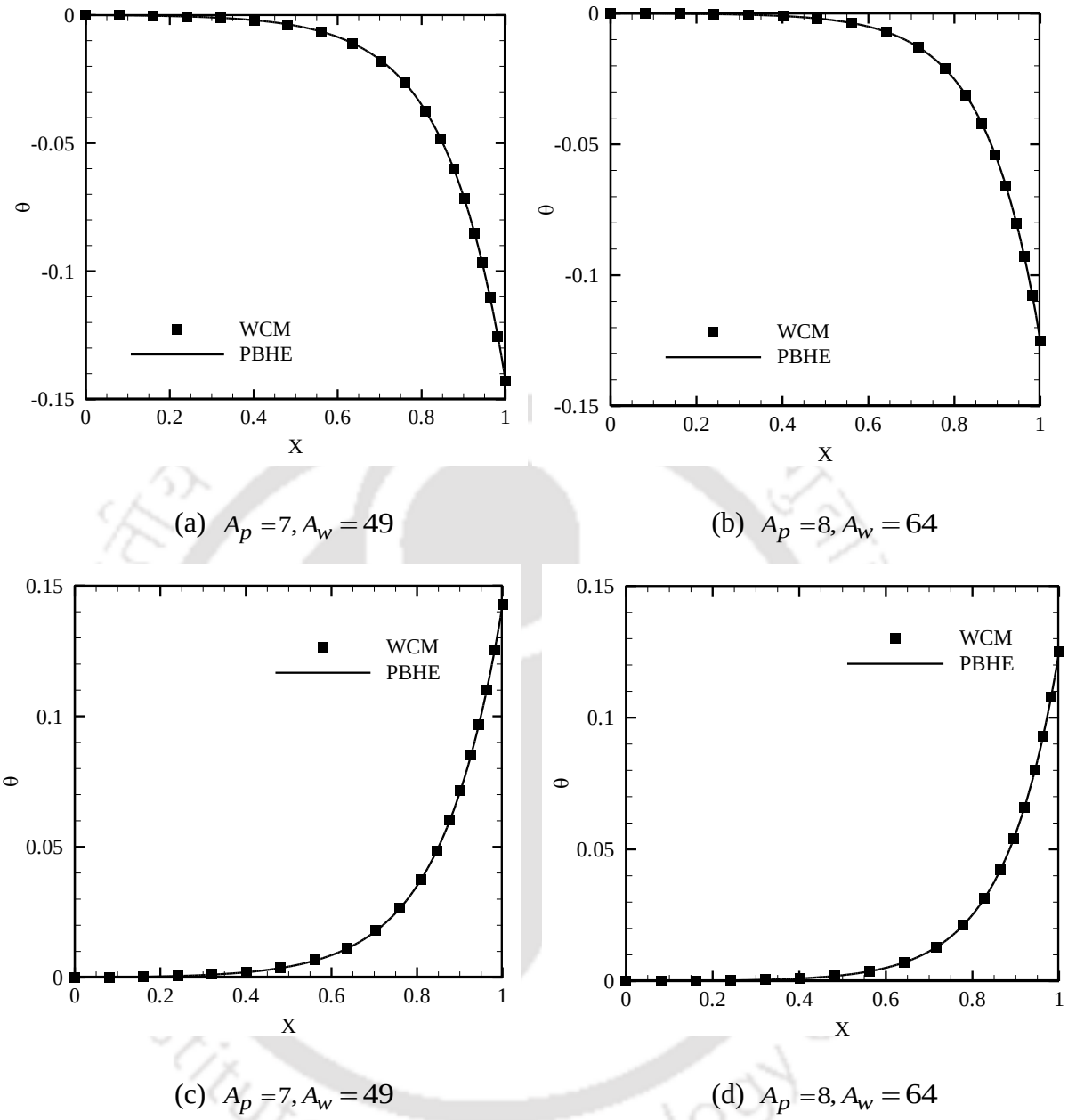

(a) $A_p = 7, A_w = 49$ (b) $A_p = 8, A_w = 64$

(c) $A_p = 7, A_w = 49$ (d) $A_p = 8, A_w = 64$

Figure 6.5 Temperature (θ) distribution along the length (X) of the 1-Ddomain of tissue showing equivalence of PBHE and WCM with heat flux of strength (a, b) $q^* = 1$ and (c, d) $q^* = -1$ on the east boundary.

6.6. Summary

Heat transfer in a breast tissue with and without a tumor was considered. The study was done with both PBHE and WCM considering a 1-D planar tissue. The equivalence of the

PBHE and WCM was shown by expressing the local mean blood velocity in the tissue as a function of blood perfusion rate. Temperature distributions obtained by solving the PBHE were benchmarked against the numerical results available in the literature. Also, the results of the present work for a 3-D hemispherical tissue were compared with the experimental results available in the literature. In all cases, a good match was obtained. Validity of the 1-D planar model was checked against the experimental results of the hemispherical (3-D) tissue. The very assumption of zero metabolic heat generation rate used in the derivation of the equivalence of the PBHE and WCM had no significant effect on temperature distribution that obtained with its consideration in the governing bioheat equation. The derived expression was also found to be independent of boundary conditions the tissue was subjected.

CHAPTER 7

CONCLUSIONS AND SCOPE OF FUTURE WORK

Presence of a tumor affects the natural temperature profiles of the breast. It is due to the difference in the thermo-physical properties of the cancerous tissues with that of normal ones. Thermophysical properties like blood perfusion rate and metabolic heat generation rate are much higher in malignant tissues compared to a healthy one. A study has been done on the human breast taking into account of a 2-D rectangular domain of the tissue. The PBHE has been solved using the FVM. The solver developed is validated, and the temperature profiles of the skin surface of the breast are analyzed considering tumors of different sizes, located at various positions. A precise measurement of temperature in such a breast tissue has been found helpful in estimation of the size and the location of the tumor, if present. The GA has been employed in the inverse analysis of the skin surface temperature profile of the 2-D breast to retrieve various parameters of the tumor. With a simultaneous estimation of blood perfusion rate, and the location of the tumor, GA has been found time consuming. With an aim to simplify the optimization procedure of the skin surface profile of the breast, an algorithm based on curve fitting has been proposed. Irrespective of the tumor size and location of the tumor, the skin surface temperature profile has been found to be a Gaussian one. For a particular tissue-tumor configuration, the Gaussian skin temperature profile was unique. This uniqueness has been in the form of the area under the curve and the amplitude of the profile. For a 2-D rectangular tissue, the algorithm has been found very efficient.

For thermal analysis of a human breast, a 2-D rectangular tissue domain is a simplified case. In order to extend the work towards a realistic scenario, the PBHE has been solved using FEM for a 2-D semicircular and the 3-D hemispherical model of the breast. For both the cases, the circumferential skin surface temperature has been found to be Gaussian. An application of the newly proposed algorithm retrieves the four unknown parameters, viz., size, radial location, two angular positions of the tumor simultaneously with good accuracy; and the method has been found to be exceedingly fast. As the estimation of the tumor attributes has been based on merely the skin surface temperature profile, the method proved to be non-invasive in nature.

Application of the WCM in any biological system required mean blood velocity of the system. Its measurement has been a difficult task. In order to calculate the mean blood velocity from the knowledge of the blood perfusion rate, an equivalence of the PBHE and the WCM was developed. Validity of the equivalence was tested for a 1-D planar tissue, and it was found to be correct. In deriving the equivalence of the PBHE and the WCM, it was found that the mean blood velocity of a tissue was directly proportional to square root of the blood perfusion rate. The derived relation was found independent of the boundary conditions the tissue was subjected.

7.1 Future Scope

In the present work, skin surface temperature profiles are used to detect cancer in a breast using the newly proposed algorithm (i.e., CFM). The work can be extended for an in-vivo analysis to check the applicability of the method. In a human breast, the grade of a tumor is decided by the rate of growth of the cells in it. An effort can be made to detect the grade of the tumor too. Though, the current work has mainly focused on human breast, the CFM may be explored to find its applicability in other tissues with tumors of random shape in the human body.

References

Agnelli, J.P., Barrea, A. A., Turner, C.V., 2011a, Tumor location and parameter estimation by thermography. *Mathematical and Computer Modelling.* 53, 1527–1534

Agnelli, J.P., Padra, C., Turner, C.V., 2011b. Shape optimization for tumor location. *Comput. Math. Appl.* 62, 4068–4081

Ahmadikia, H., Fazlali, R., Moradi, A., 2012. Analytical solution of the parabolic and hyperbolic heat transfer equations with constant and transient heat flux conditions on skin tissue. *Int. Commun. Heat Mass Transfer.* 39, 121–130.

Amri, A., Saidane, A., Pulko, S., 2011. Thermal analysis of a three-dimensional breast model with embedded tumour using the transmission line matrix (TLM) method. *Comput. Biol. Med.* 41, 76–86.

Arkin, H., Xu, L.X., Holmes, K.R., 1994. Recent developments in modeling heat transfer in blood perfused tissues, *IEEE Trans. Biomed. Eng*. 41, 97-107.

Bellil, M., Bennaoum, M., 2013. TLM modelling of Laser thermal treatment of benign prostate hyperplasia, *International Conference on Control, Engineering & Information Technology*, 4, 62-66.

Bezerra, L.A., Oliveira, M. M., Rolim T. L., Conci, A., Santos, F. G. S., Lyra, P.R.M., Lima, R.C. F., Estimation of breast tumor thermal properties using infrared images. *Signal Process*, Available from: doi: 10.1016/j.sigpro.2012.06.002 [Accessed 25th January, 2013].

Bhowmik, A., Singh, R., Repaka, R., Mishra, S.C., 2013. Conventional and newly developed bioheat transport models in vascularized tissues: A review. *J. Therm. Biol.* 38,107–125.

Byrns, G. E., Ciacco, K. H. P., Shands, L. A., Fennelley, K. P.,McCammon C. S., Boudreau, A. Y., Breysse, P. N., and Mitchell, C. S., 2000. Chemical Hazards in Radiology, *Appl Occup Environ Hyg*, 15, 203–208.

Çengel, Y.A., Boles, M.A., 2006. Thermodynamics: an engineering approach, *McGraw-Hill Higher Education*, New York.

Charny, C.K., 1992. Mathematical models of bioheat transfer, *Adv Heat Transfer*. 22, 19–155.

Cho, Y.I., 1992. Advances in transfer-Bioengineering heat transfer. Volume 22, *Academic Press*, London.

Das, K., Singh, R., Mishra, S.C., 2013, Numerical analysis for determination of the presence of a tumor and estimation of its size and location in a tissue. *J. Therm. Biol*. 38, 32-40.

Das, R., Mishra, S. C., and Uppaluri, R., 2008. Multi-Parameter Estimation in a Transient Conduction-Radiation Problem Using the Lattice Boltzmann Method and the Finite Volume Method Coupled with the Genetic Algorithms, *Numer. Heat Transfer A*, 53, 1321-1338.

Das, R., Mishra, S.C., Uppaluri, R., 2009, Retrieval of thermal properties in a transient conduction–radiation problem with variable thermal conductivity, *Int. J. Heat Mass Transfer*, 52, 2749-2758.

Dehghan, M., Sabouri, M., 2012. A spectral element method for solving the Pennes bioheat transfer equation by using triangular and quadrilateral elements. *Applied Mathematical Modelling.* 36, 6031–6049

Fan, J., Wang, L., 2011 A general bioheat model at macro scale. *Int. J. Heat Mass Transfer.* 54, 722–726.

Fisher, B., Slack, N.H., Bross, I.D., 1969. Cancer of the breast: size of neoplasm and prognosis, *Cancer*, 24, 1071-1080.

Gautherie, M., 1980. Thermopathology of breast cancer: measurement and analysis of in vivo temperature and blood flow, *Ann. N.Y. Acad. Sci*., 335, 383-415.

GLOBOCAN 2008: http://globocan.iarc.fr/factsheet.asp retrieved on 28 September 2013.

GLOBOCAN 2012: http://globocan.iarc.fr/Pages/fact_sheets_population.aspx retrieved on 10 February 2014.

Golovkin, I.E., Mancini, R.C., Louis, S.J., Lee, R.W., and Klein, L., 2002. Analysis of X-Ray spectral data with genetic algorithms, *J. Quant. Spectrosc. Radiat. Transfer*, 75, 625–636.

Gonz´alez, F. J., 2007. Thermal Simulation of Breast Tumors, *REVISTA MEXICANA DE FI´SICA*, 53, 323–326.

Gore, J.P., Xu, L.X., 2003. Thermal Imaging for Biological and Medical Diagnostics, Biomedical Photonics Handbook, *CRC Press*.

Griffeth, L.K., 2005. Use of PET/CT scanning in cancer patients: technical and practical considerations, *Baylor University Medical Center Proceedings*, Baylor University Medical Center, 18.

Jiji, L.M., 2009. Heat conduction, *Springer*, New York.

Mankoff, D.A., Dunnwald, L.K., Gralow, J.R., Ellis, G.K., Charlop, A.T., Lawton, J., Schubert, E. K., Tseng, J., Livingston, R.B., 2002. Blood flow and metabolism in locally advanced breast cancer: Relationship to response to therapy, *J. Nucl. Med.*, 43, 500–509.

Mishra, S.C., Chugh, P., Kumar, P., Mitra, K., 2006. Development and comparison of the DTM, the DOM and the FVM formulations for the short-pulse laser transport through a participating medium. *Int. J. Heat Mass Transfer*. 49, 1820–1832.

Mishra, S.C., Lankadasu, A., Beronov, K., 2005. Application of the lattice Boltzmann method for solving the energy equation of a 2-D transient conduction-radiation problem. *Int. J. Heat Mass Transfer*, 48, 3648-3659.

Modest, M.F., 2003. Radiative Heat Transfer, second ed., *Academic Press*, New York.

Muthukumaran, R., Mishra, S.C., 2008, Transient response of a planar participating medium subjected to a train of short-pulse radiation. *Int. J. Heat Mass Transfer*. 51, 2418–243

Nakayamma, A., Kuwahara, F., 2008. A general bioheat transfer model based on the theory of porous media. *Int. J. Heat Mass Transfer,* 51, 3190-3199.

National Breast Cancer Foundation: www.nationalbreastcancer.org/ retrieved on October 2, 2013.

National Cancer Institute: www.cancer.gov/ retrieved on October 2, 2013.

National Instruments: www.ni.com retrieved on 30th May, 2014

Partridge, P.W., Wrobel, L.C., 2007, An inverse geometry problem for the localization of skin tumors by thermal analysis. *Eng. Anal. Boundary Elem.* 31, 803–811

Rai, K.N., Rai, S.K., 1999. Effect of metabolic heat generation and blood perfusion on the heat transfer in the tissues with a blood vessel. *Heat Mass Transfer*. 35, 75-79.

Rayter, Z., Mansi, J., 2003. Medical Therapy of Breast Cancer. *Cambridge University Press,* New York

Shen, W., Zhang, J., Yang, F., 2005. Modeling and numerical simulation of bioheat transfer and biomechanics in soft tissue. *Math. Comput. Modell.* 41, 1251-1265.

Shih, T-C., Yuan, P., Lin, W-L., Kou, H-S., 2007. Analytical analysis of the Pennes bioheat transfer equation with sinusoidal heat flux condition on skin surface. *Med. Eng. Phys*. 29, 946–953.

Trobec, R., Depolli, M., 2011. Simulated temperature distribution of the proximal forearm. *Comput. Biol. Med.* 41, 971–979.

Versteeg, H.K., Malalasekera W., 1995. An introduction to computational fluid dynamics, the finite volume method. *Longman Group Limited*, New York.

Wang, L.Q., 1994. Generalised Fourier's Law. *Int. J. Heat Mass Transfer.* 37, 2627-2634

Wissler, E.H., 1998. Pennes' 1948 paper revisited. *J. Appl Physiol*, 85, 35-41.

World Cancer Report 2008: http://www.iarc.fr/en/publications/pdfs-online/wcr/2008/ retrieved on September 17, 2013.

Wulff, W., 1974, The energy conservation equation for living tissue, IEEE Trans. Biomed. Eng., BME-21, 494-495.

Yuan, P., 2009. Numerical analysis of an equivalent heat transfer coefficient in a porous model for simulating a biological tissue in a hyperthermia therapy. *Int. J. Heat Mass Transfer*. 52, 1734-1740.

Zhang, H., 2008, Lattice Boltzmann method for solving bioheat equation. *Phy. Med. Biol.* 53, N15-N23.

Zhao, J. J., Zhang, J., Kang, N., Yang, F., 2005. A two level finite diff scheme for 1-D Pennes bioheat equation. *Appl. Math. Comput.* 171, 320–331.

Zolfaghari, A., Maerefat, M., 2010. A new simplified thermo regulatory bioheat model for evaluating thermal response of the human body to transient environments. *Build. Environ.* 45, 2068-2076.